5-2013

The Production and Characterization of a Multi-functional Fiber-based Composite for use in Protective Clothing

Jessica Green
Clemson University, jmgreen737@gmail.com

THE PRODUCTION AND CHARACTERIZATION
OF A MULTI-FUNCTIONAL FIBER-BASED
COMPOSITE FOR USE IN PROTECTIVE CLOTHING

A Dissertation
Presented to
the Graduate School of
Clemson University

In Partial Fulfillment
of the Requirements for the Degree
Doctor of Philosophy
Materials Science and Engineering

by
Jessica Marie Green
May 2013

Accepted by:
Dr. Philip Brown, Committee Chair
Dr. Christine Cole
Dr. Gary Lickfield
Dr. Richard Marcus

Abstract

A fiber-based composite comprised of two functional components which work concurrently to adsorb toxic organic compounds was developed and characterized for use in chemical threat protective clothing. The first functional component, the sorptive layer, consists of a carded nonwoven loaded with adsorptive particles. In this layer, Capillary-Channeled Polymer[TM] (C-CP[TM]) fibers were used instead of traditional round fibers since the grooved nature of the C-CP[TM] fibers enables increased adsorptive particle loading. The species of adsorptive particles investigated, zeolite and modified PS, are considered as a replacement for more commonly used activated carbon spheres. The second functional component, the flow restrictive layer, consisted of a meltblown polypropylene (PP) nonwoven, which significantly retards air flow due its inherent nanoporous nature thus allowing increased residence time between vapor (molecules) and adsorbent particles. The fabrication of these layers into a composite structure as well as particle loading of the sorptive layer was examined. Testing of the developed composite showed that it has the adsorptive capacity required to protect the wearer from a lethal dermal dose of toxic compounds.

Acknowledgements

I would like to thank my advisor, Dr. Philip Brown, for all of the time and effort he gave to me throughout my time as a graduate student and especially for his input into the writing process of my dissertation. I would like to thank Dr. Kathryn Stevens for her help in my daily work, extensive proofreading and for always being there to listen and give advice. Thank you to Dr. Christine Cole for the opportunity to work on this project and several others throughout my time in graduate school. I would like to give a special thank you to Dr. Gary Lickfield and Dr. Deborah Lickfield for their input in to my research, academic career and for having such a positive impact on my experience at Clemson.

To the faculty and staff of the School of Material Science and Engineering, thank you for all of you help during my time at Clemson University. Thank you in particular to Kim Ivey, Robbie Nicholson, Bob Bowen, and Kathy Bolton for all of their assistance and support during my academic career. I would also like to express my appreciation and gratitude to all of my lab mates for their help along the way. In particular, I would like to say thank you to Dr. Lisa Fuller, Dr. Kyle Gipson, Dr. Jeff Moreland, Dr. Elizabeth Skomra, Julien Boyon, Brett Ellerbrock, Dr. Cody Reynolds, Katelyn Howay, Joel Barden and Steve Hipp. Lastly, I would like to thank all of the family and friends that showed me love and support while I was in graduate school, especially my parents and brothers. I couldn't have done it without you all!

Table of Contents

Table of Contents (continued)

List of Figures

List of Figures (continued)

List of Figures (continued)

List of Figures (continued)

List of Figures (continued)

List of Figures (continued)

List of Tables

List of Tables (continued)

List of Equations

1   Introduction

1.1   Protective Clothing

Protective clothing and armor have been around for at least 5 millennia and originated with the use of animal skins and furs for protection.[1] However, as weapons developed and threats changed from simple ballistic threats to include chemical, biological and nuclear, protective clothing evolved in order to attain multi-functional effectiveness. Advancements in technology have enable protective clothing to evolve from materials such as leather and chainmail (small metal rings linked together in a pattern to form a mesh) to selectively permeable polymeric membranes and bullet proof vests made from high performance fibers.[2] Today the hazards faced by military and industrial personnel are varied and can be broadly placed into the following categories: chemical, biological, physical/mechanical, radiological, and flame/thermal.[3] Regardless of the hazard, the goal of protective clothing has always been to provide the wearer with light weight, durable and effective protection. The work herein will focus on protection from chemicals hazards.

1.2   Chemical Protective Clothing

1.2.1   Brief History of Chemical Warfare Agents (CWAs)

The use of chemicals and naturally occurring poisons (snake and scorpion venom) during war to incapacitate or weaken an enemy force has been used since the late Stone Age (10,000 BC). The modern age of chemical warfare agents was ushered in by World War I

1
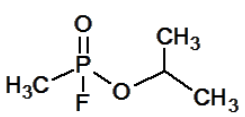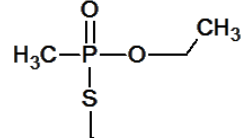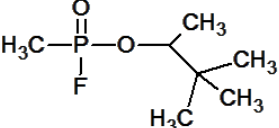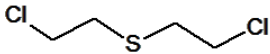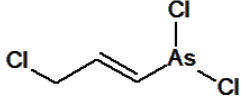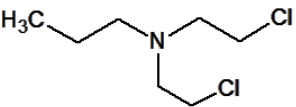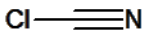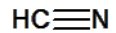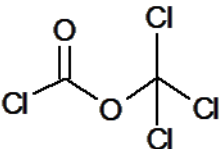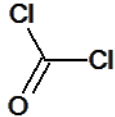
(WWI) where the use of chlorine, hydrogen cyanide, phosgene, and mustard agent occurred on large scales. The first three chemicals were typically disseminated as gases because they had to be inhaled in order to be toxic. Immediate development of protective masks followed in order to protect the soldiers. However, when the German Empire began using mustard agent in warfare the protective equipment needed to be changed. Since mustard agent is not an easily volatilized chemical it would persist on the ground and objects causing the need for full body protection.[4]

At the conclusion of WWI, many nations wanted to ban the use of chemical warfare agents (CWAs) and in 1925 the Geneva Protocol was signed in Geneva during a League of Nations conference, which prohibited the use of chemical and biological weapons in war.[5] While many nations considered it an absolute prohibition, several nations (including United States, England, France, Russia and China) viewed it as a no-first-use agreement.[6] Therefore the development and stockpiling of CWAs continued. In the 1930's a German scientist discovered the first nerve agent, O-ethyl N, N-dimethyl phosphoramidocyanidate (common name of GA or Tabun) during his development of a new insecticide. Throughout WWII and even after the war ended, research and development of new chemical warfare agents continued. It was not until 1993 that a treaty was signed by the United States, Russia and other countries which prohibited the development, production, stockpiling and use of chemical weapons at the Chemical Weapons Convention.[7] CWAs have made appearances since the treaty in several terrorist attacks, the most notable occurring in Japan in 1995 in which a Japanese

2

religious cult (The Aum Shinrikyo) released Sarin in a subway system causing 12 to die and 5,500 to seek medical treatment.[4] To date, chemical warfare agents have been placed in one of four categories (Table 1.1) based on the manner in which they affect the human body.[8]

Table 1.1. Chemical warfare agent classifications and representative chemicals agents/structures

Classification	Chemical Agent/Chemical Structure
Nerve Agents	Sarin, Soman, VX
Blister/Vesicant Agents	Mustard Gas, Lewisite, Nitrogen Mustard (HN-1)
Blood Agents	Cyanogen Chloride, Hydrogen Cyanide
Pulmonary Agents	Diphosgene, Phosgene, Chlorine

1.2.2 Toxic Industrial Chemicals (TICs) and Pesticides

While CWAs possess the greatest danger there are other chemicals that can be used as weapons or pose danger to humans such as toxic industrial chemicals (TICs) and pesticides. TICs are defined as "an industrial chemical which has a LCt50 (lethal concentration time which will kill 50% of the exposed population) value of less than 100,000 mg.min/m^3 in any mammalian species and is produced in quantities exceeding 30 tonnes per year at one production facility."[9] While these chemicals are not designed for warfare, they can be used by terrorists to make weapons of mass destruction (WMD) and are appealing because they are inexpensive, accessible, available legally and in high volumes. TICs may not cause death but can be used to incapacitate the opponent or contaminate military/civilian infrastructures.[10]

Another toxic hazard that people (agricultural workers in particular) are exposed to in large quantities are pesticides which include insecticides, fungicides, rodenticides, pediculocides and biocoides.[11] A common active ingredient in pesticides is organophosphorous (OP) compounds which are also used to produce nerve gases.[12] While pesticides obviously do not have the same level of toxicity, the health hazards they pose are still significant. Research has shown a positive association between pesticide exposure and increased risk of acute or delayed health problems such as non-Hodgkin lymphoma, leukemia, dermatologic effects, neurotoxicity, birth defects and fetal death.[11, 13, 14] According to Wolfe *et al.*, dermal adsorption rather than inhalation or ingestion is the primary route of pesticides entering the body and in 2001 the U.S.

4

Bureau of Labor Statistics reported that skin diseases and disorders accounted for almost 40% of all occupational illnesses within agriculture.[15, 16] Regardless of the chemical hazard, proper chemical protective clothing (CPC) is needed to provide a barrier and protect the wearer.

1.3   Nonwoven Manufacturing

The use of nonwovens in protective clothing is increasing at a rate of ~11% per year as they replace traditional woven materials because they provide an inexpensive and effective solution to chemical protection.[3, 17] In addition, nonwovens are capable of providing increased barrier protection due to the smaller pore sizes possible and because they can be produced at much lighter weights. Lee and Obendorf examined the barrier effectiveness and thermal comfort of nonwoven and woven materials.[18] They found an average through-pore size distribution of 3.5 to 114.4 μm for woven materials and an average of only 0.3 to 6.2 μm for nonwoven materials. In addition the basis weights for the woven materials ranged from 108 to 540 g/m^2 (gsm) whereas the nonwovens had a range of 29 to 81 gsm.[18]

There are three main manufacturing processes for producing nonwovens: wet-laid systems, dry-laid systems and polymer-based systems. The wet-laid process, which is derived from paper making, forms a web by filtering an aqueous suspension of fibers through a wire cloth, on top of which the nonwoven web is made.[19] The webs are bonded by either adding a bonding agent to the aqueous suspension and/or by passing

5

it through a resin applicator.[20] This process is used mainly for various papers including air filter paper, synthetic fiber paper, and liquid filter paper to name a few.[21] Dry-laid systems include both air-laid and carded webs. Air-laid nonwovens are typically made from cellulose fluff pulp and the web is formed by hammer milling the fluff pulp into individualized fibers, distributing the fibers in an air current and forming a fabric on a moving belt or forming wire. Air-laid webs are typically bonded by application of a latex emulsion or with thermoplastic fibers. Nonwovens made through this process are typically used for absorbent materials such as personal hygiene produces and disposable wiping products.[20] The aforementioned manufacturing processes are not commonly used to produce nonwovens which are incorporated into protective clothing and therefore will not be a focus in this work. However, the remaining manufacturing processes (carded webs and polymer-based systems) will be discussed in greater detail in the sections that follow because they are used extensively in current protective clothing and research for developing new protective clothing.

1.3.1   Carded Nonwovens

Carded webs are formed from short staple fibers and the initial processes resemble those used for yarn production. The short staple fibers are typically purchased in a bale (a bag, sack or box into which staple fibers are compressed for shipping and storage) and, therefore, there are several steps that must occur before the fibers can be made into a web.[19] Typical processing steps include opening, blending and feeding. Several stages of opening occur for processing stable fiber from a bale. Initially there is course

6

opening in which the compressed fibers are loosened into larger tufts and impurities are removed. The large tufts can then be passed through several other opening rolls until sufficient opening has been obtained. At that point the fibers are transported via a conveyor belt to a blend roll which can be used for single or multi-component blends. The opened fibers then reach the feeder which prepares a fiber mat and introduces the mat to the card. The purpose of the card is to then form a uniform mat of individualized fibers with a random arrangement.[20, 21] The card is comprised of a series of rolls with wire teeth on their surface. The density of the fiber web can be controlled by the speeds of the various rolls in the card. The carded web is then bonded using one of several possible methods including: thermal (most common), needlepunching, hydroentanglement, ultrasonic, or chemical.

1.3.2   Spunbond Nonwovens

Spunbond nonwovens fall into the classification of polymer-based systems in which webs are formed directly from polymer melt. Molten polymer is extruded through a spin pack and enters a quench chamber where cool air causes the fibers to solidify. The fibers are then introduced into a second stream of high velocity air which attenuates the fibers causing stretching of the individual filaments. These are deposited in a random manner onto a perforated moving belt that has a vacuum below it to aid in web formation. The web is then bonded thermally, chemically or by hydroentangling or needlepunching and taken up (Figure 1.1).[21, 22]

7
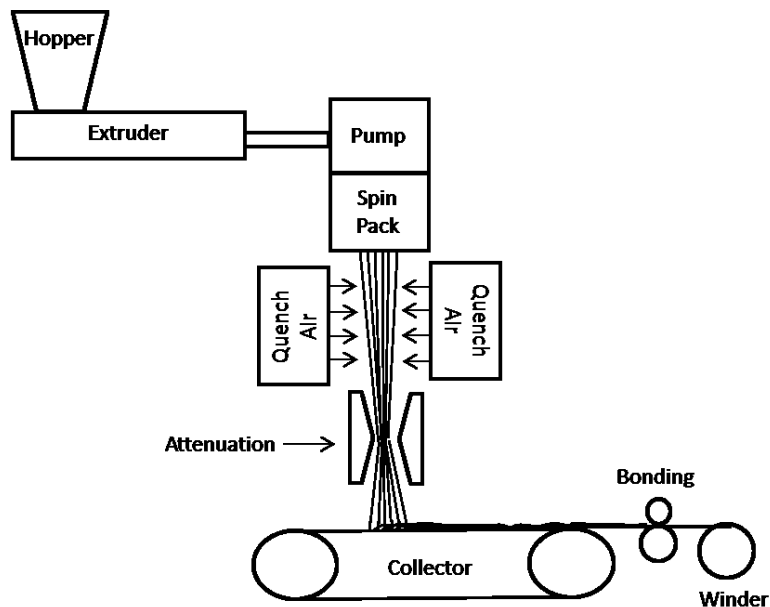
Figure 1.1. Schematic of the supnbond process

The spunbond process can achieve spinning speeds of 1,000 to 8,000 m/min which makes it the fastest and most economical way to produce nonwovens. They can be produced with basis weights of 5 to 800 gsm and fiber diameters of 1 to 50 µm.[20] Spundbond nonwovens are characterized with high strength-to-weight ratios as compared to other nonwoven, woven and knitted structures as well. As with meltblown nonwoven there are many factors which affect the resulting material properties of the web. The major process variables include polymer characteristics, melt viscosity and temperature, air temperature and flow rate, filament draw speed, polymer throughput rate, collection speed and bonding conditions.[23]

Fedorova and Pourdeyhimi investigated the use of bicomponent fibers in the spunbonding process to produce micro- and nanofibers nonwovens which have sufficient strength to be used without a support layer. The small pore sizes and

8

increased surface area, in addition to the strength of the material, would make these nonwovens desirable for use in protective clothing.[24] The production of low basis weight nonwovens with high strength was successful and it was determined that hydroentanglement was the preferred bonding method (as compared to thermal bonding). However, post treatment of the nonwoven is required in order to remove the unwanted polymer and obtain the desired fiber size. This additional step increases the cost of production and the removal of the sea creates environmental issues.[24]

1.3.3 Meltblown Nonwovens

Meltblown nonwovens are also a polymer-based system in which the web is formed from a polymer melt. They are similar to spunbond nonwovens with the key difference being the way in which the air is introduced to the molten polymer. In the spunbond process the air flows perpendicularly to the emerging fiber whereas hot air converges with the fiber in the meltblown process.[20] The polymer melt is extruded though a nozzle (or series of nozzles) directly into high velocity (6,000 to 30,000 m/min) heated air which causes the fibers to be drawn down into very small diameters, 1-5 μm. Directly below the nozzle, ambient air causes cooling of the filaments and air turbulence causes filament breaking and entanglement.[21] The self-bonded, random web is then collected on the screen below (Figure 1.2).
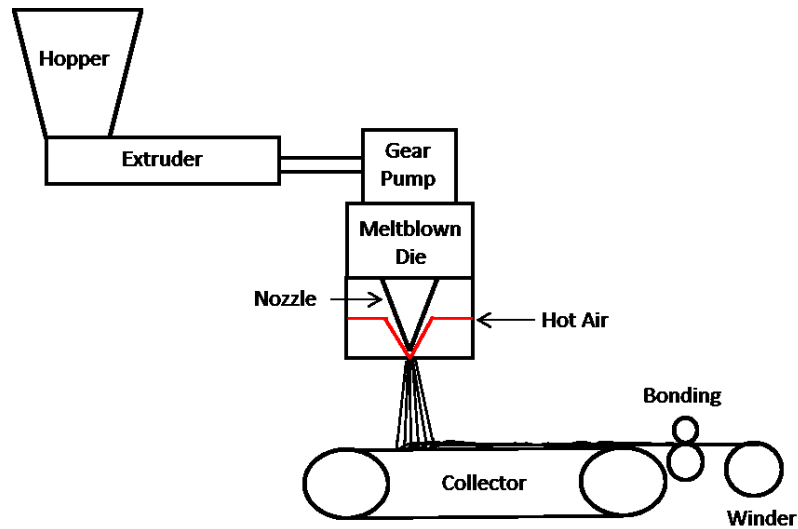
Figure 1.2. Schematic of the meltblown process

According to Hutten meltblown processes are used for thermoplastic polymers, are capable of production speeds up to 1,000 m/min, and typically produce webs with basis weights ranging from 8 to 350 gsm.[20, 25] Material properties of the web are influenced by many factors including machine variables (i.e., polymer throughput and air flow), process variables (i.e., the air gap between the extruded molten polymer and collecting belt), and polymer properties (i.e., polymer type and molecular weight). Meltblown webs are softer, bulkier and weaker than spunbonded webs but provide smaller pore sizes and fiber diameters. This is typically why meltblown webs are commonly used with additional substrates or scrims or in combination with a spunbond nonwoven such as in Kleenguard coveralls (Kimberly Clark) which are used as CPC.[26]

Meltblown nonwovens, as well as spunbond-meltblown-spunbond (SMS) nonwovens, have been investigated for use in military CPC to serve as a lightweight, more air permeable, activated carbon loaded laminate.[27] These systems were compared to

10

traditional polyurethane (PU) foams containing activated carbon. The PU foams had breakthrough capacities that were equivalent to the total adsorption capacity of the material. The meltblown and SMS nonwovens, however, had breakthrough capacities that were less than 50% of the total adsorption capacity due to the thin structure of the material.

1.3.4 Electrospun Nonwovens

The last well known polymer-based system that will be discussed is electrospun nonwovens which are made from either a polymer solution or a polymer melt. A high voltage charge is placed on the polymer solution which causes a liquid jet of polymer to be rapidly drawn from the metallic tip of the syringe onto the grounded collector below (Figure 1.3). The voltages used for electrospinning range from 5 to 30 kV depending on the force needed to overcome the surface tension of the polymer.[20]
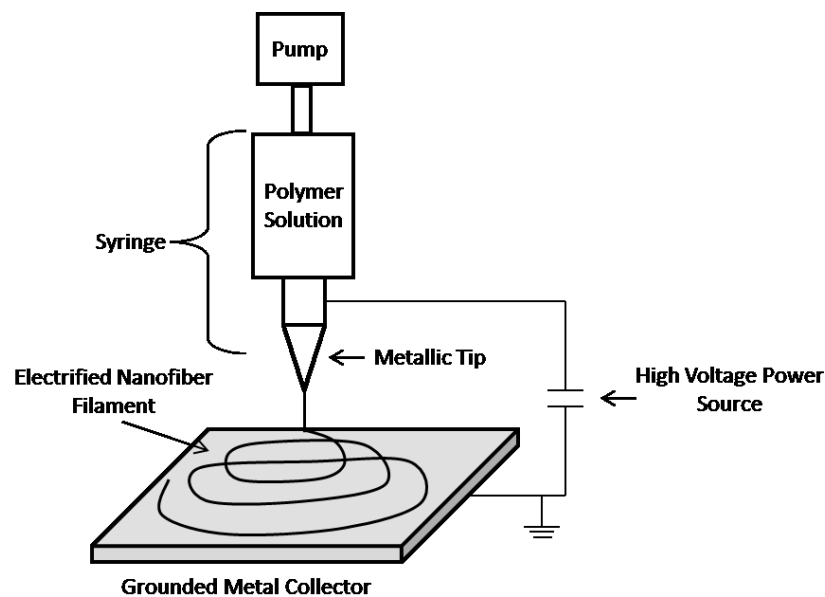
Figure 1.3. Schematic of the electrospinning process

11

Electrospinning produces the smallest fiber diameters of the three polymer-based systems described, with typical diameters between 100 to 500 nm and subsequently the thinnest web structure.[28] Due to the very small diameters the fibers also have a very high surface area and are capable of producing materials with very small pore sizes. The fiber size is dependent on several parameters such as solution viscosity, field strength and field uniformity. As with meltblown nonwovens, electrospun nonwovens are typically used in combination with another substrate due to their lack of strength and durability.[20, 29]

Electrospun nonwovens have been investigated by Schreuder-Gibson, *et al.* for improved chemical resistance to toxic chemical exposure, enhanced fabric breathability and increased wind resistance in protective clothing. Lee and Obendorf examined electrospun polyurethane nanofiber nonwovens as barriers to liquid penetration in protective clothing for agricultural workers. Several different polymers were used including nylon, poly(benzimidazole) (PBI), and polycarbonate all of which require toxic solvents that must be recovered and disposed of properly.[30, 31] The nanofibers were electrospun directly onto a polypropylene nonwoven in order to produce a layered fabric structure and to provide strength to the electrospun web. While improvements in properties were observed (increased protection against challenge liquids and reduced pore sizes for example) the web was produced with a feed rate of 0.003 mL/min which is not feasible for scale up production.[29]

1.3.5   Other Emerging Nanofiber Technologies

A new technology has been developed recently to overcome many of the issues encountered with electrospinning such as slow production rates and solvent recovery challenges. This technology has been termed Forcespinning[TM] and can be used to produce nanofibers using centrifugal forces instead of electrical forces. Forcespinning[TM] can be used to spin both non-conductive and conductive solutions as well as solid materials that melt. Fibers are produced by feeding the polymer solution or melt into the spinneret which is rotated at very high speeds (up to 20,000 rpm). When the centrifugal forces exceed the capillary forces, which prevent the flow of the polymer through the orifices, fluid polymer is ejected and attenuated as the polymer solidifies into nanofibers on the collector (Figure 1.4).[32, 33]
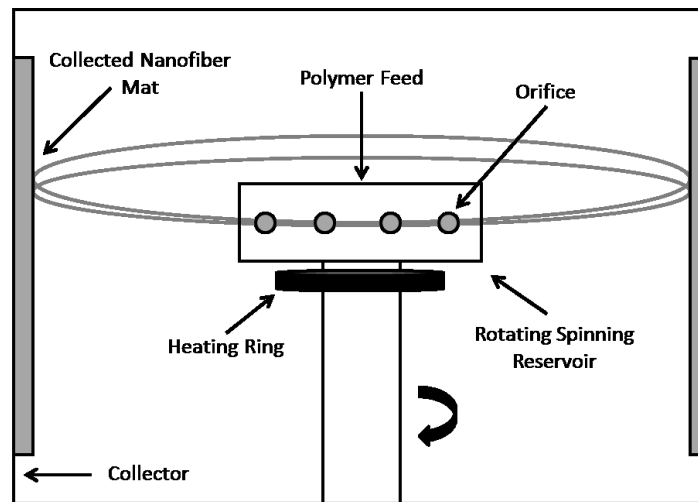
Figure 1.4. Schematic of Forcespinning[TM] process

Shanmuganathan *et al.* found that fiber morphology and diameter were most significantly influenced by the melt and/or spinneret temperature but other contributing factors were spinneret rotational speed, orifice diameter and collector

www.manaraa.com

distance.[33] Sarkar *et al* reported initial production rates of 1 g/min/spinneret orifice.[32]

To date a variety of polymers have been spun using force spinning including

polypropylene (PP), polystyrene (PS), polyethylene oxide (PEO), a hybrid of poly(2,5-

bis(2'-ethyl-hexyl)-1,4-phenylenevinylene) (BEH-PPV))and PEO, and polybutylene

terephthalate (PBT).[32-34]

1.4   Chemical Protective Clothing

1.4.1   Materials used for Chemical Protective Clothing

This research focuses on the development of a fiber based composite for use in

chemical protective clothing (CPC). To date there are four main types of materials used

for CPC which include woven material, nonwovens, microporous materials, and

monolithic films.[18] The purpose of each material is to function as a barrier and protect

the wearer from a chemical threat. The level of protection afforded by each

classification varies and is typically closely associated with the comfort level of the

garment (Figure 1.5).
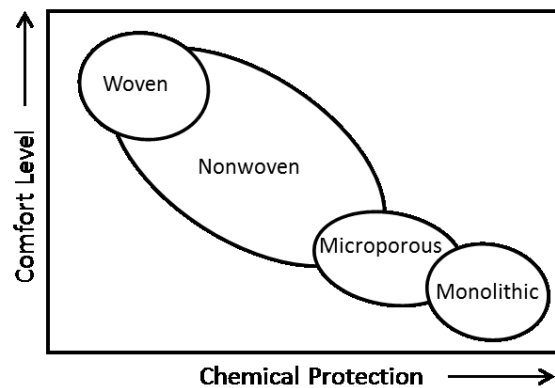
Figure 1.5. Schematic illustrating the relationship between chemical protection and comfort level for the four types of materials used for CPC

14

1.4.1.1 Woven Materials

Woven materials are commonly used to provide low levels of protection against chemicals that possess low toxicity, such as in the agricultural industry. Woven materials are desirable due to their high air permeability and comfort; however, their permeability makes them susceptible to penetration by hazardous liquids such as pesticides. Much of the research on increasing barrier protection of woven fabrics centers around fiber/yarn structures, fiber chemistries and fabric finishes because these factors influence liquid penetration.[35-37] Due to the vast number of pesticide formulations and the variety of fabrics that can be worn as protective clothing, several researchers have investigated statistical models to predict pesticide penetration and barrier efficacy of woven fabrics.[38-40] All researchers found that the viscosity of the pesticide solution and fabric thickness were the two most influential parameters of liquid penetration. In addition fabric cover, yarn twist and the difference in surface tension were found to be very important.[38]

1.4.1.2 Nonwovens Materials

Nonwovens provide a wider range of thermal comfort (breathability) and protection levels due to the variety of production methods (as discussed in Section 1.3) and the ease of fabric/fiber manipulation (fiber size, fabric thickness, pore size, etc.). An example is Kimberly-Clark's line of Kleengaurd[*] brand protective apparel which offers 8 different levels of protection, 5 of which are made either exclusively from nonwovens (spunbond or meltblown) or incorporate a nonwoven in the fabric design.[26] In addition

15

nonwovens are inexpensive which is why their use as disposable CPC has increased significantly over the past few decades.[18] Due to their successful utilization for woven materials, statistical models have also proved a useful tool for the prediction pesticide penetration through nonwoven CPC.[17, 39] Lee and Obendorf found that untreated nonwovens (those without a repellent finish such as a fluorochemical) had greater pesticide penetration as the difference in surface tension between the nonwoven and test chemical increased, the solid volume fraction of the nonwoven decreased or the fabric thickness decreased.[17] The model developed by Jain and Raheel was in agreement with these findings but also found that water vapor transmission and air permeability were significant variables that influenced liquid pesticide penetration.[39]

1.4.1.3 *Microporous Materials*

Microporous materials are used in CPC due to their ability to provide improved barrier effectiveness, compared to woven and nonwoven materials, due to their small pore sizes (diameters less than 2 nm) while still maintaining an acceptable level of wearer thermal comfort.[18] Lee and Obendorf compared thermal comfort of microporous materials, nonwovens and woven materials commonly used for protective clothing and found, while the materials containing microporous membranes had lower air permeabilities, the water vapor transmission rate was equivalent to that of the nonwovens examined.[18] It has been determined by many that there is a strong correlation between thermal comfort and moisture vapor transport in apparel fabric.[2, 3, 18] Commonly, microporous membranes are laminated to a conventional fabric

16

substrate such as a woven, knit or nonwoven for added comfort and strength. W.L. Gore & Associates, DuPont® and Kimberly-Clark offer laminated microporous materials (Gore-Tex®, Tychem® line and Kleenguard A40 and A60, respectively) which offer protection from liquids and dry particulates while remaining breathable (heat and sweat are able to escape).[26, 41] Pesticide penetration though laminate structures such as these have been investigated and shown to provide higher barrier performance as compared to woven and nonwoven materials.[42, 43] While these materials offer improved protection they are also much more expensive and do not provide the same level of comfort as traditional woven materials.

1.4.1.4 Monolithic Films

Monolithic films are continuous polymer based films which are used in cases where highly toxic chemicals present a threat. Penetration of chemicals through these materials occurs via three steps: adsorption of the chemical into the polymer matrix, diffusion of the molecules through the film and desorption of the chemical molecules from the other side of the film. Several researchers have developed predictive models to estimate the rate of permeation through monolithic films based on physical properties of the solute and polymer.[44-46] Pal *et al.* examined breakthrough and permeation rates of chemical agent simulants through protective clothing materials and found that laminate structures that contained monolithic films had the greatest resistance to permeation and had the most consistent breakthrough times.[47]

1.4.1.5 Types of Chemical Protective Materials

The materials previously described (Section 1.4.1.1 to 1.4.1.4) are used individually or incorporated into a laminate structure to produce one of four types of CPC: permeable, semipermeable, selectively permeable or impermeable (Figure 1.6).
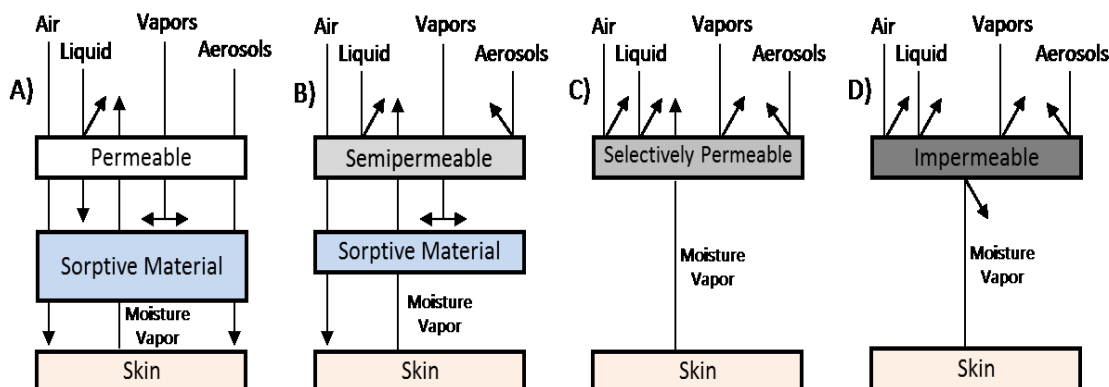
Figure 1.6. Schematic of the four types of CPC

Permeable CPC allows the passage of air, liquid, vapors and aerosols through the outer layer which is typically a woven or nonwoven material. Due to the permeability of the outer layer, a sorptive material is laminated to the back to adsorb toxic chemicals and vapors. In order to increase the level of protection further, a repellent finish, such as a fluoropolymer, is commonly placed on the outer layer to improve liquid repellency.[2, 3] This type of CCP is desirable because it maintains comfort for longer periods of time at higher activity levels. The current standard issue military chemical protective suit, the Joint Service Lightweight Integrated Suit Technology (JSLIST), is a permeable CPC with a woven outer layer, a sorptive layer comprised of activated carbon spheres and an inner knit shell.[48] Semipermeable materials typically have a microporous membrane as an outer layer backed by a sorptive material. These garments prevent passage of liquids

and aerosols but still allow passage of air and toxic vapors necessitating the sorptive layer. A well-known example of a semipermeable garment would be Gore-Tex® by W.L. Gore & Associates, Inc. or polytetrafluoroethylene (PTFE) microporous membranes.[2]

Selectively permeable membranes (SPMs) are thin, lightweight materials that are resistant to permeation by organic molecules in the form of liquids, vapors and aerosols but allow the passage of moisture vapor away from the wearers' skin. The protection mechanism is based on a selective solution/diffusion process instead of an adsorption process like that of activated carbon, which has a limited adsorption life.[2] SPMs have been made from poly(vinyl alcohol), cellulose acetate, cotton and poly(allylamine) and typically consist of a multi-layer composite system.[48] Currently several companies have been researching development of these materials including W.L. Gore & Associates, Inc., DuPont, and Innovative Chemical and Environmental Technologies (ICET).[2]

Impermeable materials are used to provide the highest level of chemical protection against all phases of toxic chemicals. Typically impermeable CPC garments are a single layer of textile material coated with a thermoplastic polymer or synthetic rubber (e.g. poly(vinyl chloride) and butyl rubber).[3] One of the impermeable CPC's for the U.S. military is the toxicological agents protective (TAP) suit which is designed for use in rugged terrain and equipped with a self-contained breathing apparatus (SCBA).[48] Many of these garments require the use of microclimate cooling/heating systems and SCBA due to the inability of sweat and heat to escape from the garment and the need of total

encapsulation. Impermeable CPC therefore cannot be worn for long periods of time or in extreme climates due to the possibility of heat stress or hypothermia. In addition they are costly, heavy and bulky which make them unsuitable for everyday use.[2]

1.5 Requirements and Classification of Chemical Protective Clothing

Chemical protective clothing is designed to protect wearers from exposure to hazardous and toxic chemicals in the workplace, emergency response situation and in the line of duty and must meet a wide range of criteria depending on the level of protection required and the use environment. Additionally garment requirements such as flexibility, strength, durability and water vapor transmission as well as aesthetic elements (i.e. color, appearance, size and comfort) must also be met. Since protective clothing falls under governmental regulation in most countries, mandated standards and safety regulations must also be met. These are issued by the respective government agency such as the US Department of Labor and Occupational Safety and Health Administration (OSHA) for Occupational Safety and Health Standards in the US.[3]

1.5.1 Civilian

In the civilian sector OSHA and the Environmental Protection Agency (EPA) have designated four levels of classifications (Level A-D) to personal protective equipment (PPE), which is the broader term used for all protective items (respirator, gloves, clothing, boots, etc.). A description of the PPE required is shown in Table 1.2. Level A provides the greatest protection and is required when hazards which pose a significant threat to skin, eyes and respiratory system have been either identified/suspected or if

personnel are working in an area where the hazards have not been fully characterized.

Level B still provides the highest level of respiratory protection but a lower level of skin

protection due to a lower presence of skin hazards. Level C PPE is used when the

hazards have been well identified and provides increased mobility as compared to Level

A or B. The final classification, Level D, provides the lowest level of respiratory and skin

protection and is worn when there are no known hazards in the atmosphere and very

low possibility for unexpected skin contact with environmental hazards.[49, 50]

Table 1.2. OSHA and EPA classification and requirements for PPE

Level	Required Personal Protective Equipment (PPE)			
	Respiratory Protection	Clothing	Gloves	Boots
A	Full face piece self-contained breathing apparatus (SCBA)	Impervious chemical protective suit with chemical resistant inner suit (e.g. Tyvek coveralls)	Chemical resistant gloves	Chemical resistant boots
B	Full face piece self-contained breathing apparatus (SCBA)	Hooded chemical-resistant clothing with chemical-resistant inner suit	Chemical resistant gloves	Chemical resistant boots
C	Full face or half mask air purifying respirator	Hooded chemical-resistant clothing with chemical-resistant inner suit	Chemical resistant gloves	Chemical resistant boots
D	Face mask (optional)	Water-repellent surgical gown	Surgical gloves	Chemical resistant boots

However, before a material can be used as PPE, or more specifically CPC, it must meet

the requirements set forth by regulatory institutes such as the following:

- Occupational Safety and Health Administration (OSHA)

- American Society for Testing and Materials (ASTM)

21

- National Fire Protection Association (NFPA)

- National Institute for Occupational Safety and Health (NIOSH)

- American National Standard Institute (ANSI)

- American Association of Textile Chemist and Colorist (AATCC)

Each organization has a series of standards for protective clothing ranging from general requirements such as OSHA's general PPE standards (29 CFR 1910.132) to specific performance goals such as moisture vapor transmission rate (ASTM E96 the Standard Test Method for Water Vapor Transmission of Materials).

1.5.2 Military

Chemical protective clothing worn by military personnel must not only provide protection but functionality and identification since the garment is being worn as the soldier's uniform.[2] The standard issue chemical protective combat clothing is the Joint Service Lightweight Integrated Suit Technology (JSLIST) which is designed for extended use in the field and is disposed of after 45 days.[3] Just as OSHA/EPA designated PPE classifications, the military has identified PPE levels for mission oriented protective posture (MOPP) gear which is used when military personnel are in toxic environments such as a chemical, biological, radiological or nuclear (CBRN) strike. The gear consists of a protective over-garment (JSLIST), multipurpose rain/snow/chembio overboots (MULO), mask, respiratory protection, helmet cover and gloves. The MOPP levels range

from 'MOPP ready' in which the majority of the gear can be issued within in 2 hours to 'MOPP 4' where all pieces are worn.[49, 51]

Military PPE must also meet requirements set by the government. In the US, the Department of Defense (DOD) has established a Defense Standardization Program which ensures that all materials, processes, practices and methods being used in the military, such as CPC, meet certain requirements.[52] These standards include MIL-SPEC (defense specifications), MIL-STD (defense standards), MIL-PRF (performance specifications) and MIL-DTL (detail specifications). MIL-SPECs describe the technical requirements for purchased material that is unique to the military or a commercial item that has been substantially modified. MIL-STDs are documents that institute uniform engineering and technical requirements for unique military or substantially modified commercial processes, procedures, practices and methods such as test method standards. MIL-PRFs state the functional requirements for a material, such as CPC, and the environment in which it must operate by listing the required results for a particular material. MIL-DTLs specify design requirements and performance requirements such as what materials should be used, how a requirement should be achieved, or how an item should be fabricated.[52]

1.6   Strategies for Textile Decontamination

The use of a permeable or semipermeable material in CPC requires the inclusion of a decontamination mechanism. The ideal decontaminate would permanently remove the

23

toxic threat and convert it into non-harmful by-products. Three of the most common methods for CPC decontamination include enzymatic degradation, chemical degradation and adsorption.

1.6.1 Enzymatic

Many researchers have investigated the use of enzymes for the biodegradation of organophosphorus compounds which are found in both pesticides and chemical warfare agents.[12, 53-55] Enzymes possess the ability to detoxify these hazardous compounds in situ and in an environmentally friendly manner. One of the most common enzymes studied for this purpose is organophosphorus hydrolase (OPH) which is also known as phosphotriesterase (PTE). Richins *et al* stated the reason for using OPH was that it had broad substrate specificity and was capable of catalyzing the hydrolysis of organophosphate pesticides as well as chemical warfare agents such as parathion and sarin, respectively.[55] Singh *et al.* reported the use of OPH in polyelectrolyte multilayer films for self-decontamination on cotton fabrics.[56] However, the exact mechanism of degradation has only been theorized with computational studies.[57, 58] Other problems faced with enzymatic degradation include short catalytic lifetimes, thermal sensitivity which can limit process productivity and difficulties with catalyst recovery and reuse.[12]

1.6.2 Degradation

Another means of decontamination is the degradation of the toxic agents via a non-enzymatic route. Several researchers have investigated chemical modifications to the surface of textile fabrics to produce self-decontaminating materials. Chen *et al.*

functionalized electrospun polyacrylonitrile (PAN) fiber mats with oxime groups in order to hydrolytically degrade compounds such as diisopropyl fluorphosphate (DFP), a CWA simulant. However, the reaction required the presence of water to proceed at a desirable rate.[59] Salter *et al.* derivatized Nomex® with N-chloramide hydantoins because chloramides are known to decontaminate thioethers such as sulfur mustards. In addition they were able to attach to polymer substrates via siloxane or silazane linkages and they are nontoxic and regenerable. However, the breakdown of the toxic compounds can result in by products with the same level of toxicity. In addition, chloramides are ineffective against G-agents such as Sarin and Soman.[60]

The use of photocatalytic materials has also been investigated for use in layer-by-layer functionalized textiles to self-decontaminate CWA agents upon exposure to UV-A or solar illumination. While the functionalized samples were able to completely remove the toxicity of dimethylmethylphosphonate (DMMP) within 7 minutes and yperite within 20 minutes, the layer-by-layer deposition method would not be practical for scaling up to manufacturing due to slow production speeds.[61]

1.6.3 Adsorption

As previously stated the current standard issue military chemical protective suit, the JSLIST, incorporates a layer of activated carbon spheres which serves as the protective layer of the uniform and protects the wearer via physical adsorption of toxic compounds. This technology is also employed in both the British and Canadian CPC military uniforms.[2] Carbon has been used for the adsorption of toxic compounds for

25

decades due its very high surface area which increases its ability to act as an adsorbent. It was first used as a filter in gas masks during World War II. While the filters used charcoal, it was found that activation of charcoal (with steam, CO_2, or other chemicals) at elevated temperatures enhanced the porous structure resulting in an increased sorption capacity. [62] Researchers have also found that impregnation of activated carbon with chemicals such as salts of Cu(II), Cr(VI) and Ag(I) can increase the capacity for a particular adsorbate (such as CWAs) and facilitate the degradation of those compounds.[63] Impregnation, however, has disadvantages such as low reactivity towards certain CWAs (sulphur mustard), decreased specific surface area and porosity and, with prolonged exposure to humidity, temperature and storage, reduced effective life due to deactivation of the active ingredients.[62]

Nanoparticles of common metal oxides (MONPs) such as MgO, CaO, ZnO, TiO_2 and Al_2O_3 have also been heavily researched for use in the adsorption of toxic compounds such as CWAs. These materials have received a lot of attention due to their ultrahigh surface areas and their ability to not only adsorb but also degrade toxins with their high surface concentrations of reactive defect sites.[64] A review on nanomaterials for use in protection and decontamination of textiles lists the variety of synthesis methods that have been used to produce MONPs such as sol-gel method, gas phase condensation and high-energy ball milling to name a few.[65] While many synthesis routes are available, most require heating a metal hydrate or hydroxide to very high temperatures (500°C) in order to convert them to a metal oxide which is complicated and costly, especially

26

during scale up. In addition, while the detoxifying reaction mechanism is known for

several compounds it is still only theorized for others.[65]

Zeolites are microporous material that have been used as an adsorbent due to their

well-defined crystal structure, which is based on AlO_4 and SiO_4 tetrahedral building

blocks connected through oxygen atoms.[66] Zeolites have a uniform distribution of pores

that penetrate the entire volume of the material. These pores provide the zeolite with a

very high internal surface area for adsorption.[67] While zeolites have been used for years

to purify air and adsorb volatile organic chemicals, recently Hudiono *et al.* investigated

the use of sodium zeolite-Y (NaY) in an ionic liquid polymer to produce a highly

breathable organic/inorganic film which provides protection from CWAs. The results

showed that the presences of the zeolite prevented the vapor penetration of 2-

chloroethyl ethyl sulfide (CEES, a simulant for mustard gas) while the film maintained a

moisture vapor transmission rate that is commonly accepted in CPC.[68] Satya *et al.*

reported successfully electrospinning a cellulose/PET blend that was then

electrosprayed with zeolites for the detoxification of paraoxon, a nerve agent

simulant.[69]

1.7   Gas Adsorption Theory

Adsorption is the enrichment of one or more components in an interfacial layer

between two bulk phases (a gas and solid for the interest of this work). The interfacial

layers consist of two regions, the surface layer of the adsorbent and the adsorption

space where the enrichment of the adsorptive occurs.[70] Adsorption occurs via physical (physisorption) and/or chemical (chemisorption) interaction. Physisorption depends on intermolecular forces such as van der Waals while chemisorption occurs due to the formation of a chemical bond between the adsorbate (the gas) and the adsorbent (the solid). Gas adsorption measurements are widely used for the characterization of the available surface area and porosity of solid and porous materials such as industrial adsorbents, catalysts and ceramics.[70, 71] These characterizations are determined by extracting information from adsorption isotherms using adsorption theory.

An adsorption isotherm is a measure of the molar quantity of gas taken up, or released, at a constant temperature by an initially clean solid surface as a function of gas pressure.[72] Adsorption isotherms typically follow one of six forms (Figure 1.7), the first five were originally proposed by Brunauer *et al.*[73]

28
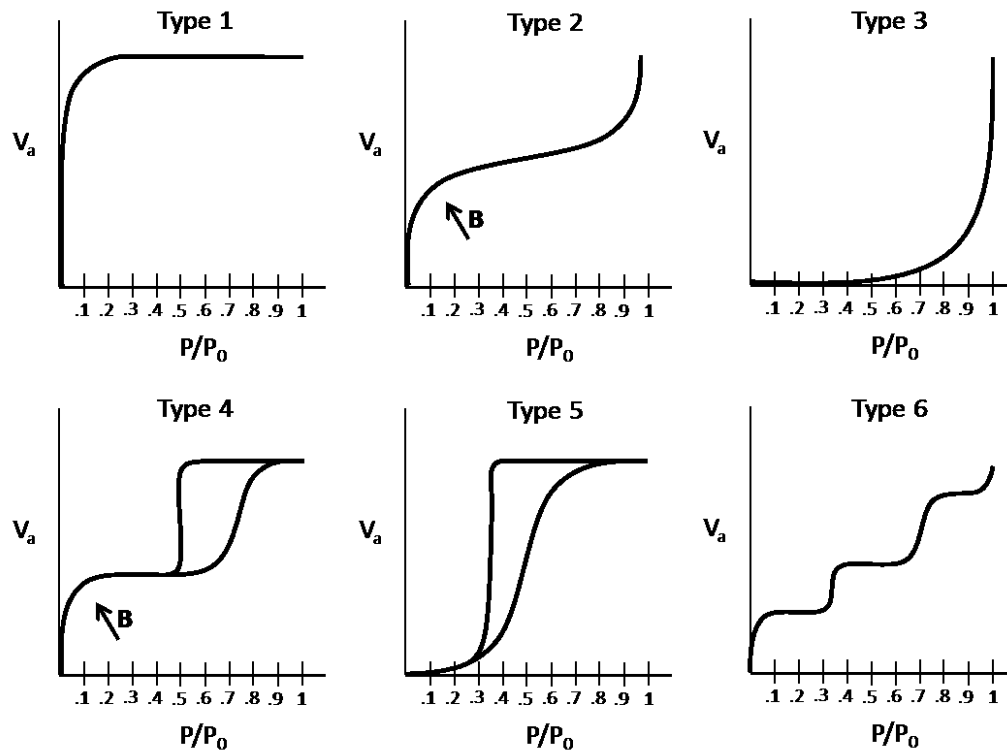
Figure 1.7. Schematics of the six basic adsorption isotherms

Type 1 adsorption isotherms (Figure 1.7) are indicative of microporous (pore widths less than 20 Å) adsorbents such as activated carbons and molecular sieve zeolites and have been termed 'Langmuir isotherms' based on Langmuir's adsorption theory (Section 1.7.1). As can be seen, they are characterized by a steep initial increase in the amount adsorbed which is associated with the filling of micropores. Once the micropores are filled the curve plateaus because there are no adsorption sites remaining.[72, 74] Type 2 isotherms are representative of either nonporous or macroporous (pore widths >500 Å) adsorbents. These isotherms are described by the Brunauer, Emmet, Teller (BET) equation which assumes multilayer adsorption (to be described in more detail in Section 1.7.2.[75] Point B, shown on the curve, indicates the completion of monolayer coverage

29

and the beginning of multilayer adsorption.[70] Type 3 isotherms occur with nonporous solids when the adsorptive molecules have a greater affinity for each other as compared to the solid. Type 4 isotherms have a characteristic hysteresis loop which is associated with capillary condensation occurring within the mesopores (pore widths between 20 Å and 500 Å) of the adsorbent. Type 5 isotherms are uncommon and indicate mesoporous solids in which adsorbate-adsorbate interactions are greater than adsorbate-adsorbent interactions at low relative pressures. A hysteresis loop is again present due to capillary condensation in the mesopores of the adsorbent.[70, 75] Type 6 isotherms are representative of stepwise multilayer adsorption, which is rare, and occurs on nonporous solids with a uniform surface.[70] While adsorption in real solids can fall into one of these distinct classifications many are borderline cases in which they can be assigned to more than one isotherm type.[71]

1.7.1 Langmuir Theory

Langmuir developed his theory of monolayer adsorption after studying electron emissions and chemical reactions at low pressures.[76] From his research and related work, he concluded that the collisions between gas molecules and the surface of a solid were inelastic. The gas molecule, after colliding with the solid, would reside on the surface for a time before returning to the gas phase. The length of time between the condensation of the gas molecule and its evaporation was dependent on the intensity of the surface forces.[72, 76] Langmuir stated this time delay was the direct result of adsorption and the equation for the amount adsorbed is given by Equation 1.1.

$$\frac{P}{V_a} = \frac{1}{V_m b} + \frac{P}{V_m}$$

<p style="text-align:center">Equation 1.1. Linear form of the Langmuir Adsorption Equation</p>

Where

V_a = volume of gas adsorbed by the sample (cm^3)

V_m = volume of gas adsorbed to form a monolayer (cm^3)

P = absolute pressure of the gas (mmHg)

b = empirical constant

A plot of P/V_a versus P should therefore yield a straight line from which the values of b and V_m can be obtained from the intercept and slope. The monolayer capacity (V_m) is then used to calculate the specific surface area of the adsorbent (Equation 1.2).

$$s = \frac{V_m \sigma N_A}{m V_o}$$

<p style="text-align:center">Equation 1.2. Specific surface area of the adsorbent</p>

Where

s = specific surface area (m^2/g)

σ = area of surface occupied by a single adsorbed gas molecule ($16.2 \times 10^{-20} \, m^2$ for N_2)

N_A = Avogadro constant (6.023×10^{23} molecules/mol)

m = molecular mass of the adsorbing sample (g/mol)

V_o = molar volume of the gas (m^3)

Langmuir's theory has been used for Type 1 and the initial portions of Type 2 isotherms but more aptly applies to chemisorption rather than physisorption because of the inherent assumptions (assumption 2) of the theory which include:[75-77]

1. The adsorbed atom or molecule is held at a definite, localized site;

2. Each site can only accommodate one atom or molecule (monolayer adsorption);

3. The energy of adsorption is constant over all sites (surface is homogeneous) and there are no interactions between neighboring sites.

In Langmuir's classical approach it was assumed that the pores present in Type 1 isotherms were so narrow that they could only accommodate a single layer of molecules or atoms, hence monolayer adsorption, and that the plateau of the Type 1 isotherm indicated the competition of monolayer coverage. However, it is now known that, due to the close proximity of the pore walls, micropore filling occurs within pores of microporous samples and that the plateau of the Type 1 isotherm indicates multilayer adsorption on the external surface area of the solid.[70, 71]

1.7.2 BET Theory

Researchers expanded upon Langmuir's theory to make it more applicable to situations that fell outside of his assumptions such as considering lateral adsorbate-adsorbate interactions and adsorption on non-uniform surfaces.[78, 79] However, the most widely known extension is the BET equation by Brunauer, Emmet and Teller.[73] After

examination of others' theories on multilayer adsorption including DeBoer and Zwicker and later Bradley who stated multilayer adsorption occurred due to dipole induced layer formation Brunauer, Emmet and Teller developed their own theory.[80, 81] They concluded that the forces responsible for condensation of gases were also responsible for the binding energy that produced multilayer adsorption. The BET equation (Equation 1.3 where C is a constant related to the energy of adsorption) was developed from their theory which has the following assumptions:[71, 73, 77]

$$\frac{P}{(P_0 - P)V_a} = \frac{1}{V_m C} + \frac{C-1}{V_m C}\left(\frac{P}{P_0}\right)$$

Equation 1.3. Linear BET equation

1. Each site can accommodate 0 to i (where i approaches infinity) molecules or atoms (multilayer adsorption, see Figure 1.8);

2. Molecular interactions occur between a single adsorbed molecule or atom and another that adsorbed onto it (i.e. there are no interactions between neighboring sites);

3. The rate of condensation is equal to the rate of evaporation when a single layer is present;

4. Second and subsequent layers are treated as the same and viewed as having properties of the bulk liquid;

5. At the saturation pressure there are i layers present which is equivalent to the sample being surrounded by a liquid.

33
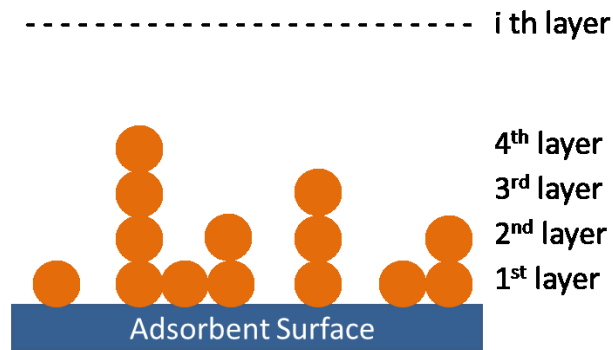
Figure 1.8. Schematic of the BET model for adsorption

As with the Langmuir equation, a plot of the BET equation ($P/[V_a(P_0-P)$ vs P/P_0) should yield a straight line from which the values of V_m and C can be obtained from the slope and intercept. The monolayer capacity is then used to calculate the specific surface area using Equation 1.2. However, for most isotherms obtained when using nitrogen as the adsorptive, the linear portion of the plot is only observed for values of P/P_0 between 0.05 and 0.3. Typically the BET equation is applied to Type 2 and 4 isotherms and Type 1 only with modification. A more in-depth discussion of the BET equation and its application to nitrogen adsorption isotherms will be covered in Section 3.4.

1.8   Aim of Research

The focus of this research is to develop and characterize a new fiber-based composite for use in CPC. The composite will be comprised of two functional components working concurrently to adsorb toxic organic compounds. The first functional component, the sorptive layer, will incorporate two different adsorptive particles, zeolites and modified polystyrene (mPS), as a replacement for the more commonly used activated carbon spheres. Since the mode of decontamination of the fiber-based composite will be

34

adsorption, the available surface area of each particle type will be determined as well as the particle size. The base of the sorptive functional layer will be a carded nonwoven comprised of Capillary-Channelled Polymer™ (C-CP™) fibers. CC-P™ shaped fibers are used instead of traditional round fibers since the grooved nature of the C-CP™ fibers enables increased adsorptive particle loading. The second functional component, which will be referred to as the flow restrictive functional layer, consists of a meltblown polypropylene (PP) nonwoven. This layer is expected to significantly retard air flow due its inherent nanoporous nature thus allowing increased residence time for interaction between vapor molecules and the adsorbent component. The fabrication of these layers into a composite structure as well as particle loading of the sorptive layer will be examined. In addition, the adsorption capacity of the material will be assessed to determine its feasibility in providing adequate protection to the wearer.

2 Experimental

2.1   Materials

Chemical/Material	Supplier	Description
0.84 IV PET	Wellman	Small clear pellet; molecular formula $(C_{10}H_8O_4)_n$
BEEM embedding capsules	Electron Microscopy Sciences	Model No. 1001-SPC
Low Viscosity Embedding Media	Electron Microscopy Sciences	Embedding resin; CAT# 14300
Instant Krazy Glue®	Krazy Glue®	Ethyl cyanoacrylate; fast acting adhesive
Low melting PET Binder Fiber	Hoechst Celanese	3dpf copolyester bicomponet fiber; 80°C melting point
Modified PS Particles	SAIC	Modified PS Particles
HiSiv 1000	UOP LLC Corporation	Zeolite Particle
Isopropanol	BDH	MW 60.1, 19L, 99% pure, CAT# BDH1133
Methyl Isobutyl Ketone	Aqua Solutions	MW 100.2, 1L, Reagent ACS, CAT# 101203-594
Diisopropyl Ketone	Alfa Aesar	MW 114, 100ml, 98% pure, CAT# A12875-22
Diphenyl Chlorophosphate	Acros Organic	MW 268.6, 100ml, 98% pure, CAT# 200012-142
Diethylketone Gas	Airgas Specialty Gases	86.0 PPM Diethylketone in balance of nitrogen

Table 2.1. Materials Utilized

2.2   Fiber Extrusion and Characterization

2.2.1 Melt Spinning

Fibers were made on a Research Melt Extrusion Machine, Model REM-3P-24

constructed by Hills R & D, Inc. Three different size C-CP^{TM} shaped fibers were produced

using a 0.84 dL/g intrinsic viscosity (IV) polyethylene terephthalate (PET) (provided by

Wellman, Inc). The extrusion conditions for making C-CP^{TM} fibers of the desired linear

36

densities per filament 6, 15, and 30 are described in Table 2.2. The linear densities per filament were confirmed after each spinning run.

Fiber dpf	Extrusion Temperature (°C)	Pump Speed (rpm)	Pump Size (cc/rev)	Mass Throughput (grams/min/hole)	Spinneret Shape	Number of holes	Spin Finish
6dpf	285	10.2	.584	0.51	C-CP™	16	Yes
15dpf	285	14.1	.584	0.69	C-CP™	16	Yes
30dpf	285	17	.584	0.84	C-CP™	16	Yes

Table 2.2. Extrusion conditions for 6, 15 and 30 dpf C-CPTM PET fibers

2.2.2   Linear Density Measurements

A 100 meter skein was made of each sample using a Yarn Reel from Industrial Laboratory Equipment Co. Inc. (model #ILE-5-SKRH-1M and serial #1192909). Each skein was weighed on a Sartorius BP221S four place balance to determine the mass. The mass was used to calculate the linear density in denier (grams per 9000 meters) per filament (dpf) using Equation 2.1, where M is the mass of the skein in grams, and N is the number of filaments in the fiber sample.

$$dpf = \frac{M \times 90}{N}$$

Equation 2.1. Denier per filament calculation for a 100m skein

2.2.3   Fiber Crimping

Prior to nonwoven production the fibers used for nonwoven sets 2 and 3 (Table 2.3) were crimped. A TWISTEC Model TWV-4/200 was used to add 2-3 turns per inch (TPI) to each fiber size in order to provide increased strength for the crimping process.   Four

37

ends of the twisted fiber were then run into the TechTex 1 Threadline crimper to obtain

crimped fibers.

2.3   Microscopic Examination of Fibers

2.3.1   Sample Preparation

Cross-sectional samples of un-crimped fibers were prepared for microscopic

examination using BEEM embedding capsules (Model No. 1001-SPC) and a Low Viscosity

Embedding Media (Electron Microscopy Sciences). The samples were mounted as

shown in Figure 2.1.
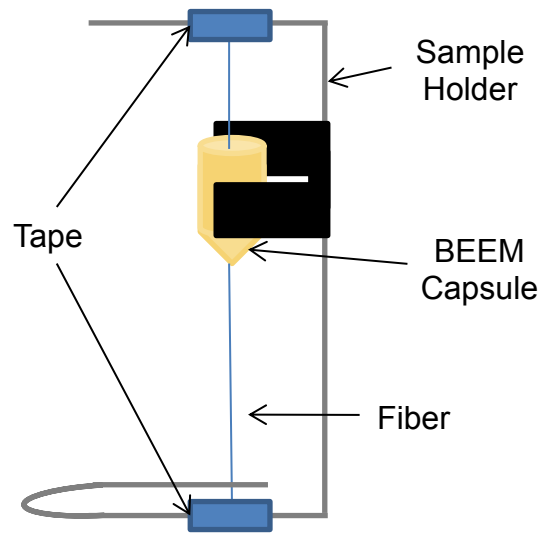
Figure 2.1. Stand and BEEM capsule setup used for microscope sample preparation.

The fiber was drawn through the bottom of the capsule using a needle and the resulting

hole was sealed with ethyl cyanoacrylate (Krazy Glue®). A 10 ml syringe with a 20 gauge

needle was used to fill the capsule with the embedding resin. The sample was then

placed into a Sheldon Manufacturing, Inc. oven at 70°C for 8 hours to cure. Once cured,

the Beem capsule was cut from the stand and the embedded sample was removed.

2.3.2 Microtoming of Fiber Samples

Prepared samples were placed into the microtome holder and microtomed using a Reichert-Jung Ultracut E Microtome. A glass blade was used to remove sections approximately 200 nanometers thick from the tip of the resin sample. This process was repeated until a smooth surface was achieved. The resin sample was then examined under a scanning electron microscope (SEM).

2.3.3 Microscopy

A Hitachi Scanning Electron Microscope (SEM) 3400 was used to obtain cross-sectional images of the embedded fiber samples. The resin samples were mounted onto an aluminum stand and a piece of copper tape was applied around the tip of the resin sample to reduce the charging of the sample by making it more conductive. Samples were examined under the variable pressure setting with a pressure of 30 Pa, a beam current of 20 kV, and a working distance of approximately 10 mm. This pressure and current setting were chosen to reduce the charging of the sample during viewing.

2.3.4 Analysis of Microscopy Images

SEM images were analyzed using Universal Desktop Ruler v3.0.1211 from AVPSoft.com. Measurements were made of tip-to-tip fiber length, groove entrance width, groove base width, and groove depth measurements for C-CP^{TM} shaped fibers. These are illustrated in Figure 2.2. Measurements were made on all visible grooves of each fiber observed at a magnification of 200X, approximately 20-30 filaments per fiber size. The highest, lowest, average and standard deviation of these measurements were then calculated.
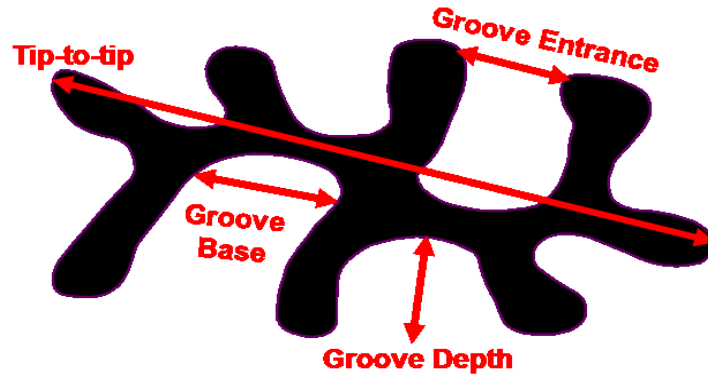
Figure 2.2. Schematic diagram showing tip-to-tip, groove entrance, base, and depth measurements

2.4 Nonwoven Production

C-CP[TM] fibers of different dpfs were wound off into skeins and cut to lengths of 2 inches. These were then hand mixed to the ratios presented in Table 2.3. In addition, low melting point PET binder fibers were added to the C-CP fiber mixtures at 20 and 30 weight percent ratios.

The various fiber blends were then placed into a CMC Rando for mechanical opening and mixing. Nonwovens were produced by running the fibers through a 20" Proctor & Schwartz Roll-Top Card immediately followed by calendaring on a 20" Benz Thermal Bonding Calendar which was set to 100°C and 20 kPa/cm. After nonwoven production the basis weight was determined in units of g/m^2.

Set	Shaped Fiber Content				Added Binder Fiber (%)	Crimped
	3dpf (%)	6dpf (%)	15dpf (%)	30dpf (%)		
1	0	33	33	33	20	No
2	0	55	40	5	30	Yes
3	30	40	30	0	30	Yes

Table 2.3. C-CP[TM] fiber and binder fiber content for nonwoven Sets 1-3

40

2.5   Nonwoven and Composite Testing

2.5.1   Elongation Testing

A constant-rate-of-extension tensile testing machine was used to determine the breaking force and elongation of composite samples. These tests were performed using an Instron 1125 equipped with Blue Hill software following ASTM D 5034. Five samples, 4" by 6", were tested from each construction in both the machine and cross-machine direction. The gauge length was set at 3 inches and the crosshead speed was set so that the maximum breaking load occurred at 20 ± 3 seconds. The percent elongation and load at initial break were obtained.

2.5.2   Air Permeability

The air permeability test is a nondestructive method used to determine the air permeability of textile fabrics. The instrument measures the air flow passing perpendicularly through a known area of the sample. The flow rate of the air is adjusted to obtain a prescribed air pressure differential between the two fabric surfaces and from this the air permeability of the fabric is determined.   Samples were tested on a Texttech 3300 Air Permeability Tester using a test area of 38 cm^2 following ASTM D 737. Each sample was securely clamped under the test head and then the air flow was adjusted until an accurate, stable reading was displayed on the flow meter, which was then recorded for each sample.

2.5.3 Capillary Flow Porometer

The Capillary Flow Porometer (CFP), model CFP-1100-AEXS, manufactured by Porous Materials, Inc., was used to measure the porosity of textile materials. Compressed air is incrementally passed through the sample and data points are taken at each equilibrium point as long as both pressure and flow rate continue to increase. Once maximum flow rate or pressure is reached the air flow is stopped and the test is complete.

Each sample was 2" by 1.5", and was placed into the sample chamber between two O-rings to ensure an air tight seal and then the chamber lid was sealed. Each sample was run in triplicate. The test method used for all samples was a wet up, dry up test using Galwick as the wetting agent. Galwick has a surface tension of 15.9 dynes/cm and can be used to detect effective pore sizes of ≥0.05μm with 100psi of pressure. The data calculated with the CFP software package included smallest pore diameter, mean flow pore diameter and bubble point pore diameter.

2.6 Particle Characterization

2.6.1 Particle Size Measurements

Hitachi Scanning Electron Microscopes (SEM), 4800 and 6600, were used to obtain images of the particles types used for this research; zeolite particles (Molsiv Adsorbent HISIV 1000 from UOP LLC) and modified polystyrene (mPS) particles (SAIC). Prior to examination both zeolite and mPS particles were placed onto double sided carbon tape which was adhered to an aluminum mounting stub for sputter coating. Both particle types were sputter coated with platinum for five minutes in order to reduce the

charging. Samples were examined under the variable pressure setting with a pressure of 30 Pa, a beam current of 20 kV, and a working distance of approximately 10 mm to aid in reducing the charging of the sample during viewing.

The images obtained from the SEM were analyzed using Universal Desktop Ruler v3.0.1211 from AVPSoft.com to obtain diameter measurements on approximately 50 particles.

2.6.2 Thermogravimetric Analysis

Thermogravimetric analysis (TGA) is a technique used to measure the change in mass over a temperature range. This technique can be used to determine the amount of water or solvent present in a sample, the mass loss of the sample over a specific temperature range, or the final degradation temperature of a sample.

A Hi-Res TGA 2950 Thermogravimetric Analyzer was used. Each sample had a mass of approximately 5 mg and was placed into a clean platinum pan. The instrument was purged with nitrogen after the sample was loaded and the precise sample mass was measured. Samples were run at a heating rate of 20°C/min up to a maximum temperature of 600°C under a flow rate of 40 mL/min nitrogen. From the thermograms the amount of water present in the zeolite particles was obtained as well as the degradation temperature of the mPS particles.

43

2.6.3 Surface Area Measurements

The Accelerated Surface Area and Porosimetery (ASAP) 2010 manufactured by Micrometrics was used to obtain information regarding the surface area and porosity of both types of particles and the textile fabrics. Particle loaded samples were prepared as discussed in Section 2.7 for smaller samples. Prior to analysis samples were dried in an oven at 60°C overnight and then degassed at 300°C (zeolite), 200°C (mPS) or 25°C (zeolite or mPS) under vacuum for 2 hours to remove any water or other volatiles present.

Before testing the sample tube is evacuated and the sample is cooled to cryogenic temperature using LN_2. The sample is then dosed with a precise quantity of the adsorptive gas (N_2 for all tests) via the adsorptive valve, Figure 2.3. As the sample adsorbs the gas, the system pressure decreases. The sample is then dosed again until adsorption equilibrium has been established at the target pressure. The quantity of gas adsorbed at this equilibrium is calculated from the total gas quantity dosed onto the sample and the gas quantity that remains. This process is repeated until a relative pressure, which is the actual gas pressure divided by the vapor pressure of the adsorbing gas, of 1 is reached. BET and Langmuir surface area, average and total pore volume, BJH pore size distribution and micro-pore analysis is obtained from the nitrogen isotherm data.

44
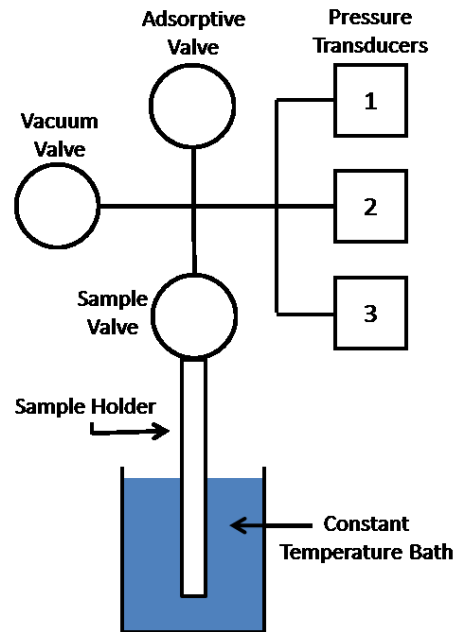
Figure 2.3. Schematic of the essential elements of the ASAP 2010

2.7   Particle Loading onto Nonwoven Fabrics

Sample size and particle loading was varied throughout the research and the method

used for loading particles was therefore adapted for the sample size needed. Larger

samples (>.2 m^2) were conditioned in a controlled room at 70°F and 65% relative

humidity for 24 hours. Smaller samples were cut to the desired sample size and placed

in a Fisher Scientific Isotemp vacuum oven (Model 285A) with a GAST vacuum pump

(Model 1HAB-25-M100X) at 60°C and dried to a constant mass. The initial mass of each

sample was recorded before particle loading.

As stated in Section 2.6.1, two particle types were studied during this research: zeolite

particles and modified polystyrene (mPS) particles. Both particle types were used as

received and then suspended in isopropanol before being applied onto the nonwoven

samples.

45

The smaller nonwoven samples (typically 14.5 cm^2) were either sprayed with only zeolite or mPS particles, or a 50/50 mixture of the two. Particles were applied to the nonwoven samples using a glass reagent sprayer connected to an airline. In order to obtain an even coating the sprayer was held at a constant distance from the fabric (approximately 20 cm) and moved across the fabric at a constant rate (4 sec/m). Each side of the nonwoven was sprayed with half of the required solution, placed in a vacuum oven at 60°C to remove the isopropanol and re-weighed after each spray. Samples were re-sprayed and dried until the target loading was achieved within 10% of the target mass (46.5 g/m^2).

The larger nonwoven samples (approximately 0.45 m by .06 to 5 m), which were produced for prototype production, were sprayed with both particle zeolite and mPS particles in order to obtain equal masses of each on the fabric samples. Particle solutions were applied to the samples in the same manner as the smaller samples but a paint sprayer was used instead of a glass reagent sprayer. Each layer was sprayed with half of the required solution, allowed to dry, and then weighed. The second particle solution (typically mPS particles) was then sprayed in the same manner and this procedure was repeated until the desired particle loading was achieved within 10% of the target mass (85.3 g/m^2 for earlier samples and 46.5 g/m^2 for later samples).

46

2.8 Microscopic Investigation of Particle Loaded Nonwovens

2.8.1 Sample Preparation

Samples were cut to fit aluminum mounting stubs and secured to the surface using double sided carbon tape. Thereafter samples were sputter coated with platinum for time periods that were sufficient to eliminate charging in the electron beam.

2.8.2 Microscopy

Hitachi Scanning Electron Microscopes (SEM), 3400 and 4800, were used to take images of the particle loaded samples. Samples were examined under the back scattered electron compositional (BSECOMP) mode with a beam current of 10 kV and a working distance of approximately 10 mm. These settings were chosen to reduce the charging of the sample during viewing.

The images were used to determine how the particles were loading onto the surface of the nonwovens and to ensure that the particles were loading into the grooves of the fibers.

2.9 Static Testing

2.9.1 Test Compounds

Four test compounds were used for static testing. All compounds were used as received and consisted of isopropanol (BDH), methyl isobutyl ketone (MIBK) (Aqua Solutions), diisopropyl ketone (DIPK) (Alfa Aesar), and diphenyl chlorophosphate (DPCP) (Acros Organic). The physical properties of each test compound are presented in Table 2.4 and their structures are presented in Figure 2.4. Each test compound was also drawn in

ACDLABS 11.0 ChemSketch in order to determine the relative size of each molecule

using the 3D viewer and measuring tool. The approximate length, width and depth of

each molecule are listed in Table 2.5. In addition the molecular volumes were

calculated using Molinspiration Cheminformatics software and are listed in Table 2.5.

Compound	Molecular Weight (g/mol)	Density (g/ml)	Vapor Density (Air=1)	Vapor Pressure (mmHg)
Isopropanol	60.1	0.785	2.10	33.00 @ 20°C
Diisopropyl Ketone	114.0	0.806	3.90	3.75 @ 20°C
Methyl Isobutyl Ketone	100.2	0.802	3.45	15.70 @ 20°C
Diphenyl Chlorophosphate	268.6	1.290	9.26	10.00 @ 20°C

Table 2.4. Physical properties of all test compounds

Compound	Length (Å)	Width (Å)	Depth (Å)	Molecular Volume (A°³)
Isopropanol	3.815	4.149	3.095	64.74
Diisopropyl Ketone	6.866	4.297	5.359	131.518
Methyl Isobutyl Ketone	6.368	4.094	3.109	131.733
Diphenyl Chlorophosphate	13.561	5.538	3.032	218.329

Table 2.5. Approximate measurements of the length, width and depth of each test compound as well as the calculated molecular volume of each test compound

Isopropanol   Methyl Isobutyl Ketone   Diisopropyl Ketone

Diphenyl Chlorophospate
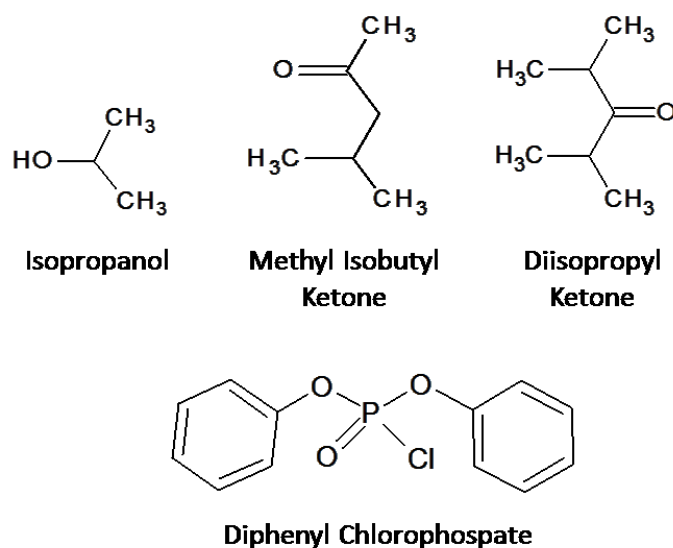
Figure 2.4. Chemical structures of each test compound

2.9.2 Static Testing

A Dynamic Contact Angle Analyzer (DCA) was used as a recording micro-balance during

static testing. Duplicate samples were tested for each sample type (blank nonwoven,

zeolite loaded nonwoven, mPS loaded nonwoven, and 50/50 loaded nonwoven) for

each test compound. The temperature of both the test compound and the chamber

were monitored using Thermochron iButtons (Embedded Data Systems), one of which

was placed in a waterproof capsule before submerging in the test compound liquid. The

mass of the sample and s-hook were off-set by placing an equal mass on the reference

stirrup. The instrument, Figure 2.5, was sealed along all of its edges and around the

door once the sample was placed in the chamber. The chamber was set up as shown in

Figure 2.6 with the sample being placed in the chamber last and the projector bulb

being turned on once the chamber door was shut and sealed. The test was then

immediately started. The test ran for 4 hrs with mass measurements being made every

49

30 seconds. The temperature data was retrieved after each test with a USB 1-Wire iButton Adapter and One Wire Viewer software Version 3.14.16. From this data the maximum adsorption in static conditions could be determined for each sample and each test compound.

Figure 2.5. Dynamic Contact Angle Analyzer (DCA) Instrument used as a microbalance
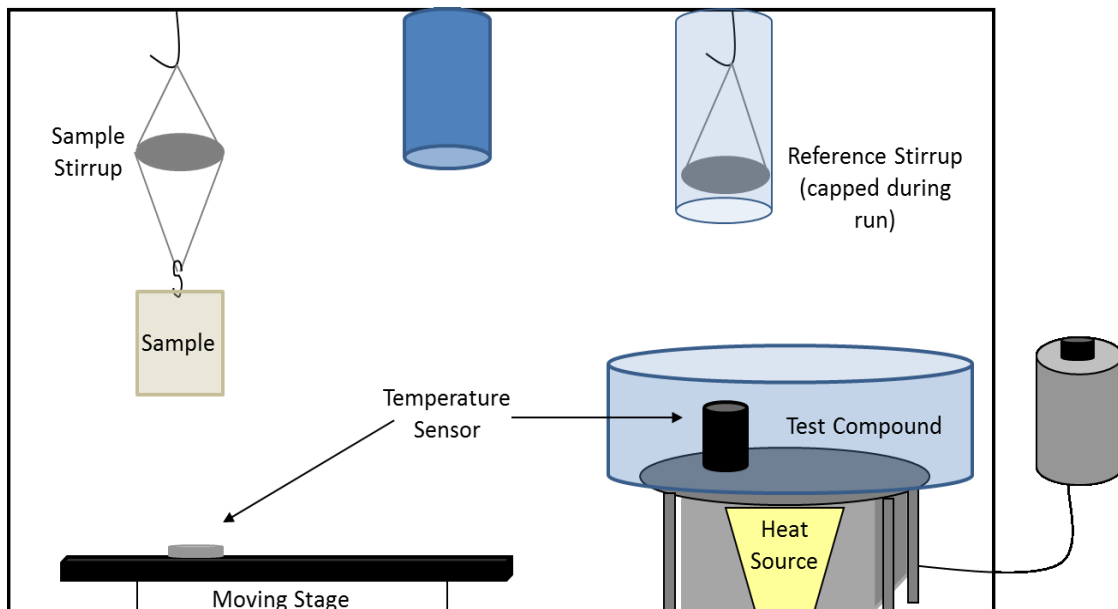
Figure 2.6. Final microbalance set up for static testing

3 Results and Discussion: Particle Characterization

3.1 Particle Size Measurements

SEM images of each particle type, zeolite and mPS, were obtained in order to determine

the average particle diameter as described in Chapter 2 (Figure 3.1 and Figure 3.2).

Measurements were successfully made on the zeolite particles (~50 particles) (Table

3.1) however; measurements were not possible for the mPS particles. While both

particle types had a tendency to agglomerate the mPS particles agglomerated to the

extent that it was not possible to distinguish one particle from the next.
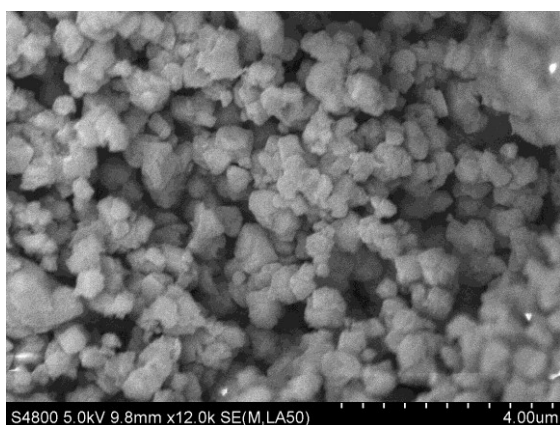
Figure 3.1. SEM image of neat zeolite particles at 12kX magnification
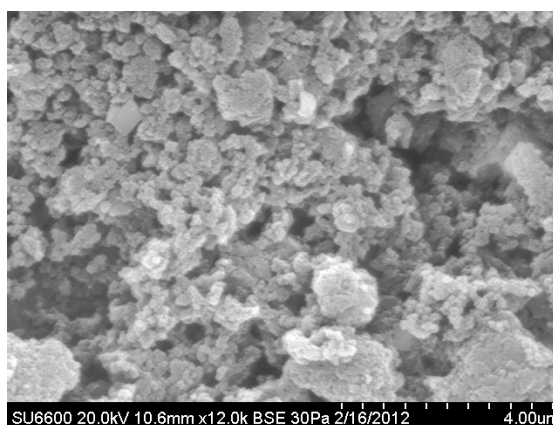
Figure 3.2. SEM image of neat mPS particles at 12kX magnification

Zeolite Particle Diameter Measurements	
Largest Diameter (µm)	0.870
Smallest Diameter (µm)	0.145
Average Diameter (µm)	0.426
Standard Deviation (µm)	0.186

Table 3.1. Summary of diameter measurements on the zeolite particles

The average particle size provided by SAIC for the mPS particles was 0.357μm ± 0.169 μm. Since measurement via SEM images were not possible, a U.S.A. Standard testing sieve with an opening of 45μm was used to ensure no agglomerations larger than that were used during application.

3.2 Thermal Analysis of Particles

Both particles were selected based on their ability to be absorbents, therefore it was important to determine the amount of water adsorbed from the atmosphere by each particle type. The thermogram (Figure 3.3) displays the results for both the zeolite and mPS particles from 0 to 250°C, which can be attributed to water. At approximately 100°C the mPS particles have a mass loss of 1.3% while the zeolite particles have a much higher mass loss of 7%.
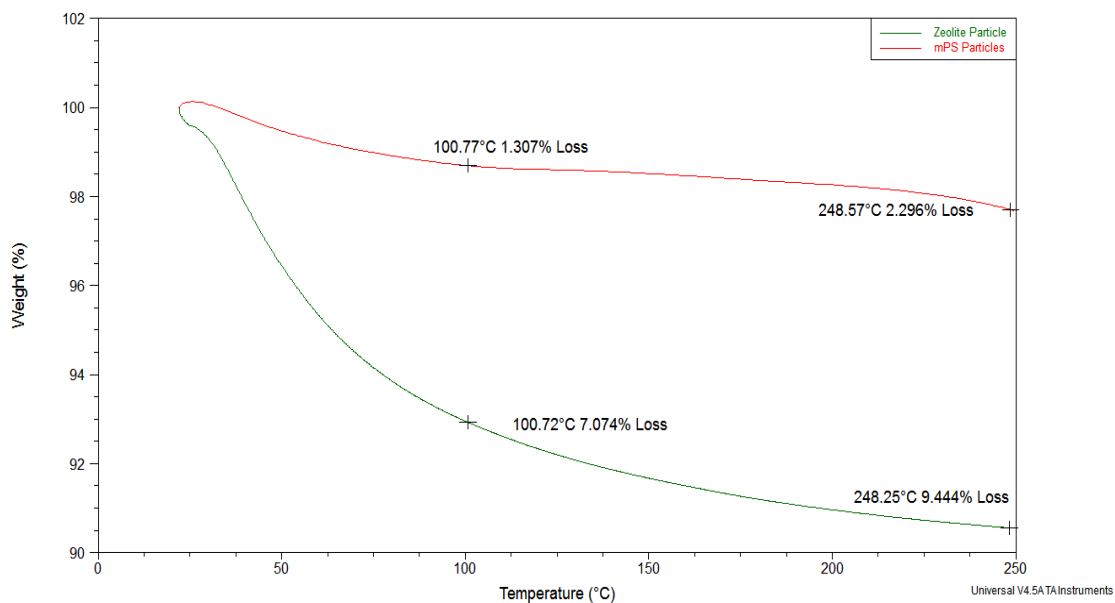
Figure 3.3. Thermograms of water loss for zeolite and mPS particles heated at a rate of 20°C/min to 250°C

52

Examination of the full thermogram of the zeolite particles (Figure 3.4), which was run from 0 to 1000°C, shows a continual decrease in mass up to 1000°C with a total mass loss of 11.23%. This mass loss is also credited to the removal of water from the microporous structure. Balci stated that hydroscopic water, which adsorbs to the surface, and portions of the zeolitic water, which fills the pores, are removed by 100°C. The remaining zeolitic water and the about half of the bound water are removed by 300°C with the remainder of the bound water being lost from 300-500°C. Lastly structural water molecules are removed at temperatures >700°C.[82] The results confirm the need to dry the zeolite particles before testing to ensure maximum adsorption for laboratory testing.
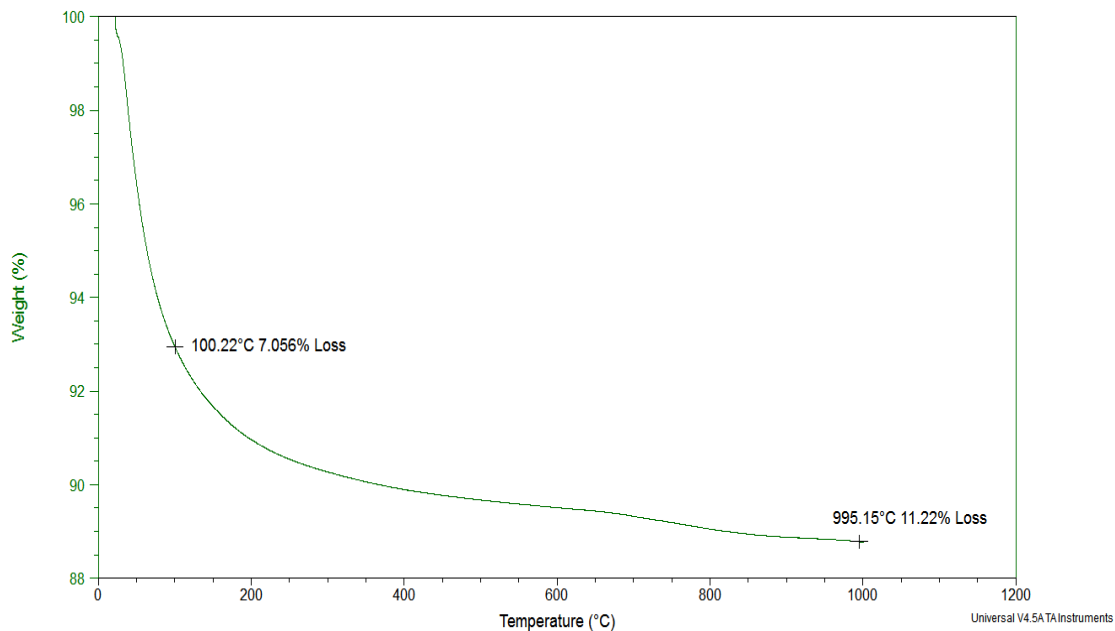
Figure 3.4. Thermogram of zeolite particles heated at a rate of 20°C/min to 1000°C under nitrogen purge (25 mL/min)

53

The results for the mPS particles (Figure 3.5) are significantly different than those obtained for the zeolite particles since the mPS sample degrades in the temperature range used, 0-800°C. In addition there is a multi-stage decomposition of the sample. The initial decomposition, mass loss of 4.7%, is due to the modification of the mPS particle with the bulk degradation, 82.7%, being that of the polymer.[83] The onset of degradation occurred around 300°C which was within the normal range (300-400°C) for PS.[84]
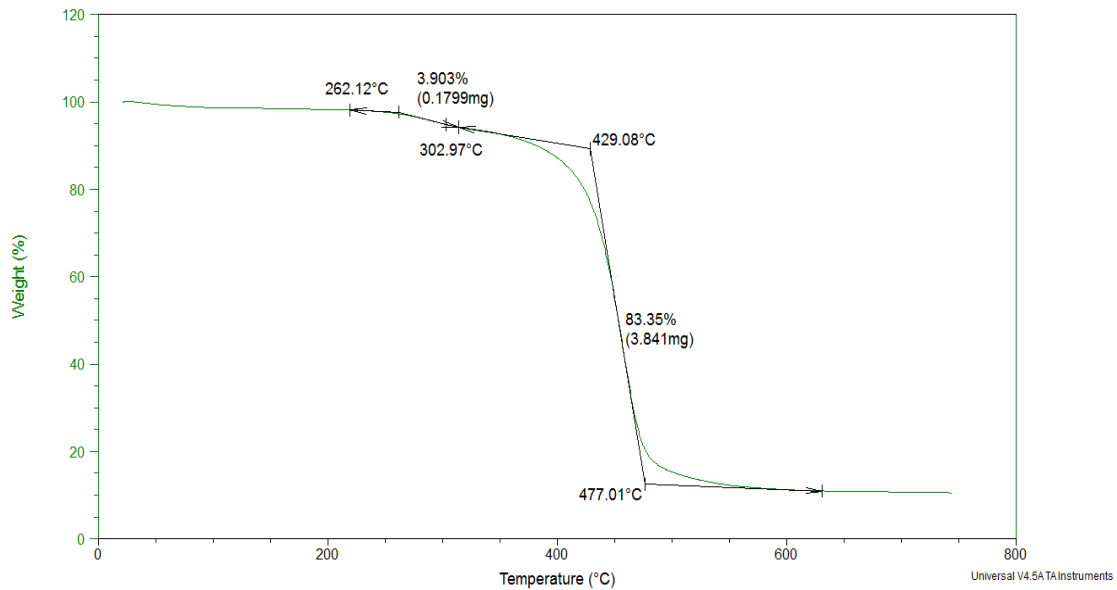
Figure 3.5. Degradation of mPS particles heated at a rate of 20°C/min to 750°C under nitrogen purge (25 mL/min)

3.3   Surface Area Measurements

The available surface area of each particle type was measured using a Micromeritic Accelerated Surface Area and Porosimetry analyzer (Section 2.6.3). The surface area results are based on gas adsorption theory (Section 1.7). For both particle samples

nitrogen adsorption isotherms were measured and the BET and Langmuir surface areas were calculated (Table 3.2).

	BET Surface Area (g/m^2)		Langmuir Surface Area (g/m^2)	
Sample	Average	Standard Deviation	Average	Standard Deviation
Zeolite	436.9	1.4	555.6	23.5
mPS	104.2	2.9	227.8	2.6

Table 3.2. BET and Langmuir surface area measurements for all tested samples

As might be expected, a significant difference was observed between the calculated values for the BET and Langmuir surface area for each particle type. This is because the BET theory assumes multilayer adsorption while the Langmuir theory assumes only monolayer adsorption. Due to this assumption, the Langmuir theory applies to chemisorption situations more aptly than physisorption.[72] Therefore the BET surface area was used for both particle types.

The BET plot (which was generated using Equation 3.1) for the nitrogen adsorption isotherm should result in a straight line between a relative pressure (P/P$_0$) of 0.05 and 0.3.

$$\frac{P}{V_a(P_0 - P)} = \frac{C-1}{V_m C}\left(\frac{P}{P_0}\right) + \frac{1}{V_m C}$$

Equation 3.1. Linear BET equation

Where

P = absolute pressure of the gas (mmHg)

P$_0$ = saturation pressure of the gas (mmHg)

V$_m$ = volume of gas adsorbed to form a monolayer (cm^3)

55

V_a = volume of gas adsorbed by the sample (cm^3)

C = constant related to the energy of adsorption

From the BET plot the values of V_m and C can be obtained. According to literature the value of C should always be positive and most likely between 10 and 300. When the value is either significantly higher or negative it indicates that the measurement is not suitable to be analyzed by the BET equation without modificiations.[1] The monolayer capacity (V_m) is then used to calculate the BET surface area. The BET method is applicable to both Type II and Type IV isotherms (Figure 1.7) without modification, such as in the case of the mPS particles.[70] The nitrogen adsorption isotherm for the mPS particles (Figure 3.6) follows a Type IV isotherm and has an average C value of 56.
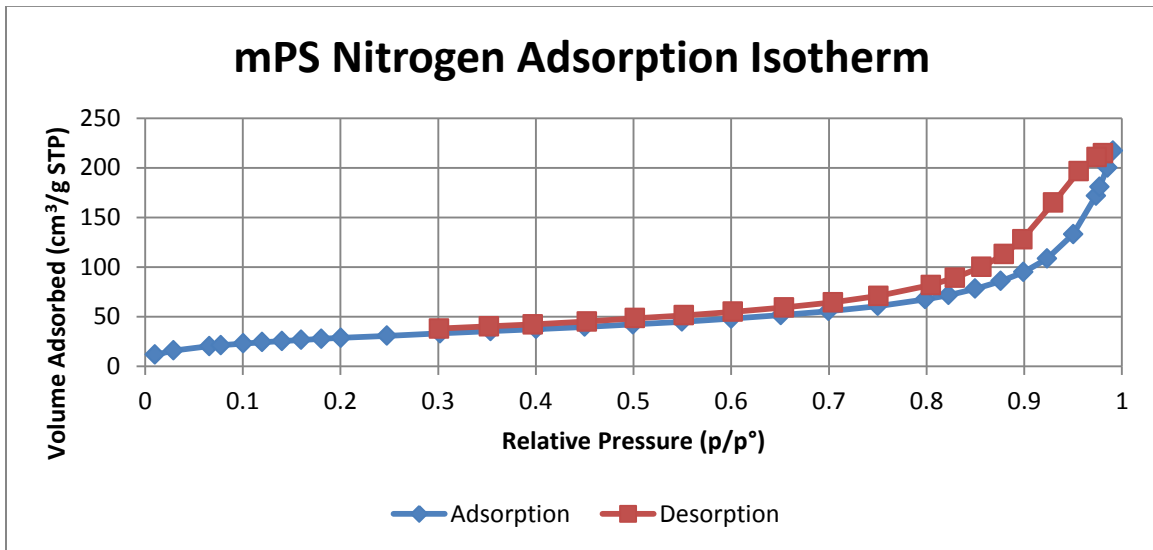
Figure 3.6. Type 4 adsorption isotherm for nitrogen on mPS particles at 77K

The zeolite particles, however, have a Type 1 nitrogen adsorption isotherm (Figure 3.7) and an average C value of -767 using the standard BET pressure range (0.05 < P/P_0 <

56

0.3). Sing *et al.* states that the value of C gives an indication of the magnitude of the adsorbent-adsorbate interaction energy and therefore, as stated by Moellmer *et al.,* a negative C value is 'unphysical' and indicates the BET equation is invalid.[70, 85]
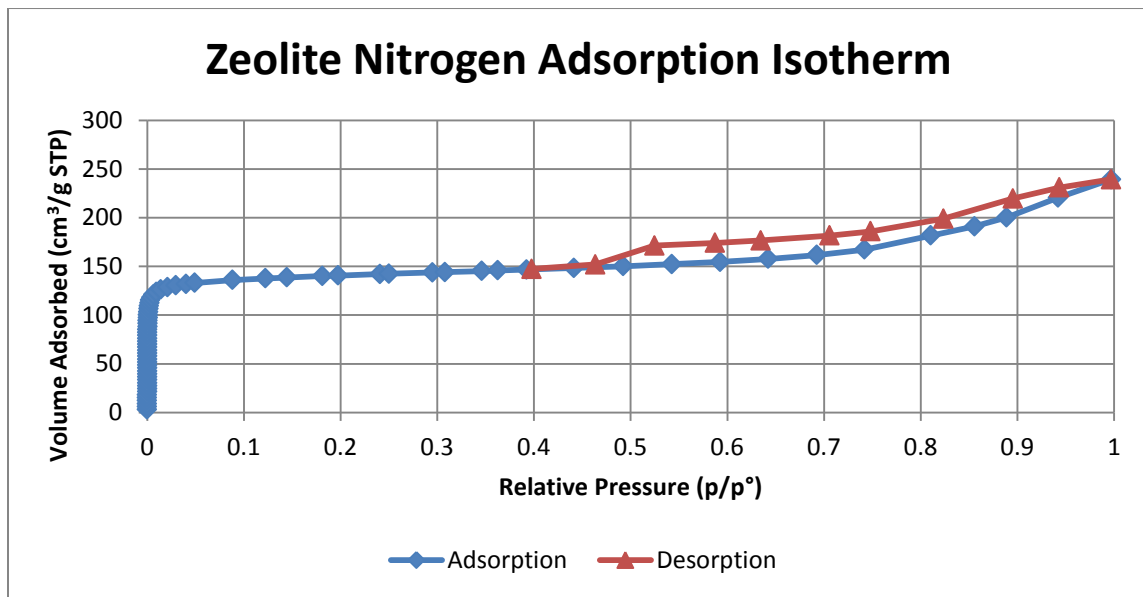
Figure 3.7. Type 1 adsorption isotherm for nitrogen on zeolite particles at 77K

The BET theory does not hold for microporous solids due to micropore filling which occurs at low P/P_0 regions therefore shifting the linear BET region to much lower P/P_0 values (often below P/P_0 of 0.05).[74] While this is a known fact it is still common practice to use the BET surface area but with modifications.[72, 74, 85-87] Rouquerol *et al.* suggested two criteria that should be followed in order to determine a linear BET region. First, the value of $V_a(P_0-P)$ should increase with increasing P/P_0 for the pressure range chosen. Second, the y intercept of the linear region being used must be positive in order to have a meaningful C value.[88] Čejka *et al.* states that, when following this criteria, a linear region can be found in the range of $1.4 \times 10^{-5} < P/P_0 < 0.016$.[74]

57

The data obtained for the zeolite particle samples was therefore transformed (Figure 3.8) using the above criteria to obtain the BET surface area values reported in Table 3.2. The criteria was met using a pressure range of $0.0005 < P/P_0 < 0.015$ which resulted in an average C value of 3,986. Very high values of C indicate strong attraction of nitrogen for the microporous solid.[74]
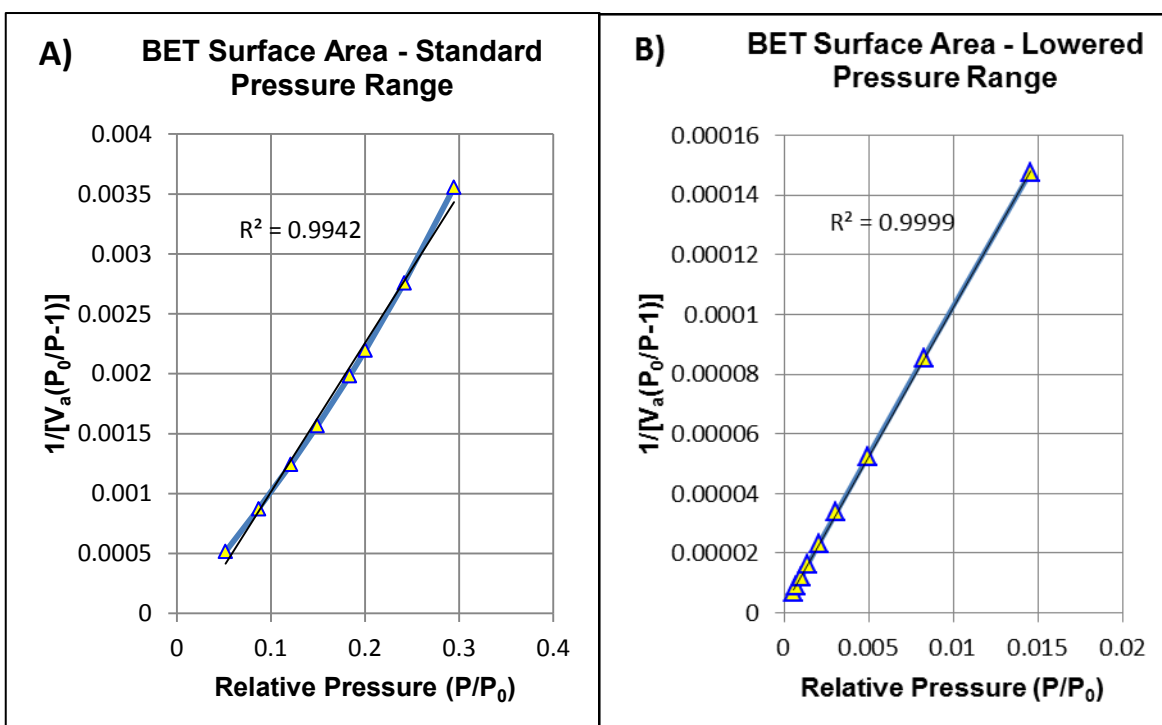
Figure 3.8. BET surface area plots for zeolite particles using a) the standard pressure range of $0.05 < P/P_0 < 0.3$ b) the pressure range determined by Rouquerol *et al.* criteria which was found to be $0.0005 < P/P_0 < 0.015$

3.4 Theoretical Maximum Adsorption Calculations of Test Compounds

The area of surface occupied by an adsorbed molecule must be determined before the theoretical maximum adsorption can be calculated. This value is different for each test compound and is calculated using Equation 3.2.

58

$$A_m = f \left(\frac{M}{\rho N}\right)^{\frac{2}{3}} \times 10^{16}$$

Where

A_m = area of surface occupied by an adsorbed test compound molecule (Å^2)

f = packing factor (1.091 is used which assumes a spherical shape for the

molecule)

M = molecular mass of the test compound molecule of interest (g/mol)

ρ = density of the test compound in the state used (vapor) (g/cm^3)

N = Avogadro's number (mol^{-1})

Physical constants for each test compound were previously listed in Table 2.4 in Section

2.9.1 and were used to calculate A_m. The final value for each test compound is

presented in Table 3.3.

Compound	A_m (Å2/molecule)
Isopropanol	27.58
Diisopropyl Ketone	41.53
Methyl Isobutyl Ketone	38.22
Diphenyl Chlorophosphate	53.74

Table 3.3. Calculated area occupied by an adsorbed test compound

The theoretical maximum adsorption is calculated in two parts. First the maximum

mass of gas that can be adsorbed per mass of sample present must be calculated for

each sample using Equation 3.3.

$$\frac{g \ of \ gas}{g \ of \ sample} = \frac{SA_s M}{N(A_m \times 10^{-20})}$$

Equation 3.3. Part one of theoretical maximum adsorption calculation

Where

SA_s = surface area of the sample being tested (m^2/g)

M = molecular mass of the test compound (g/mol)

N = Avogadro's number (mol^{-1})

A_m = area of surface occupied by an adsorbed test compound molecule (Å^2)

The calculated theoretical maximum mass of each test compound that could be adsorbed per mass of zeolite or mPS particle is listed in Table 3.4.

Compound	Zeolite Particle (g/g)	mPS Particle (g/g)
Isopropanol	0.158	0.038
Diisopropyl Ketone	0.199	0.047
Methyl Isobutyl Ketone	0.190	0.045
Diphenyl Chlorophosphate	0.363	0.086

Table 3.4. Theoretical maximum mass of each test compound per mass of particle present

The values in Table 3.4 can then be multiplied by the sample mass of the tested sample to determine the theoretical maximum adsorption for that particular sample. This calculation was performed for samples examined with static testing method.

4   Results and Discussion: Development of Composite Structure

Textile composites developed during this project were ultimately intended to be used as a wearable protective garment; therefore many design considerations must be taken into account. According to Scott well designed protective clothing must have the following properties:[3]

- Meet functional requirements (hazard dependent)

- Appropriate for task and aesthetically pleasing

- Fit for purpose, durable and performs to or exceeds required standards

- Acceptable to both the user and the client with respect to culture, traditions, specifications, manufacturing and costs.

Functional requirements are directly dependent on the end use of the garment and the hazard they will be used to protect the wearer from (chemical, biological, physical/mechanical, radiological, flame, or thermal). Aesthetic elements such as color, appearance, size, handle, touch, fit, and comfort must be found acceptable to the user or the protective clothing may not be used. In addition basic garment requirements must be met such as flexibility, strength, durability, and water vapor permeability in conjunction with structural uniformity. Since protective clothing falls under governmental regulations in developed countries, materials must also meet requirements mandated by standards and safety regulations issued by the respective

61

agency such as the US Department of Labor, Occupational Safety and Health

Administration for Occupational Safety and Health Standards.

4.1   Design Rationale

The composite was designed such that two different functional layers (sorptive and flow

restrictive layers) could be assembled into chemical protective clothing (CPC) in order to

provide protection for the wearer. The sorptive functional layer was comprised of a C-

CP^{TM} nonwoven fabric loaded with particles that can adsorb/absorb toxic compounds.

The flow restrictive functional layer was included in order to increase the residence time

for gas molecules to interact with the adsorptive particles. The flow restrictive layer

used was a PP 'nanofiber' meltblown nonwoven and was utilized because meltblown

micro/nanofibers materials have much smaller pore sizes compared to nonwovens,

wovens and knitted fabrics made from conventional melt spun fibers. Therefore longer

residence times can be expected once such materials are incorporated into textile

composites. In order for these layers to work as one cohesive material that does not

delaminate, a binder was required.   The binder served to bind the functional layers to

the outer layers of the garment. The first generation layering arrangement for the

composite was as follows in Figure 4.1.

Outer Layer
Binder
Sorptive Functional Layer
Binder
Flow Restrictive Functional Layer
Binder
Outer Layer
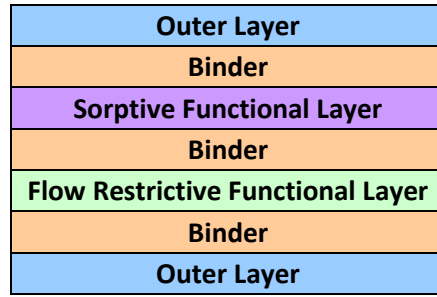
Figure 4.1. Layering arrangement for the first generation composite structure

4.2   Functionality

The sorptive functional layer was made of poly(ethylene terephthalate) (PET) CCP^{TM}

fibers. PET was chosen because it is extensively used in the textile industry due to its

tractability, good inherent chemical stability and tunable physical/mechanical properties

depending on the chosen manufacturing process parameters (e.g. IV, fiber spinning

variables, heat treatments and heat setting). C-CP^{TM} fibers (Figure 4.2) were chosen to

produce the nonwoven (as described in Section 2.4) because the material would have

several inherent advantages over traditional round cross-sectional fibers. These include:

1. The ability to load and retain absorbing species into the grooves of the

     fibers;

2. Increased surface area of ~2.3-2.8 times that of a round fiber cross-

     section of the same denier;[89]

3. The ability to spontaneously wick fluids which allows the material to

     move the threatening compound away from the body;[89]

4. The ability to provide increased rubfastness for the particles due to

     loading into the grooves of the fiber.

63
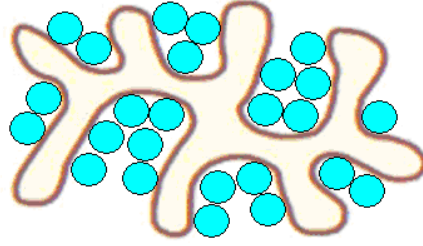
Figure 4.2. Schematic of C-CP^{TM} fiber cross-section loaded with particles

4.2.1 Sorptive Functional Layer: Characterization of C-CP™ Fibers

Fibers were made to ensure the dimensions of the C-CP^{TM} fiber grooves were large enough to accommodate the zeolite and mPS particles. The width of the groove entrances and bases, as well as the depths of the groove, were measured on individually mounted fibers and these results are tabulated in Table 4.1. The average width of the groove entrance for the smallest fiber used was 6.8 μm ± 2 μm with the base being 5.4 μm ± 2.2 μm and the depth of the groove being 7.1 μm ± 2.7 μm. The average particle size reported in Section 3.1 of the mPS particles was 0.357 μm ± 0.169 μm and for the zeolite particles it was 0.426 μm ± 0.186 μm. While it is known that the particles will agglomerate, the measurements show that the grooves are sufficiently large enough to accommodate individual particles of either type.

	End-to-end				Groove Entrance			
	3dpf	6dpf	15dpf	30dpf	3dpf	6dpf	15dpf	30dpf
Max (μm)	38.2	49.5	99.1	163.4	13.2	16.3	38.0	36.0
Min (μm)	29.6	32.4	64.5	110.1	2.9	4.2	8.3	22.3
Average (μm)	32.9	39.2	78.6	139.1	6.8	9.5	17.1	27.7
Standard Deviation (μm)	2.2	4.2	9.1	12.2	2.0	2.5	4.8	4.1

	Groove Base				Groove Depth			
	3dpf	6dpf	15dpf	30dpf	3dpf	6dpf	15dpf	30dpf
Max (μm)	10.2	15.8	29.2	36.2	13.9	17.7	26.6	58.8
Min (μm)	2.2	2.9	5.3	19.8	2.7	3.4	4.6	15.1
Average (μm)	5.4	7.4	11.9	26.3	7.1	9.0	14.5	33.0
Standard Deviation (μm)	2.2	3.1	6.0	5.3	2.7	3.5	6.4	13.7

Table 4.1. Tip-to-tip, groove entrance, groove base, and groove depth measurements for 3, 6, 15, and 30 dpf C-CP[TM] PET fiber cross-sections

It should be noted that these measurements could vary once the fibers are placed into a nonwoven structure. When the fibers were measured they had little to no interaction with other fibers (Figure 4.3). However as they are processed and made into a nonwoven material the fibers can be mechanically twisted, compressed or flattened (due to thermal bonding for example) or groove availability can be altered due to fiber interlocking (Figure 4.4).
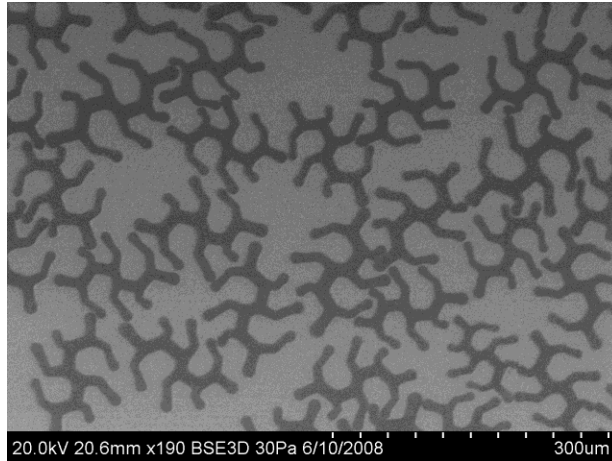
Figure 4.3. SEM image of 30 dpf C-CP^{TM} PP fiber cross section 190X magnification and scale bar of 300μm
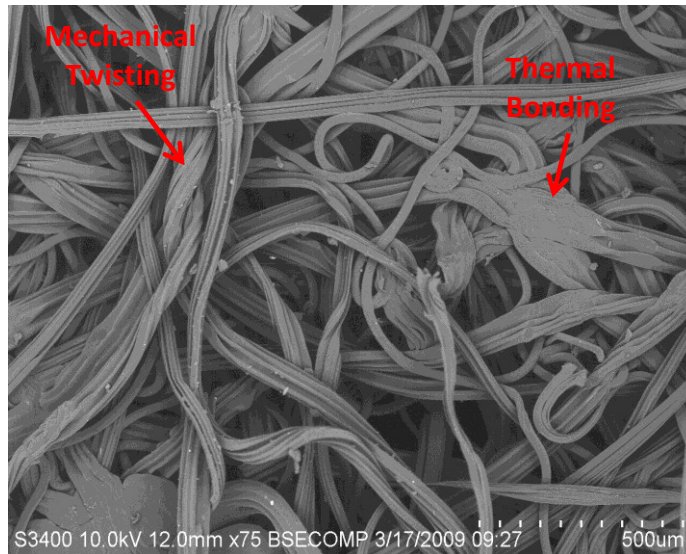
Figure 4.4. SEM image of a 3 layer mixed dpf C-CP^{TM} PET nonwoven 75X magnification and scale bar of 500μm

4.2.2 Sorptive Functional Layer: Production of C-CP™ Nonwovens

Having ensured the grooves were of a suitable size for the particles, the evenness of the

nonwoven web had to be addressed. It was noted that the webs produced by carding

were inconsistent, having dense and sparse areas of fiber coverage (Figure 4.5 a). This

66

posed a significant problem as it would make even particle dispersal in the composite impossible.

Cards were originally built to process natural fibers, such as cotton and wool, which inherently have bulk or crimp enabling them to entangle themselves more easily within the combs of the card and form a consistent web. The fibers used for making the primary functional nonwoven layer lacked any such texture and therefore a significant amount fell out during the carding process. The webs obtained were not only uneven but also contained an unknown ratio of fiber as a result of the fiber loss during production. An initial solution to this problem was to layer 3 webs of the nonwoven together. Since the unevenness of the web was random, layering several nonwovens would increase the overall evenness and then all layers would be bonded together using the calendar. The calendar consists of two heated metal rolls that are pressurized and as the nonwoven passes between them the combination of heat and pressure (100°C and 25 kPa/cm) causes the binder fibers to melt and the shaped fibers to soften (T_g of PET C-CP^{TM} fibers ~80°C) resulting in a thermally bonded material.

In order to reduce fiber loss during nonwoven production, a new piece of fiber crimping instrumentation was obtained, i.e. a TechTex 1 Threadline crimper. The Threadline crimper was used to place crimp in the fibers prior to nonwoven production (~19 crimps per inch). The resulting nonwoven webs were significantly more even (Figure 4.5 b) and the fiber fall out was dramatically reduced. This also ensured that the final percentage

67

of fiber type present in the end product was close to the input percentage. Thus

improvements in C-CP^{TM} PET nonwoven uniformity were achieved by a) improving the

uniformity of each layer due to fiber crimping and b) by bonding three layers of the

crimped fiber nonwoven together via the calendar.
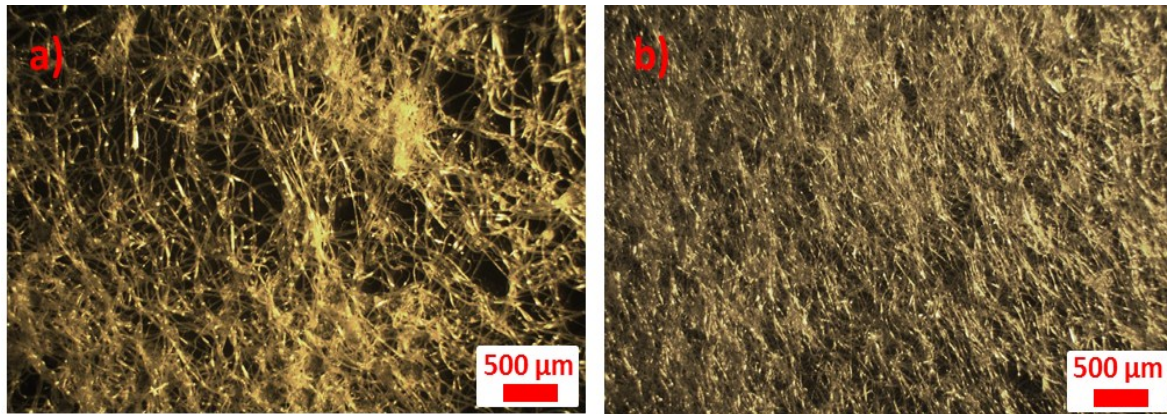
Figure 4.5. Optical images of mixed dpf C-CP^{TM} PET nonwoven with a) un-crimped fibers b) crimped fibers

4.2.3   Flow Restrictive Functional Layer: PP Meltblown Nonwoven

The secondary functional layer was a meltblown PP nonwoven made by Hills, Inc., which

was added to the composite design due to the small fiber diameters (Figure 4.6) which

range from 0.05 μm to 5.7 μm with an average of 0.67 μm. The meltblowing process

allows for the formation of small fiber diameters due to the polymer melt being

extruded through a nozzle directly into high velocity (6,000 to 30,000 m/min) hot air

which draws the fiber immediately. Below the nozzle air turbulence causes the fiber to

cool and form a web on the moving belt located directly below the nozzle.[21]

68
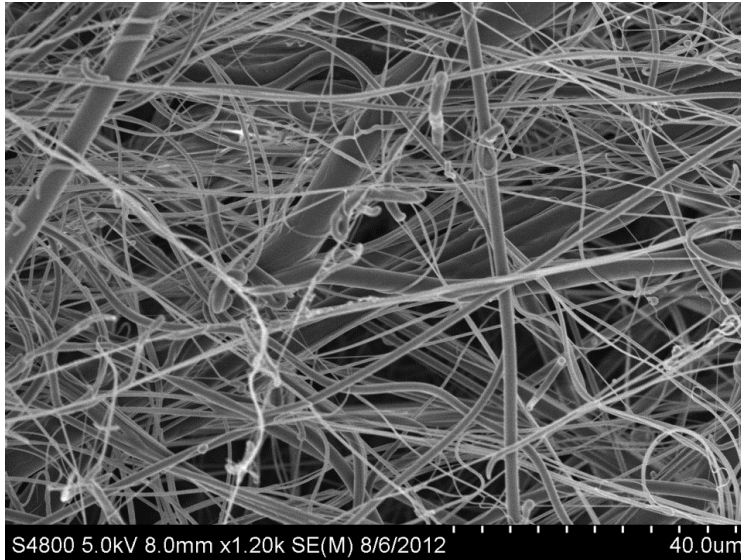
Figure 4.6. SEM image of Hills, Inc PP meltblown nonwoven 1.2kX magnification with 40μm scale bar

In addition to the increased surface area due to small fiber diameters, the structure of

the meltblown provided small pore sizes (6.6-34 μm) which helped to increase residence

time of the gas molecules within the composite structure. The meltblown nonwoven

used for this research was produced by Hills, Inc. under the processing conditions listed

in Table 4.2.

Meltblown PP Processing Conditions
Throughput: 0.0046 g/hole/min
Run speed: 3.5 mpm
Forming table distance: 8 in
Air heat: set @ 263°C
Extrusion temp: 230°C
Basis Weight: 6 g/m2

Table 4.2. Processing conditions for meltblown PP nonwoven

4.2.4   Thermal Bonding Techniques: Point Bonded Roll vs Flat Roll

As stated in Section 4.2.2 the sorptive functional layer of the first generation composite

consisted of three layers of mixed dpf C-CP^{TM} PET nonwovens. A layer of meltblown PP

was added within the mixed dpf C-CP™ PET nonwoven layers to act as a barrier in order to reduce the amount of particles lost during spraying (discussed further in Section 5.1.1). For this construction to be handled and sprayed all of the layers were bonded together using a calendar (20" Benz Thermal Bonding Calendar).

The calendar used had two different top rolls; a roll with a smooth surface (flat roll) or one with evenly spaced raised points (point bonding roll). The first would provide bonding across the width of the fabric where binder fibers were present; the second option would bond the binder fibers at the contact points and thus produce a point bonded fabric. One concern with the smooth roll was that it could possibly flatten the grooves of the C-CP™ fibers which would in turn decrease their particle loading capacity.

In order to determine the best bonding method for the sorptive functional layer samples were prepared using both rolls. The layering arrangement of the samples is shown in Figure 4.7, both were calendared at the same temperature (100°C) and speed (5.2 ft/min) however the pressure used for the flat roll was slightly higher in order to obtain sufficient bonding in the sample (1524 kPa compared to 1270 kPa). Samples were placed through the calendar with the double layer of mixed dpf C-CP™ facing the top roll.

2 Layer Mixed dpf C-CP™
Melt blown
1 Layer Mixed dpf C-CP™

Figure 4.7. Schematic of the layering arrangement of the sorptive functional layer with the addition of the meltblown nonwoven

After calendaring, the samples were examined using both optical and scanning electron

microscopy, Figure 4.8 to Figure 4.12. The optical image clearly showed that the point

bonding calendar roll punched holes through the meltblown layer (Figure 4.8).   When

examined further using SEM, bonding points were seen as areas where the fiber had

been melted and the grooves had been deformed (Figure 4.9).
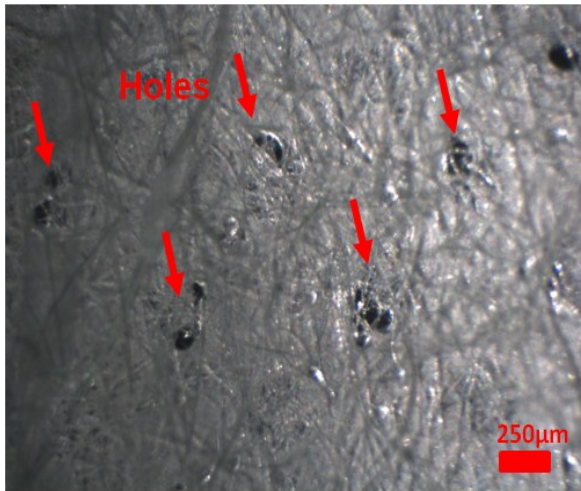
Figure 4.8. Optical image of the sorptive functional layer thermally bonded with the point bonded calendar roll at a magnification of 40X
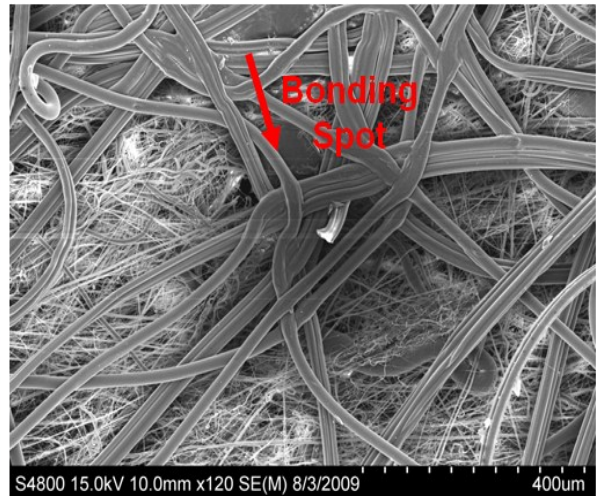
Figure 4.9. SEM image of the sorptive functional layer thermally bonded with the point bonded calendar roll at a magnification of 120X

The optical image of the sorptive functional layer bonded with the flat roll showed

melted bonding areas but no holes, Figure 4.10. The SEM images (Figure 4.11 and

Figure 4.12) of the same sample showed, in addition to the melted spots, that many

more of the fibers appeared to have been flattened by the combined effect of heat, pressure and the smooth surface of the roll. This flattening was detrimental to the final product as it may reduce the groove depth or completely obliterate the grooves which were essential for particle loading.
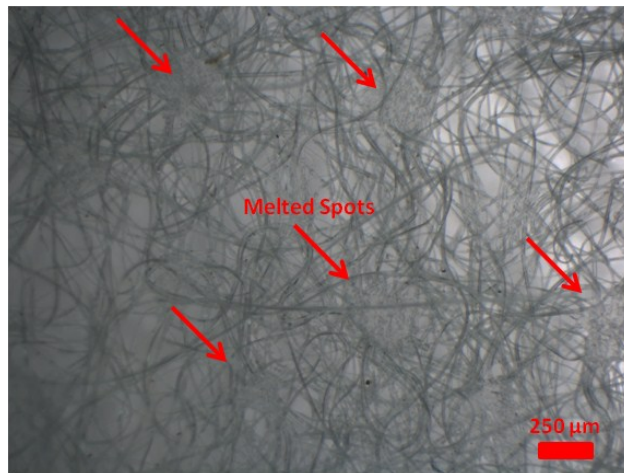
Figure 4.10. Optical image of the sorptive functional layer thermally bonded with the flat calendar roll at a magnification of 40X
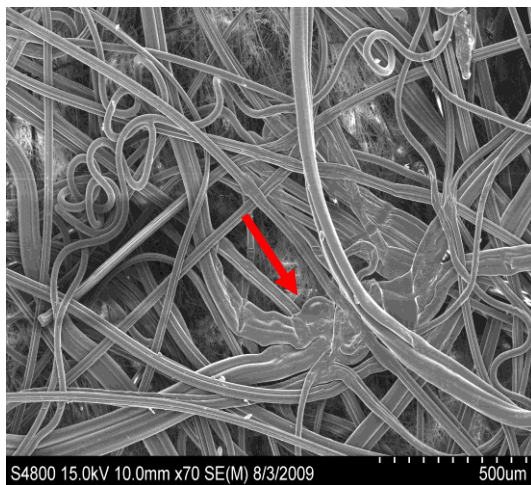
Figure 4.11. SEM image of the sorptive functional layer thermally bonded with the flat calendar roll at a magnification of 70X
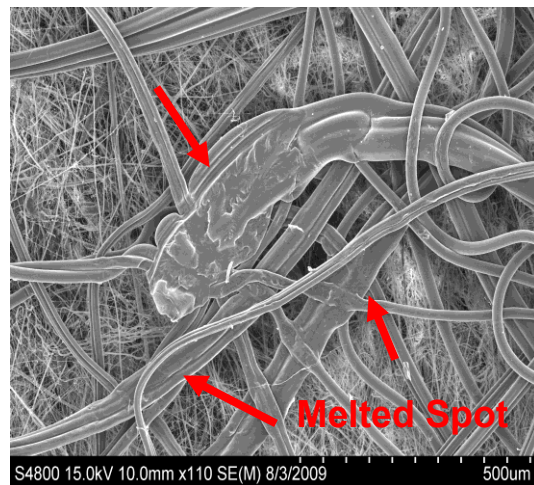
Figure 4.12. SEM image of the sorptive functional layer thermally bonded with the flat calendar roll at a magnification of roll 110X

Since the flat calendar roll reduced or eliminated access to a significant number of the grooves it was determined that its use was not optimal for thermally bonding the sorptive functional layer. In addition it was noted the meltblown nonwoven used within this layer would have holes in it and therefore could not serve as the flow restrictive functional layer. In the final composite (discussed in Section 4.5) additional meltblown layers were placed to either side of the sorptive functional layer to serve as the flow restrictive functional layer. However there was still concern that calendaring would cause hole formation in these additional meltblown layers. To determine if this would be a problem, samples were made of a final composite calendared together with the flat roll and one with the point bonded roll and tested by an outside laboratory. The results indicated that the type of roll used on the final composite had no effect on the ability of the material to pass testing conditions. Therefore the point bonded roll was used for all thermal bonding processes.

4.3   Material Properties

One of the most important properties of a composite used within a garment is flexibility while preventing rupture of any interior functional layers. For the current research, the flow restrictive functional layer was of greatest concern. It was suspected that the layer having the greatest impact on flexibility would be the binder. A binder is defined as a thermoplastic which is melted to bond fibers together in a web or to bind one web to another.[19] The initial binder material used was a meltblown polyamide made by

73

Freudenberg, Vilene ZG902, which had a basis weight of 10.3 g/m^2 and a melting point of 82°C (as compared to a melting point of 156°C for the meltblown PP).

Due to its delicate nature it was thought the meltblown PP component would be the limiting factor in terms of overall strength of the composite. Ideally the layers shown in Figure 4.1, which surround the meltblown PP, would provide enough support to prevent a breach from occurring while the garment was being worn. In addition the composite should be designed to minimize the number of layers without risking structural failure when donned as a garment. If the composite could withstand a 22.5 lb load, which is the theoretical load placed on a fabric due to the bending of an elbow or knee, before a breach in the meltblown layer then the composite would be able to sufficiently protect the flow restrictive layer.[90] Therefore the strength of the composite and each of its components were determined as well as the extension at which an initial breach occurs in the meltblown PP layer. The composite sample tested was fabricated following the layering schematic shown in Figure 4.1 with Freudenberg as the binder. The composite, as well as the individual components, were tested according to ASTM D 5034 the Standard Test Method for Breaking Strength and Elongation of Textile Fabrics (Grab Test) and the average results are presented in Figure 4.13 and Figure 4.14.
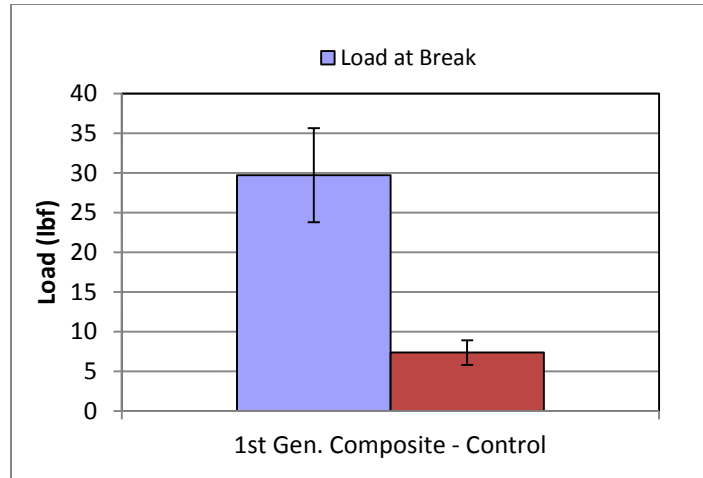
Figure 4.13. Average load at break and average load at initial breach of the meltblown PP layer of the 1st generation control composite
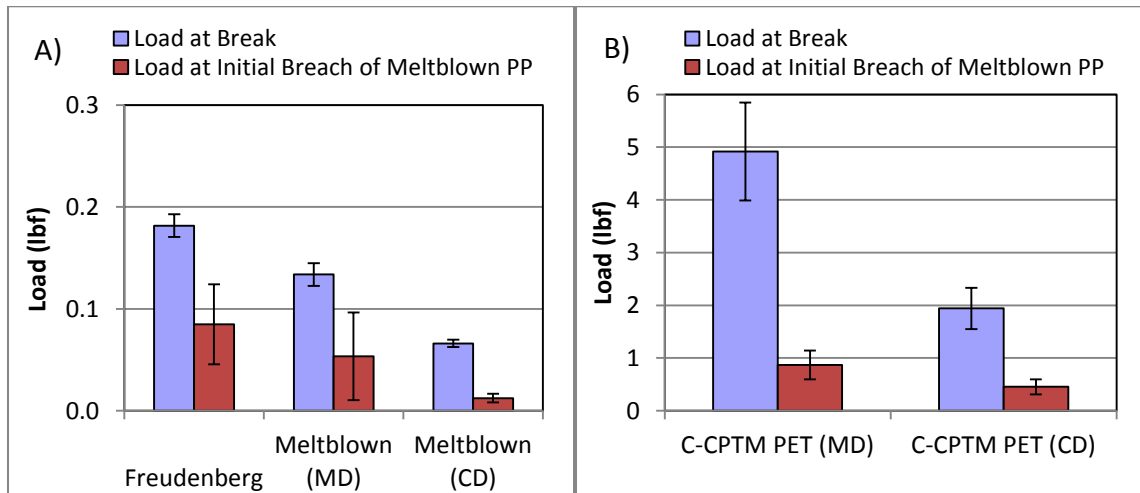
Figure 4.14. Average load at break and average load at initial breach of the meltblown PP layer for A) Freudenberg (the binder) and the meltblown PP nonwoven and B) 3 layers of the carded C-CP^{TM} PET nonwoven of the 1st generation composite (Note: Scales vary between A and B)

The control composite sample (Figure 4.13) had a load at break of 29.7 lbf ± 5.9 lbf

which is comparable to that of Kleenguard A40, 30.6 lbf, and Tyvek, 24 lbf, both of

which are commercially available nonwoven composites used as protective garments.[26]

The results for the individual layers (Figure 4.14 A and B) show that the meltblown

nonwoven (Figure 4.14 A) was indeed the most delicate layer present in the composite

with a load at break of 0.13 lbf and 0.07 lbf in the machine (MD) and cross directions (CD), respectively. With this confirmation the raw data was re-examined to determine the extension at which an initial breach occurred in the meltblown. An initial breach was indicated by the first decrease in load on the plot of extension vs. load.   The sample had an initial gauge length of 3 inches and a cross-head speed of 3 in/min. The initial breach occurred in the meltblown nonwoven at 1.37 mm (1.8% elongation). Therefore the composite must not extend more than 1.37 mm at a load of 22.5 lbf in order to properly protect the meltblown nonwoven during wear.

The data from the other samples was then examined to determine the load each could withstand at an extension of 1.37 mm, shown in red on Figure 4.13 and Figure 4.14. As expected the load at 1.37 mm was lower than the load at break for all samples. At this extension (1.8%) the composite was able to withstand a load of 7.4 lbf ± 1.5 lbf which did not meet the garment requirements.

4.3.1   Approach to Improve Material Properties

Since the 1st generation composite structure did not provide sufficient protection for the flow restrictive layer, the use of a different binder, modifications to a current layer or inclusion of an extra layer (such as a support layer) would be needed. In addition, due to its delicate nature a second layer of meltblown PP was placed within the composite structure to serve as a failsafe in case a breach occurred in one of the flow restrictive layers.

76

4.3.1.1 Carded Nonwoven Binder

A new approach was taken in an attempt to find another binder layer. Three carded

nonwovens were made consisting of high percentages (>20 % by weight) of a 3dpf low

melting point polyester binder fiber (binder) and a 3dpf round PET fiber (matrix). The

three ratios used for the binder/matrix carded webs were 80/20, 50/50, and 20/80 (by

weight). In addition two different basis weights were made, a light and heavy (7-12

g/m^2 and 20-35 g/m^2, respectively). The binder and matrix fibers were weighed out,

hand mixed and then placed into a CMC Rando for further mechanical opening and

mixing. Nonwovens were produced using a 20" Proctor & Schwartz Roll-Top Card.

The new binder layers were placed into composites (Figure 4.15) using the same

layering arrangement with only the binder changing for each sample. Samples were

thermally bonded using a calendar (100°C, 5.2 ft/min and 1524 PSI) and tensile

properties were determined according to ASTM D 5034 (Grab Test). The raw data from

each test was evaluated to establish the load withstood by each sample at an extension

of 1.37 mm, which corresponds to the initial breach of the meltblown layer.

Outer Layer
Binder
Sorptive Functional Layer
Binder
Flow Restrictive Functional Layer
Binder
Outer Layer
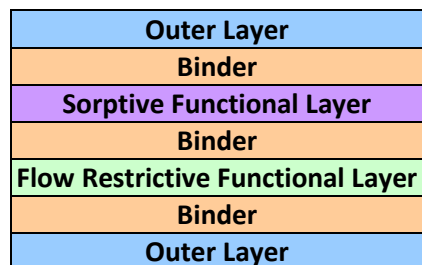
Figure 4.15. Schematic of the layering arrangement used for composites with trial binders

77

It was expected that as the percent of binder increased there would be greater adhesion between layers which would cause the load withstood at 1.37 mm to increase. However, Samples 2-6 in Figure 4.16 all have similar average loads from 3.2-4.3 lbf with varying percent's of binder. Only Sample 7, containing the 80/20 heavy binder, had a significantly different average load, 7.7 lbf, which was slightly greater than that of the control, 7.4 lbf. The basis weight of the 80/20 binder was three times that of the Fruedenberg and performed at the same level, which was not sufficient. Therefore the Fruedenberg was used as the binder for all future samples.
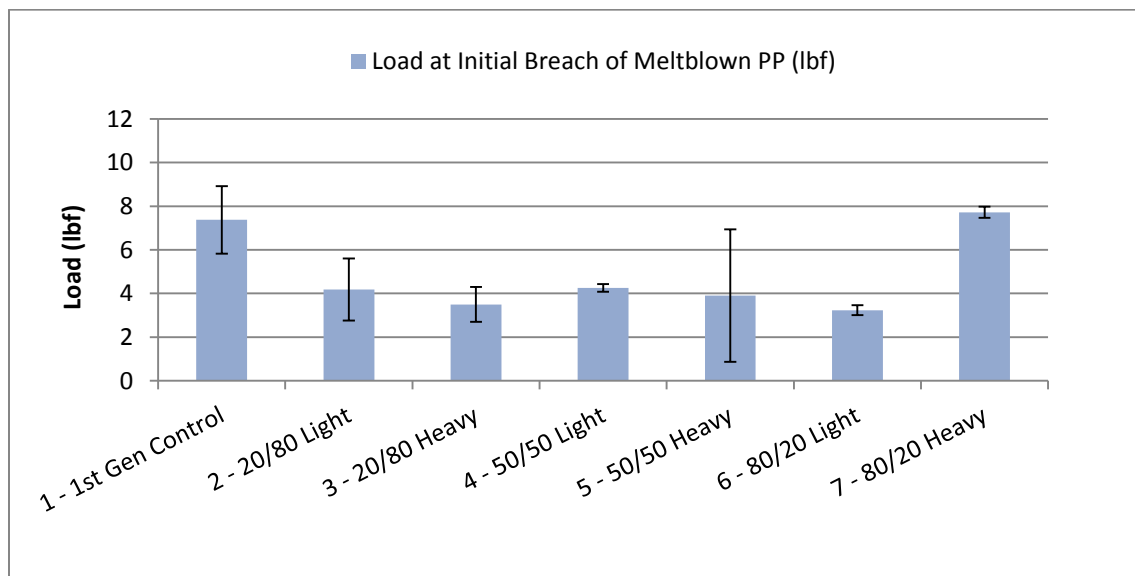
Figure 4.16. Average load at 1.37mm elongation for control and binder/matrix samples

4.3.1.2 Freudenberg Modifications

Since all of the alternative binders investigated failed to withstand 22.5lbf at 1.8% elongation, a support layer was be required in the composite structure. The addition of a support layer would necessitate more layers of Freudenberg. It was suspected that extra binder layers would result in increased stiffness and weight of the composite.

78

Therefore, modifications to the Freudenberg layer were examined to determine if the structure could be altered to obtain an intermittent binding. Two approaches were undertaken in an effort to produce a grid like binding system from the original Freudenberg utilizing 1) a point bonding calendar roll and a 2) a 12" hydro-entanglement water jet system.

In the first case a single layer of Freudenberg was placed between two sheets of Teflon coated material and passed through the calendar, fitted with the point bond roll, at temperatures in the range of 75-85°C and pressures of 762-1524 kPa. It was thought that the bonding roll points would place holes in the Freudenberg at precise intervals forming a grid pattern. The presence of holes would reduce the binding between layers and make the composite more flexible. However, the resulting samples did not show consistent pattern formation (Figure 4.17) and holes were not actually formed in the Freudenberg. The temperatures used for point bonding were close to the melting point of the Fruedenberg (82°C) and as the sample was heated it melted and flowed to form a very thin film instead of being mechanically removed to form a hole.
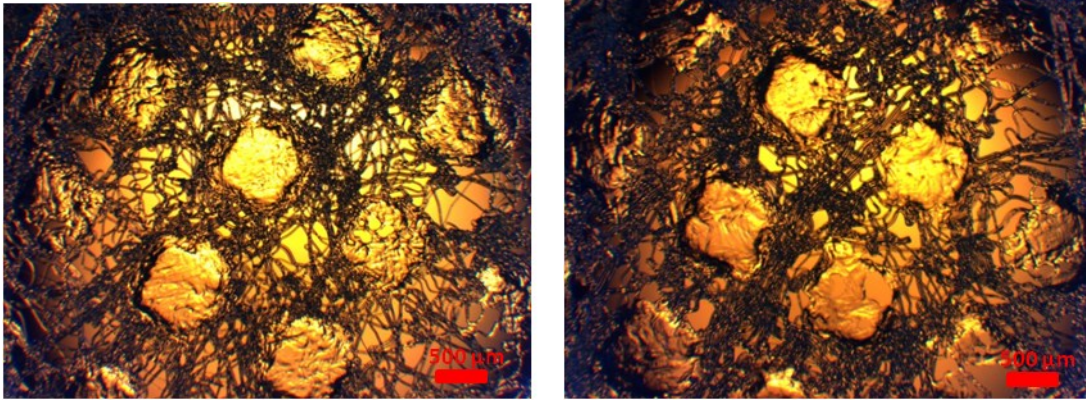
Figure 4.17. Optical images of Freudenberg samples calendered at 80°C and 1524 kPa (left) and calendered at 85°C and 1270 kPa (right)

In the second method, a single layer of Freudenberg was run through the water jet system starting with a pressure of 100 psi which was increased incrementally up to 800 psi, 8 total samples were made. This system is commonly used for hydroentangling nonwovens and in this case it was thought that the pressure of the water jet could cause a disruption of the Freudenberg nonwoven structure.

After the samples were run through the water jet, each was examined optically. It was found that regardless of pressure, the water jet did not produce any changes in Freudenberg nonwoven. These results clearly demonstrated that the modification of the Freudenberg was not a suitable approach to obtain the desired characteristics of mass reduction and intermittent adhesion and that its use was limited to an adhesive layer in the manner in which it was supplied.

4.3.1.3   Composite with Support Layer
It was clear that trying to solve the problem posed by the meltblown layer using only the binder would not work. Hence structural supports were investigated that could be

included in the composite to prevent breach of the flow restrictive layer in the 2nd generation composite. The concept of a scrim like material was desirable because it was expected to have least impact on the stiffness of the final composite. Samples of two extruded nets were obtained from DelStar Technologies, Inc. and two lightweight woven fabrics were obtained from BGF Industries, a lightweight woven Kevlar® fabric and a lightweight woven fiberglass fabric. All samples were constructed using the same layering arrangement as in Figure 4.18. The support layer was changed for each sample as shown in Table 4.3. In all cases the binder incorporated was the Freudenberg meltblown material and layered composites were thermally bonded using a calendar (100°C, 5.2 ft/min and 1524 PSI).

| Outer Layer |
| Binder |
| Secondary Functional Layer |
| Binder |
| Primary Functional Layer |
| Binder |
| Secondary Functional Layer |
| Binder |
| Support Layer |
| Binder |
| Outer Layer |
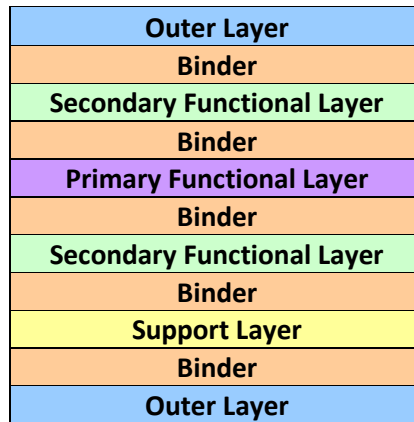
Figure 4.18. Schematic of the layering arrangement used for 2nd generation composites with trial support layers

Sample ID	Support Layer	Basis Weight
8	None	N/A
9	Fiberglass	20 g/m^2
10	Lightweight Woven Kevlar®	60 g/m^2
11	Nylon 14936 Extruded Net	155 g/m^2
12	PP 14526 Extruded Net	65 g/m^2

Table 4.3. Description of support layer and associated basis weight used in composites

81

The tensile properties of each sample were determined according to ASTM D 5034 (Grab Test). The raw data was evaluated to establish the load withstood by each composite at an extension of 1.37 mm, which corresponds to the initial breach of the meltblown layer.

An increase in strength was noted for the 2nd generation control composite (Sample 8), Figure 4.19, due to the addition of a binder layer and flow restrictive layer, but it was still not sufficient for the garment requirements. Three of the five samples (Samples 9-10 and 12), however, did meet the required load of 22.5lbf at an elongation of 1.8% (Figure 4.19).

As expected the samples containing fiberglass and Kevlar® as support layers were able to withstand the highest load, 80.8 lbf ± 18.1 lbf and 233.8 lbf ± 40.6 lbf in the machine direction respectively. Both extruded net samples had a sufficient average load in the machine direction, 37.5 lbf ± 0.5 lbf and 25.1 lbf ± 3.8 for Samples 11 and 12, respectively, but Sample 11 did not meet requirements in the cross machine direction. While the average load in the cross machine direction was greater than 22.5lbf for Sample 12 (extruded PP net) there were issues with delamination due to poor binding between the extruded net and the Freudenberg. Therefore the PP extruded net was eliminated as an option for the support layer leaving just the fiberglass and Kevlar® fabrics as feasible support layers.
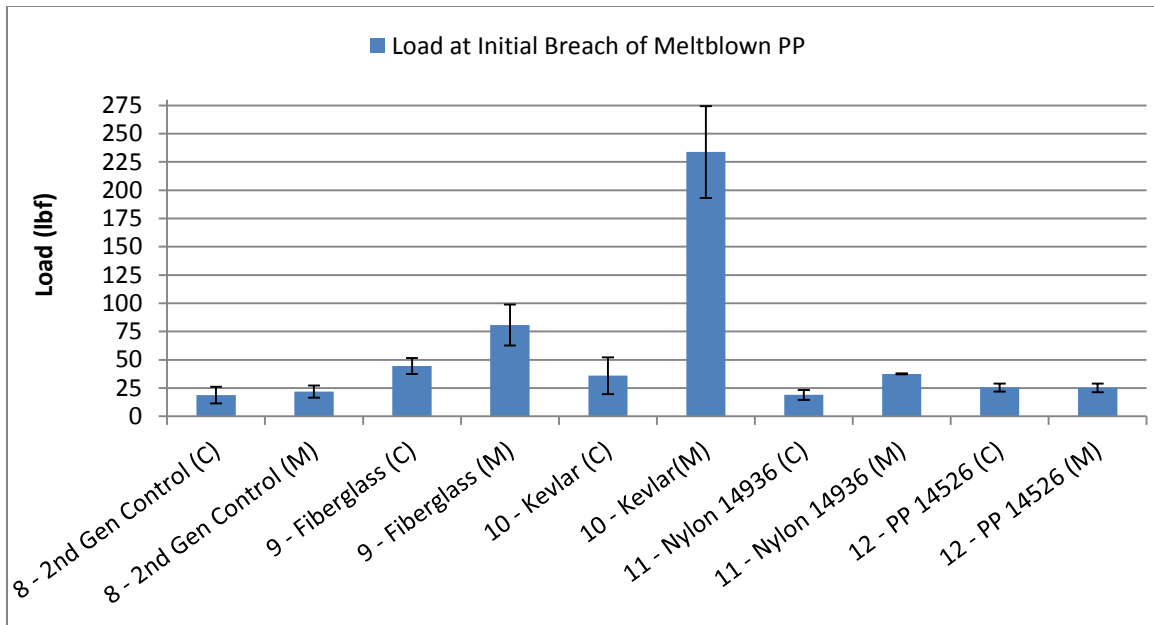
Figure 4.19. Average load at 1.37mm extension for trial support layer samples in both machine (M) and cross-machine (C) directions

Bias direction testing was also carried out to ensure that all directions could withstand the desired load of 22.5 lbf at an extension of 1.37 mm. At this extension the fiberglass sample had an average load of 25.44 lbf ± 9.58 lbf and the Kevlar® sample had an average of 29.68 lbf ± 6.29 lbf, both of which met the criteria. While both samples were sufficient, the woven fiberglass fabric was utilized due to the basis weight of 20 g/m^2, a third less than that of the lightweight woven Kevlar®.

4.3.2 Air Permeability

As structural modifications were made to the composite, the resulting effects on the air permeability of the material were investigated. Air permeability is an important property of the composite in its end use (i.e. protective clothing) and researchers have used it as both an indication of thermal comfort and to predict protection

performance.[17, 18, 29] As might be expected they found an inverse relationship between air permeability and chemical protection performance.

The samples containing the alternative binders (no Freudenberg) from Section 4.3.1.1 and those containing the trial support layers (containing Freudenberg binder) from Section 4.3.1.3 were tested using an Air Permeability Tester as described in Section 2.5.2. For the binder/matrix composites (which consisted of a 3dpf low melting point polyester binder fiber and a 3dpf round PET fiber) it was expected that as the percent binder increased the air permeability would decrease due to greater bonding throughout the composite structure. This trend was observed for all but Sample 2 which contained the 20/80 light binder (Figure 4.20). While the average air permeability for Sample 2 did not follow the expected trend, the results obtained were not significantly different from those for 20/80 heavy, 50/50 light or 50/50 heavy.
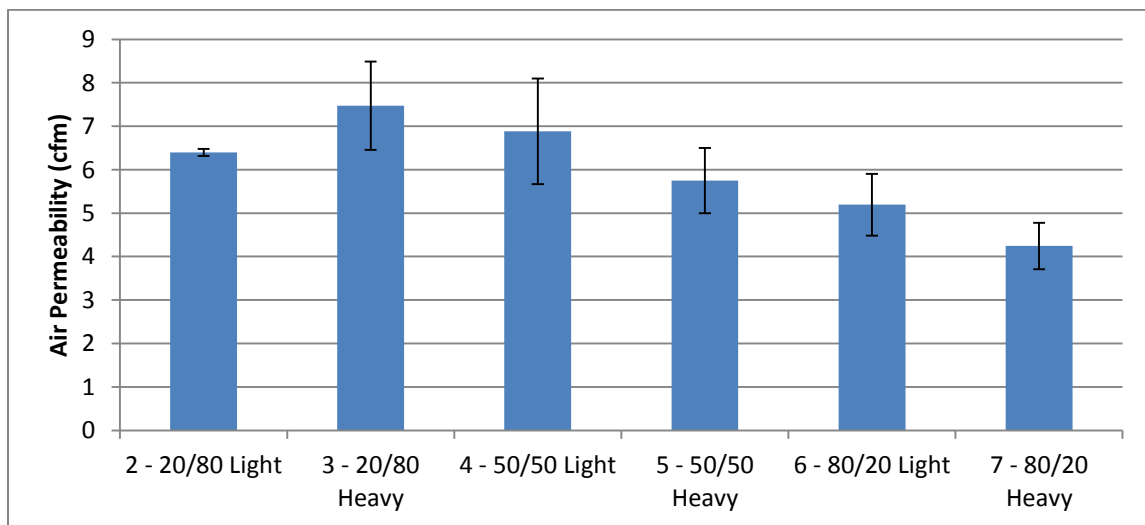
Figure 4.20. Air permeability results for binder/matrix composite samples

All samples containing Freudenberg as the binder (Figure 4.21) had a significantly lower air permeability as compared to the binder/matrix samples (0.7-2.9 cfm/ft^2 as compared to 4.2-7.5 cfm/ft^2). It is thought that the Freudenberg binder becomes 'film' like after thermal bonding within the composite due to its low melting point (82°C) and the combination of temperature and pressure (100°C and 1524 PSI) used for calendaring. This, however, could not be confirmed visually due to the inability to deconstruct the composite. While the Freudenberg provides excellent binding throughout the sample it also causes a decrease in the air permeability of the composite material. This was further confirmed by testing a duplicate of Sample 9 that was not thermally bonded together. The resulting air permeability was 37.6 ± 1 cfm/ft^2.

Samples 11 and 12, which contained the extruded nets, had significantly higher air permeability than the other composite containing Freudenberg (2.3-2.9 cfm/ft^2 as compared to 0.7-0.9 cfm/ft^2) due to the structure of the extruded net. Both extruded nets were thicker and stiffer than either of the woven supports used in Samples 9 and 10 and because of these properties bonding between the extruded net and the Freudenberg was insufficient. This disruption in the composite structure allowed for an increase in air permeability.
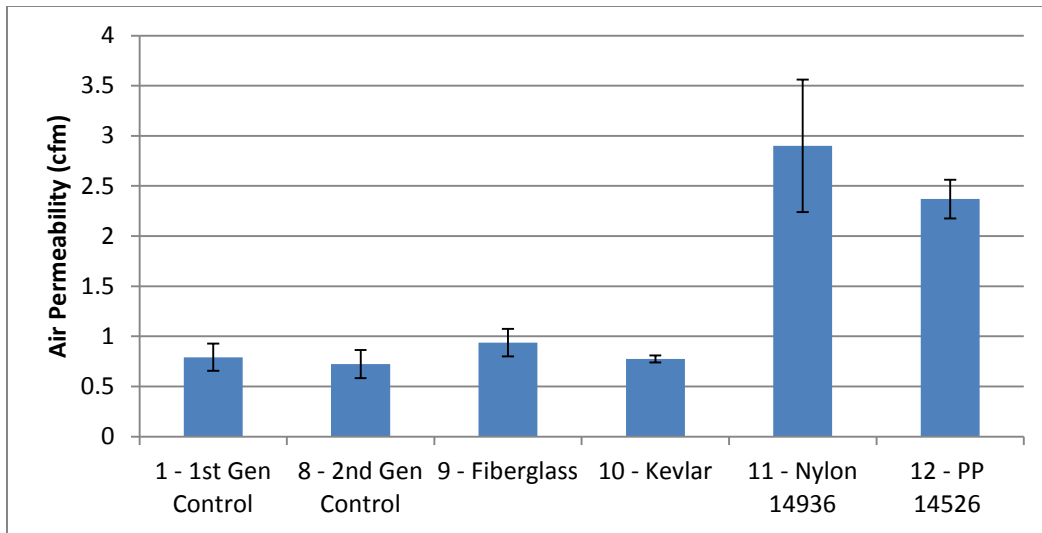
Figure 4.21. Air Permeability of control composites and composites containing trial support layers

While a range of air permeabilities were observed, most materials used for protective clothing have an air permeability of 0 to 197 cfm/ft^2.[29] The average air permeability was 4.2-7.5 cfm/ft^2 for the binder matrix samples, 2.3-2.9 cfm/ft^2 for the extruded net sample and 0.7-2.9 cfm/ft^2 for the control composites and woven support composites. All of which fall within the commonly accepted range for material used in protective clothing applications.

4.3.3 Pore Size Measurements

The samples containing the alternative binders (no Freudenberg), Section 4.3.1.1, were also examined using a Capillary Flow Porometer (CFP), as described in Section 2.5.3, to determine pore sizes. The instrument elicits pore size information from two measurements (through a wetted sample and a dry sample) of flow rate and the corresponding pressure difference across the sample. A wetting agent (Galwick) of known surface tension is used to saturate the sample (Section 2.5.3). Air is then

incrementally passed through the sample until the pressure is sufficient to overcome

the capillary action of the liquid within the largest pore of the sample, also known as the

bubble point. The flow rate and pressure are increased until all accessible pores are

opened and the sample is considered dry. The dry sample is then run again and the flow

rate and pressure through the sample are recorded. A comparison of the two curves

and a third calculated curve, the ½ dry curve, provides the data necessary to calculate

the smallest detected pore, mean flow pore diameter and largest detected pore (Figure

4.22).
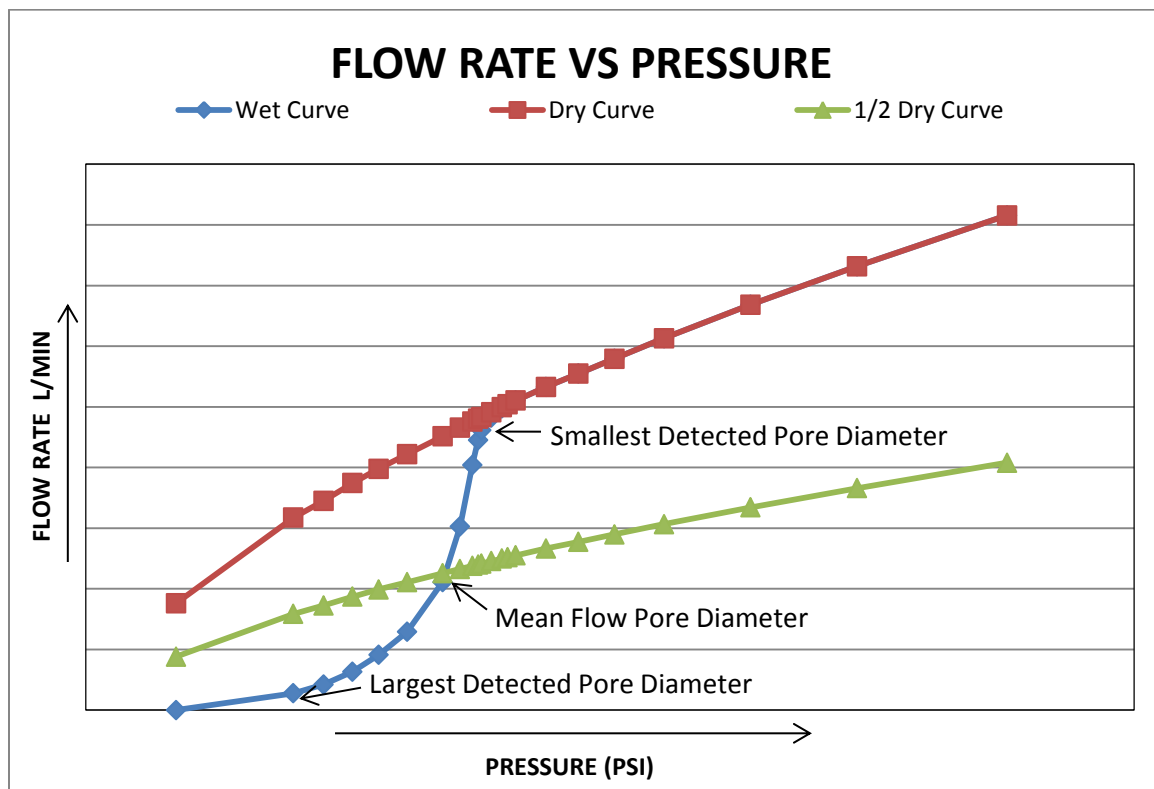
Figure 4.22. Example data obtained from Capillary Flow Porometer

It was expected that the smallest detected pore would be similar for all composite

samples because it would be governed by the meltblown layer which consists of the

www.manaraa.com

smallest diameter fibers. However, there was a range amongst the samples from 0.35 μm to 1.0 μm, Figure 4.23, for the smallest detected pore size. The control composite had the smallest average pore size which was attributed to the presence of the Freudenberg binder, which was not used in samples 2-7.   These results also correspond with the trend observed for the air permeability samples. The samples containing Freudenberg adhesive had lower air permeability than those without (0.8-3 cfm/ft^2 vs 4-7 cfm/ft^2). As previously mentioned, due to the processing conditions used for thermal bonding of the composite, the Freudenberg binder melts which causes partial blockage of pores present in the sample.
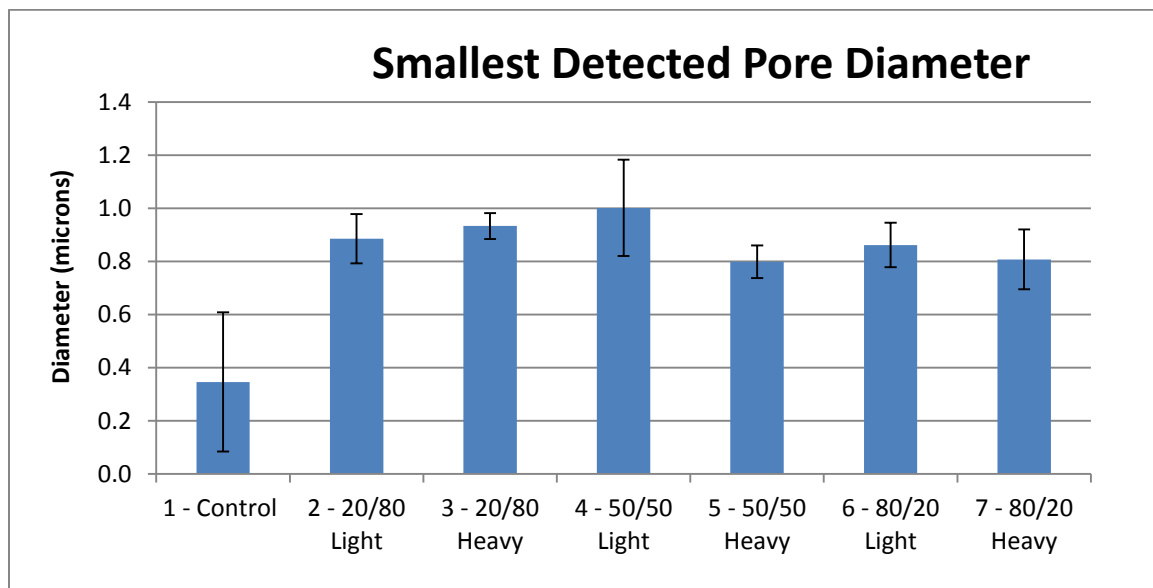
Figure 4.23. Smallest detected pore diameter for the 1st Generation control composite and composites with trial binders

The mean flow pore diameter is the pore diameter at a pressure drop at which the flow through a wetted sample is 50% of the flow through the dry sample.[20] While it is not the mean pore diameter, because the flow through larger pores can be

88

disproportionately larger than the flow through smaller pores, it is the most common pore size in the sample. The data shows that most of the samples fall within the same range, 2-3.5 µm, Figure 4.24. This was expected since 4 of the 7 layers present the sample, Figure 4.15, were the same. The samples containing the binder/matrix layers had slightly larger mean flow pore diameters, 2.4-3.5 µm, as compared to the control which had an average of 2.0 µm. This data corresponds with the results from air permeability in which the binder/matrix samples had higher air permeability than the control.
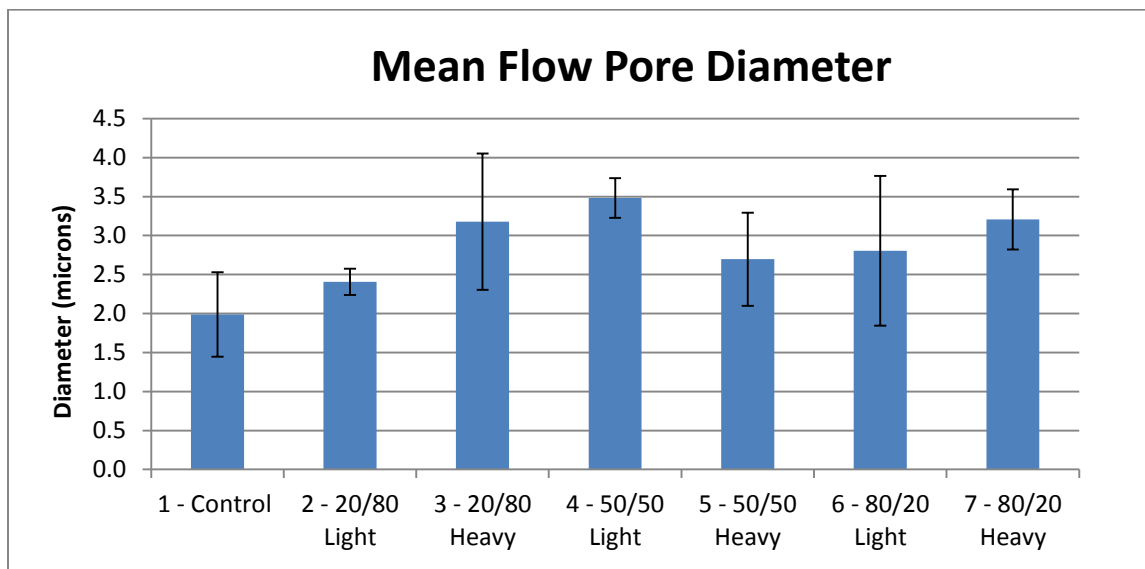
Figure 4.24. Mean flow pore diameter for the 1st Generation control composite and composites with trial binders

The final measurement commonly provided by the CFP is the bubble point pore diameter, which is the largest pore present in the sample. This measurement is not listed because huge variations were obtained for the samples. The lamination process at this point in the research project had not been perfected. As the air would flow

89

through the sample (if the layers were not in intimate contact) it could pass through one layer, move parallel to the fabric and then return to moving perpendicularly through the sample. This action replicates a pore and causes larger values to be obtained.

4.4   Individual Component Layers

The individual components used in the composite structure were analyzed using a using a Capillary Flow Porometer (CFP) and an air permeability tester, as described in Section 2.5.2 and 2.5.3, to determine their contributions to the overall composite structure.

A comparison of the pore sizes for each layer is presented in Table 4.4. The meltblown PP nonwoven, as expected, had the smallest detected pore size (6.58 ± 0.3 µm) but the 3 layer PET C-CP^{TM} carded nonwoven and the knitted outer layer (tested under minimal tension) had similar diameters for the smallest detected pore (6.86 ± 1.3 µm and 7.82 ± 0.25 µm, respectively). The pore size distribution of the meltblown PP nonwoven, however, was significantly different than what was obtained for the carded nonwoven and knitted outer layer (Figure 4.25 to Figure 4.27). The majority of the pores present in the meltblown PP nonwoven are between 7-8 µm whereas for the 3 layer PET C-CP^{TM} carded nonwoven they are between 30-80 µm and for the knitted outer layer they are between 60-100 µm.

Sample	Average Smallest Detected Pore Diameter (µm)	Average Mean Flow Pore Diameter (µm)	Average Largest Detected Pore Diameter (µm)
Meltblown PP	6.58 (0.30)	8.11 (1.1)	34.22 (3.5)
Carded 3 layer PET C-CP™	6.86 (1.3)	72.83 (7.0)	211.88 (46.5)
Knitted Outer layer	7.82 (0.25)	74.08 (4.1)	202.62 (12.6)
Freudenberg Binder	12.60 (0.84)	N/A	N/A
Woven Fiberglass	26.12 (6.5)	N/A	N/A

Table 4.4. Average smallest detected pore diameter, mean flow pore diameter and largest detected pore diameter for each component in the composite. Standard deviation listed in parenthesis.
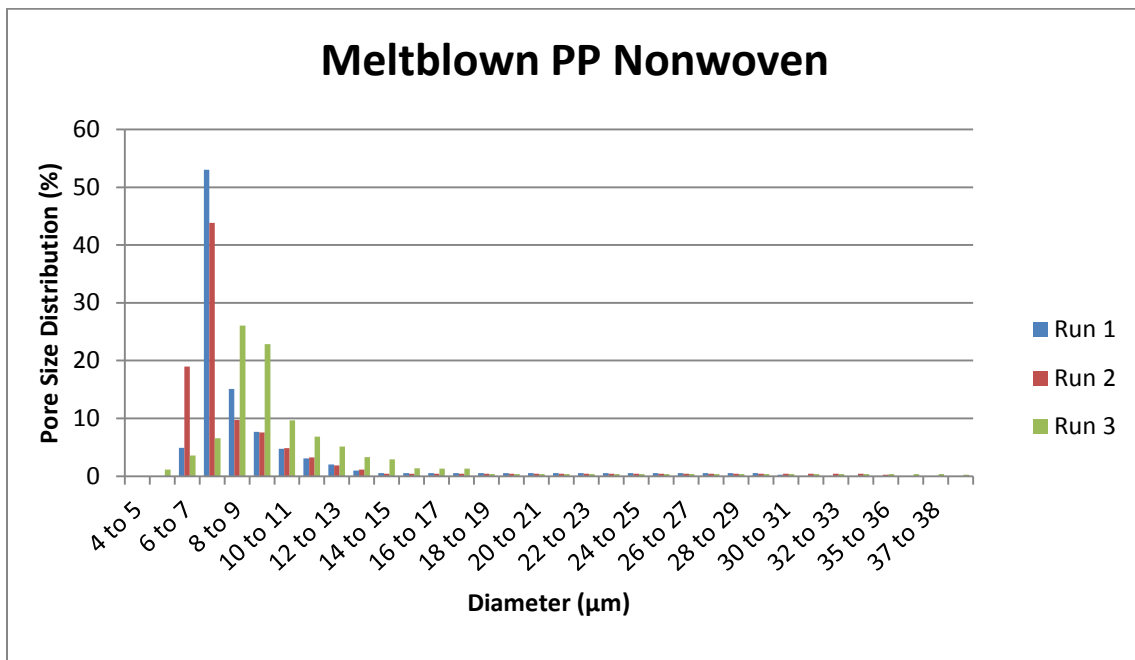
Figure 4.25. Pore size distribution for the meltblown PP nonwoven
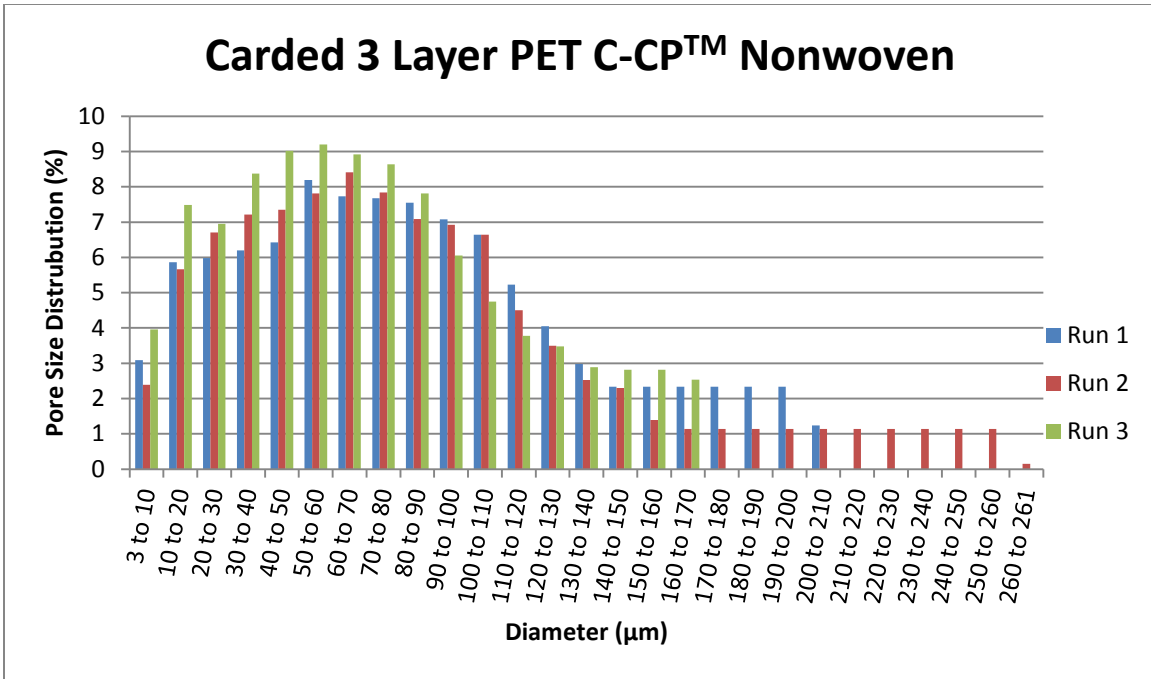
Figure 4.26. Pore size distribution for the carded 3 layer PET C-CP^{TM} nonwoven
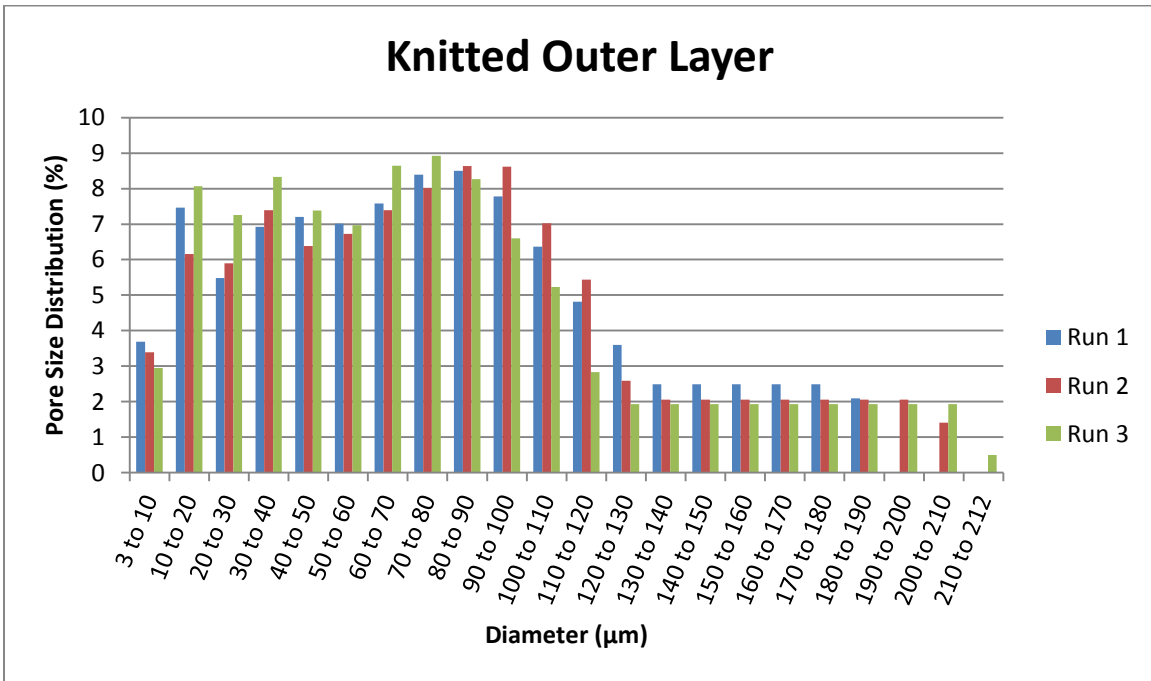
Figure 4.27. Pore size distribution for the knitted outer layer

The two layers with the largest values for the smallest detected pore size were the Freudenberg binder and woven fiberglass fabric (12.6 ± 0.84 µm and 26.12 ± 6.5 µm respectively), as expected. Due to the openness of both materials (Figure 4.28) reliable measurements were not obtained for either the mean flow or largest pore diameter.
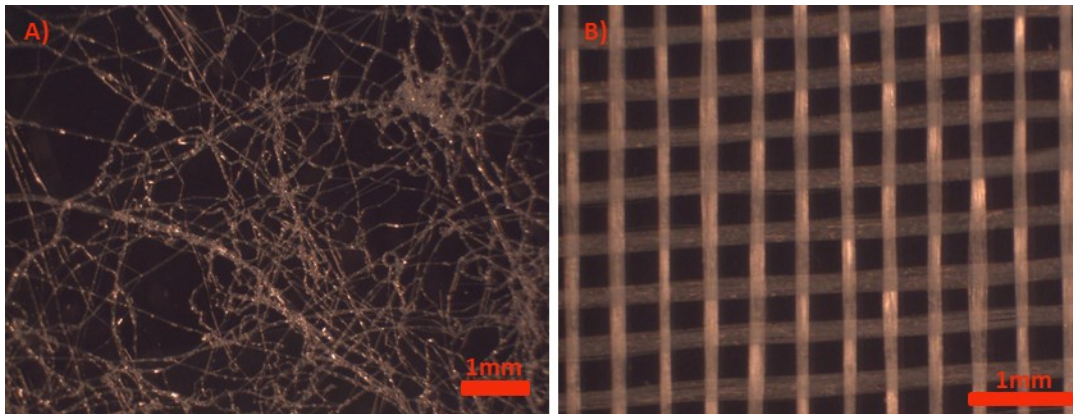
Figure 4.28. Optical images of A) Freudenberg binder and B) woven fiberglass at 20x

The CFP also provides data regarding the pressure drop across each sample (Figure 4.29). As has been stated previously, the meltblown PP nonwoven was placed in the composite to be used as a flow restrictive layer. The results show that the meltblown PP does have the highest pressure drop confirming its purpose in the composite structure. At a flow rate of ~80 L/min the pressure drop across the meltblown PP is ~2.1 PSI, the knitted outer layer is ~1.8 PSI and the 3 layer PET C-CP^{TM} carded nonwoven/Freudenberg binder/woven fiberglass is ~1.4 PSI. These results also correlate with the pore size measurements in which the meltblown layer contained the smallest detected pore diameter and had a pore size distribution with the majority of its pores being ~8 µm (the smallest).
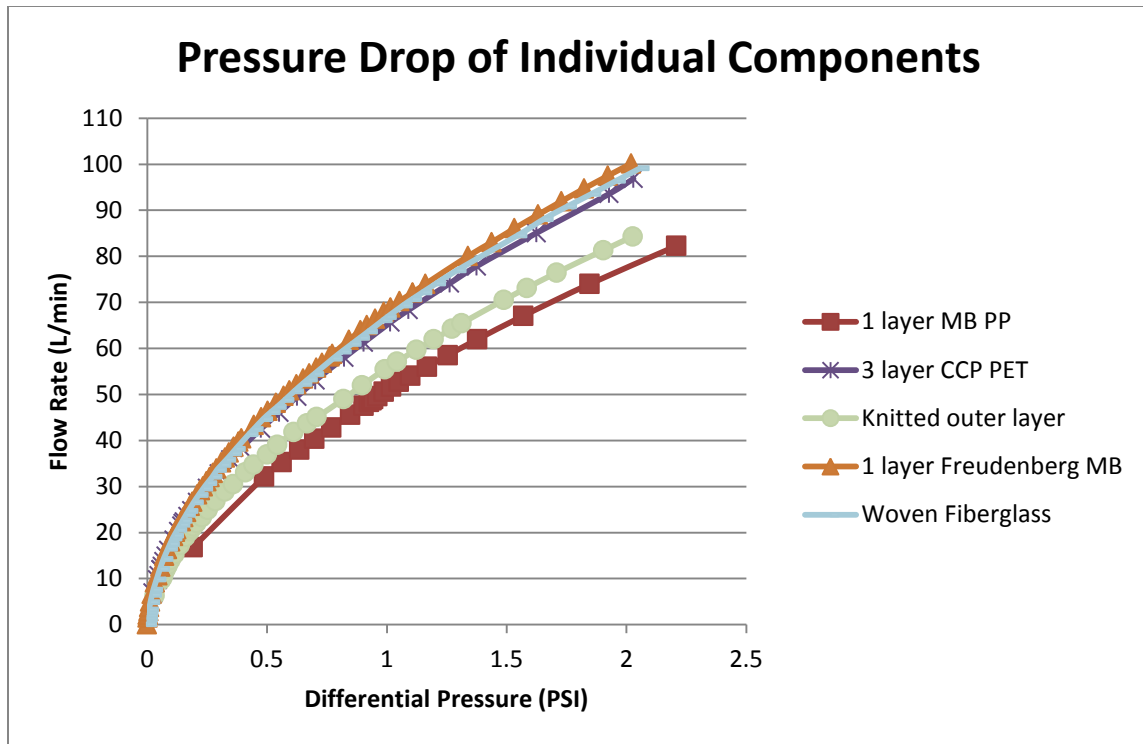
Figure 4.29. Pressure drop for each component in the composite structure

The results from air permeability measurements, which were made on the Texttech 3300 Air Permeability Tester, again coincide with the data from CFP testing. The meltblown PP nonwoven, which was shown to have the smallest pore sizes and the largest pressure drop, had the lowest air permeability of all the individual component layers (80.3 ± 13 cfm/ft^2 as compared to 274.4 ± 10.3 cfm/ft^2 for the knitted outer layer). Air permeability measurements could not be made on the 3 layer PET C-CP^{TM} carded nonwoven, Freudenberg binder or woven fiberglass fabric due to the openness of their structures (Figure 4.28).

Finally the absolute permeability of each layer was calculated using Equation 4.1

$$p^* = \frac{QL\mu}{\Delta PA} \times 1.01 \times 10^8$$

Equation 4.1. Calculation of absolute permeability

Where

 p^* = absolute permeability (D, 1 Darcy = 1.01×10^8 cm)

Q = flow rate of air through the sample (cm^3/s)

L = thickness of the sample (cm)

μ = dynamic viscosity of air at 20°C (Pa·s)

ΔP = pressure drop (Pa)

A = area of tested sample (cm^2)

Permeability is the ability of a fluid (air in this case) to pass through a porous material such as a woven or nonwoven fabric. The equation for absolute permeability allows for a direct comparison of materials by normalizing the permeability by the thickness of the sample. A comparison of the absolute permeability of each component layer will determine which layer has the largest contribution to the reduction of the flow of toxic compounds through the composite. As shown in Figure 4.30, the meltblown layer has the lowest absolute permeability which agrees with the results from air permeability, pore size measurements and pressure drop.

95
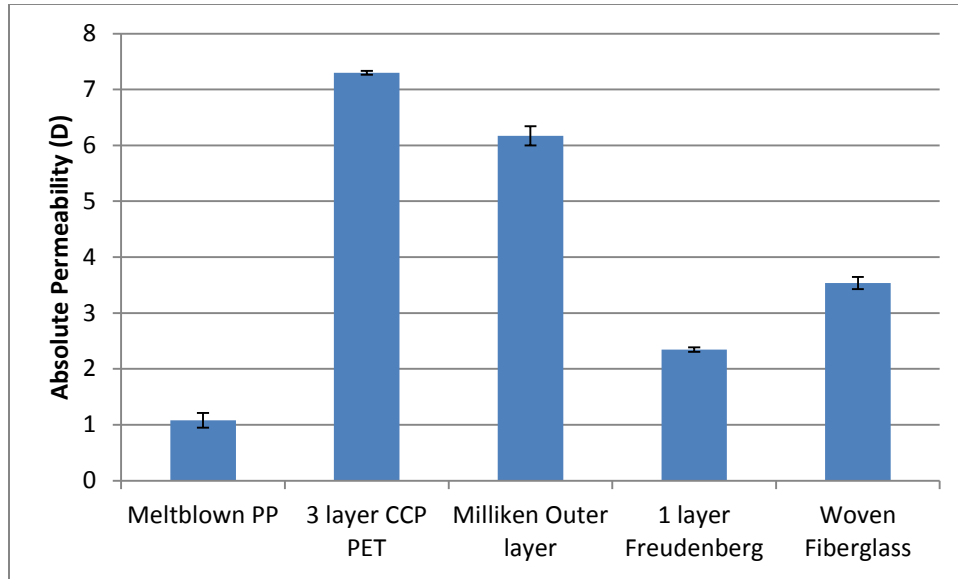
Figure 4.30. Absolute permeability of each component in the composite structure

4.5   Composite Structure

The 2nd generation composite structure design based on material properties is

presented in Figure 4.31. The uniformity of the sorptive functional layer, shown in

purple, was increased significantly by crimping the fibers prior to making the mixed dpf

nonwovens. In addition the incorporation of a layer of meltblown PP within the 3 layers

of mixed dpf C-CP[TM] PET nonwovens displayed a decrease in particle loss in preliminary

particle spraying.

96

Outer Layer
Fruedenberg
Meltblown PP
Fruedenberg
2 Layers Mixed dpf C-CP^{TM} PET
Meltblown PP
1 Layer Mixed dpf C-CP^{TM} PET
Fruedenberg
Meltblown PP
Fruedenberg
Woven Fiberglass
Fruedenberg
Outer Layer

Figure 4.31. Final composite structure layering schematic

Two flow restrictive functional layers, shown in green, were placed in the final

composite design to act as a fail-safe in case a breach occurred in one of the two layers.

The results obtained from tensile testing also demonstrated the need for a support,

shown in yellow, to be present in order to prevent breach of the meltblown layer during

wear. While several alternative binders were investigated it was determined that the

Freudenberg nonwoven provided the best bonding within the sample. It was also seen

that the Freudenberg helped to reduce pore sizes which should be beneficial for

increasing the residence time of the vapor within the composite allowing for adsorption

by the particles. Lastly, the data obtained from the CFP confirmed that the pore sizes

throughout the composite samples are fairly consistent which confirms that the

materials used are also consistent.

5 Results and Discussion: Composite Characterization and Testing

5.1 Composite Characterization

5.1.1 Particle Loaded Nonwoven Characterization

Several particle loading methods were explored before determining which method resulted in the most uniform and consistent application. Preliminary studies involved loading of particles by pipetting the particle solution (5% (w/v) in water in 2.5 mL aliquots) onto the sorptive functional layer, which was placed in a Buchner funnel, as shown in Figure 5.1. The particle solution was applied to one side of the nonwoven, allowed to sit for 5 minutes and then the nonwoven was placed in a vacuum oven (60°C which was below the T_g of the PET fibers used) for 2.5 hours to dry. This was repeated for the opposite side of the sample and continued until the target loading of 16g/ft^2 of was achieved. After preparing the first set of samples it was decided to disperse the particles in a different liquid due to the time required to dry the samples. Isopropanol was chosen due to its lower boiling point (82.5° as compared to 100°C for water) and because it was readily available.
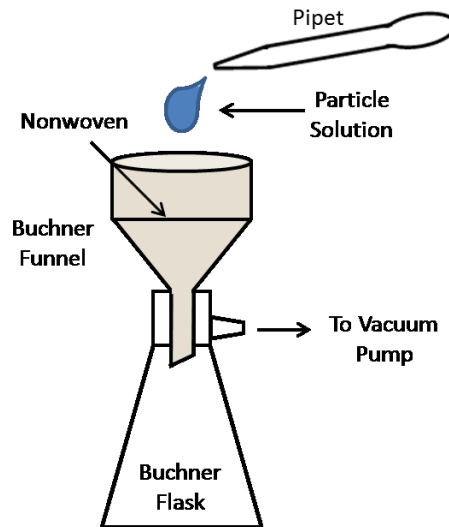
Figure 5.1. Schematic of particle loading via pipetting

It would be expected that the particles would coat the interior of the grooves due to the wicking nature of the fiber; however, the degree to which the grooves could be filled was unknown. Figure 5.2A shows what appears to be a groove completely filled with mPS particles and, under further investigation using higher magnification (Figure 5.2B), this was confirmed. While groove filling was seen in several areas of the sample there were also sections that resembled Figure 5.3 where loading only occurred on the tops of the grooves.
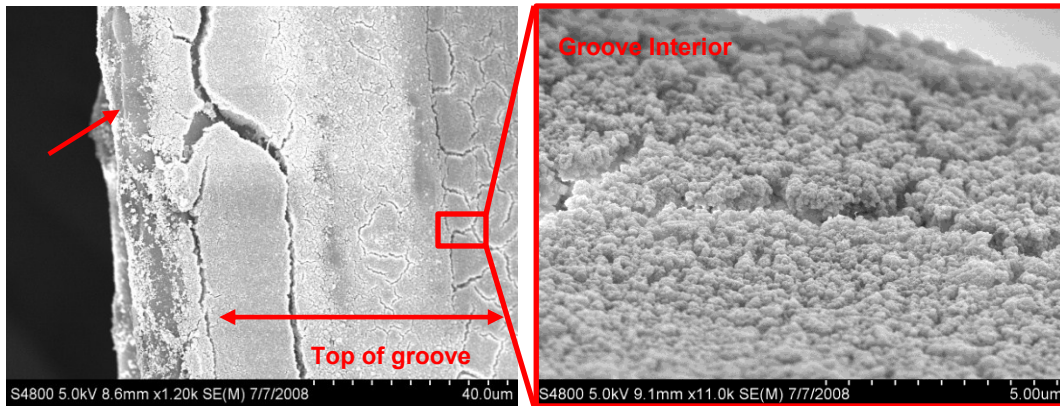
Figure 5.2. SEM image of mPS loaded sorptive functional layer with loading occurring in the interior of the groove A) at 1.2kX magnification with scale bar of 40 μm B) at 11kX magnification with scale bar of 5 μm
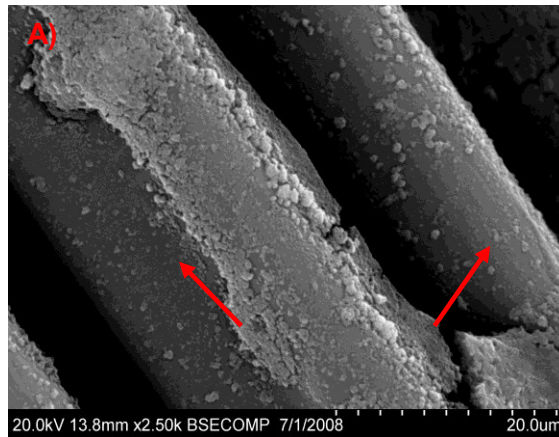
Figure 5.3. SEM image of mPS loaded sorptive functional layer with loading occurring on the top of the groove at 11kX magnification

Similar loading was observed for the samples loaded with zeolite particles, Figure 5.4 and Figure 5.5. While particle loading into the grooves of the fiber was desired, the loading uniformity was far from providing adequate coverage. With both particle species it was observed that the particles would agglomerate and settle onto or into the grooves of the fiber but did not dispersed evenly along the sample. It was concluded that this was probably an artifact of the application method. While the particles were suspended in a solution prior to application they readily fell out of suspension if not

100

constantly or consistently agitated. In addition the pipetting procedure did not evenly

disperse the particles across the nonwoven surface. Thus an application method was

developed to a) obtain a more even particle distribution over the nonwoven surface and

b) to break up particle agglomerates during the application method.
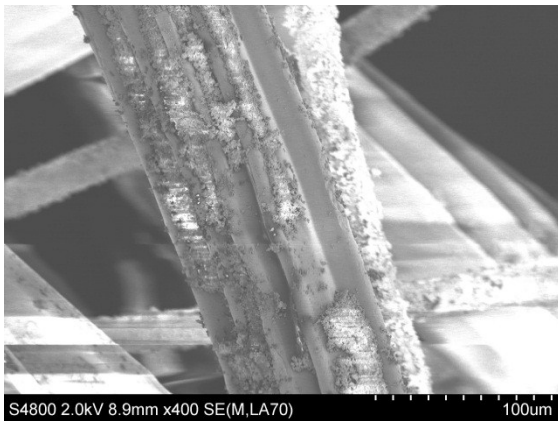
Figure 5.4. SEM image of zeolite loaded sorptive functional layer with loading occurring in the interior of the groove at 400X magnification
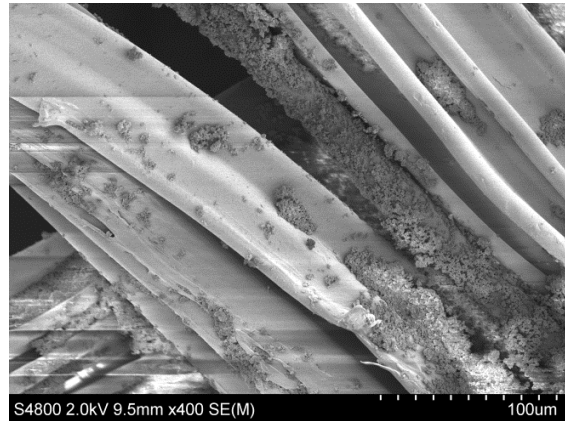
Figure 5.5. SEM image of non-uniform loading of zeolite particles onto the sorptive functional layer at 400X magnification

The next approach was to spray the particles, which were suspended in isopropanol,

using either a paint sprayer or a glass reagent sprayer (depending on scale) connected

to an airline (as described in Section 2.7) onto the nonwoven surface. Observations

from SEM images, Figure 5.6 to Figure 5.8, show that this method provides significantly

more uniform particle coverage. Additionally these images, in particular Figure 5.6,

confirm that the loading level of $16g/ft^2$ was overloading the grooves present and the

nonwoven as a whole. This excessive mass of "free"particles, those not physically

retained by the groove or direct interaction with the fiber surface at the groove tip,

www.manaraa.com

caused significant dusting from the samples. This was found later to also negatively

impact the bonding of the composite layers.
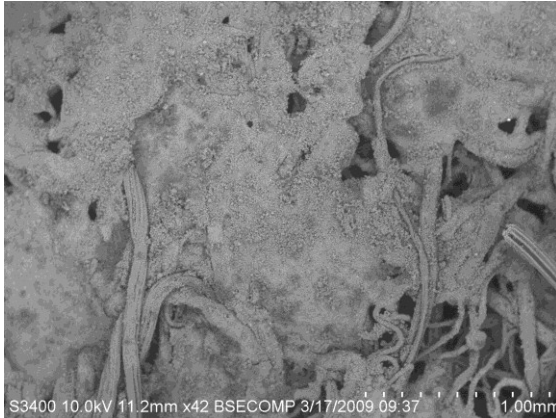
Figure 5.6. SEM image of zeolite loaded sorptive functional layer showing overwhelming particle loading at a loading level of 16g/ft^2 at 42X magnification

Figure 5.7. SEM image of zeolite loaded sorptive functional layer showing excessive particle loading at a loading level of 16g/ft^2 at 210X magnification
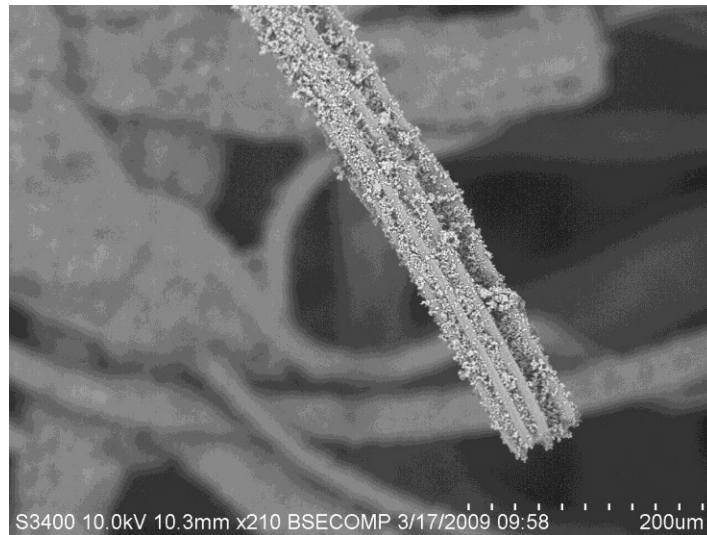
Figure 5.8. SEM image of zeolite loaded sorptive functional layer showing fully loaded grooves at a loading level of 16g/ft^2 at 210X magnification

In order to obtain the target mass of particles on the nonwoven several applications had

to be carried out. It was noted that with each additional particle spray application

needed it became increasingly more difficult to reach the target loading mass of $16g/ft^2$ due to two different mechanisms. As the grooves become filled with particles, the momentum of a new application of sprayed particles causes particles already present to be knocked off. In addition, due to the openness of the carded nonwoven web, particles are lost due to flying through the fabric.

An approach to mitigating this problem was to incorporate a meltblown layer within the three layers of mixed dpf PET which make up the sorptive functional layer (as previously mentioned in Section 4.2.4). The meltblown layer would now serve two purposes; first it would decrease the amount of particles lost during spraying since the average pore diameter present in the meltblown nonwoven is significantly smaller (~ 90%) than those present in the mixed dpf nonwoven ($73\mu m$). Second, it would allow for particles to be loaded onto its surface which would prevent the grooves from becoming overloaded with particles and allow the target loading to be achieved (Figure 5.9).

Figure 5.9. SEM image of zeolite loaded primary functional layer showing loaded grooves at a loading level of 16 g/ft^2 at magnification of 600X

Fabric samples were sprayed to have particle loading levels of 16 g/ft^2 both with and without the meltblown layer. These were then compared under SEM (Figure 5.6 to Figure 5.9). Samples that did not have a layer of meltblown present are shown in Figure 5.6 to Figure 5.8. Figure 5.9 shows that samples prepared with the meltblown layer in place reduced groove overloading in comparison to those without the meltblown layer as shown in Figure 5.6 to Figure 5.8.

However, dusting and adhesion issues were still prominent in addition to the continuing difficulty in reaching the desired particle loading level. The target loading level of 16 g/ft^2 was provided by SAIC based on their preliminary studies to ensure samples would pass further testing. A non-dusting loading level was experimentally determined to be 4.3 g/ft^2 which, when tested by SAIC, still passed testing conditions and no longer manifested adhesion issues when incorporated in the composite structure. This was

104

confirmed via SEM, Figure 5.10 and Figure 5.11, where it can be seen that the particles

were evenly dispersed on the fibers without the excessive build up previously observed.
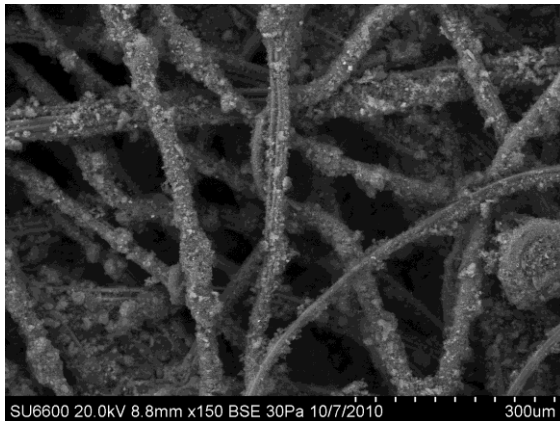
Figure 5.10. SEM image of zeolite loaded primary functional layer showing loaded grooves at a loading level of 4.3g/ft^2 at magnification of 150X
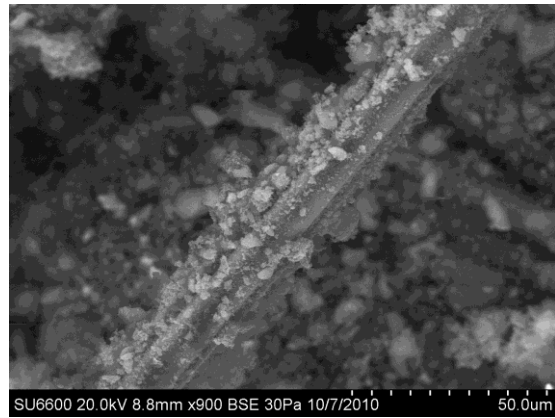
Figure 5.11. SEM image of zeolite loaded primary functional layer showing loaded grooves at a loading level of 4.3g/ft^2 at magnification of 900X

5.2   Composite Testing

In order to determine the protective capacity of the composite, it was exposed to test

compounds under both static and dynamic conditions. The goal of static testing was to

determine the maximum amount of a test compound vapor that could be adsorbed.

Determining maximum adsorption, or adsorption equilibrium, has been approached in

various ways for protective garments. Pal *et al*. examined maximum uptake via

complete immersion of chemical protective material into liquid stimulants, Wester *et al*.

investigated percutaneous vapor adsorption through naked and uniformed skin over a

period of 96 hours and Rivin determined equilibrium adsorption by exposing strips of

adsorbent fabric with and without activated carbon to challenge vapor and measuring

the mass gain.[47, 91, 92] Maximum adsorption capacity is important because, in military situations, the soldier typically must wear the same uniforms for extended periods of time. However the performance of the composite also depends on factors such as adsorptive diffusivity and flowrate. Therefore dynamic testing was also completed to determine the break through time of a penetrating test compound.

Live agents were not used for either static or dynamic testing due to the level of hazard they impose to the experimentalist. It is common practice to instead choose a compound that mimics the chemical agent sufficiently to provide useful data without the level of toxicity that a chemical warfare agent (CWA) possesses. Since the adsorption mechanism of the zeolite particles being used was physisorption it was desirable to choose chemical compounds that were of similar molecular size to common CWAs (Figure 5.12) and had vapor pressures that would allow for vaporization. The test compounds chosen for static testing were isopropanol, diisopropyl ketone (DIPK), methyisobutyl ketone (MIBK), and diphenyl chlorophosphate (DPCP). The chemical and physical properties of each were listed in Section 2.9.1 and approximate size measurements, as well as size measurements of CWAs, are listed in Table 5.1.
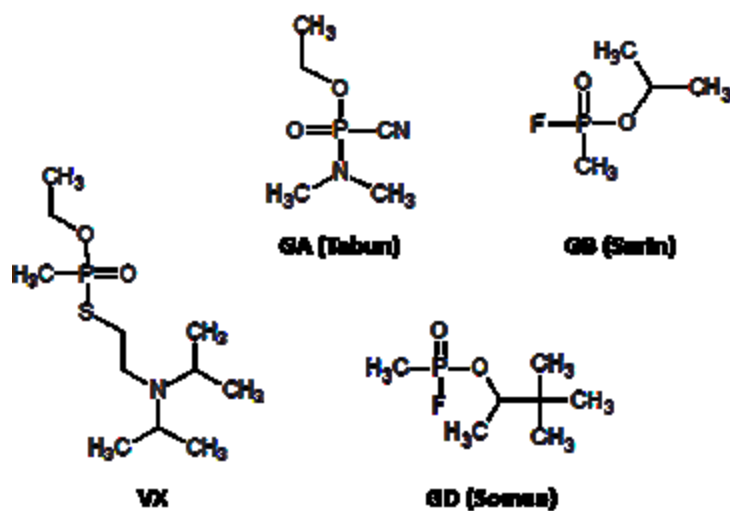
Figure 5.12. Chemical structures for common CWAs

Compound	Length (Å)	Width (Å)	Depth (Å)
VX	11.15	6.97	4.85
GA (Tabun)	8.26	6.20	3.50
GB (Sarin)	6.93	4.28	3.36
GD (Soman)	8.05	5.31	6.22
Isopropanol	3.82	4.15	3.10
Diisopropyl Ketone	6.87	4.30	5.36
Methyl Isobutyl Ketone	6.37	4.09	3.11
Diphenyl Chlorophosphate	13.56	5.54	3.03
Diethyl Ketone	6.74	4.319	4.291

Table 5.1. Approximate measurements of length, width and depth for common CWAs and chosen test compounds

DPCP was chosen to mimic VX based on size with a length slightly larger than that of VX, 13.56Å compared to 11.15Å, and a width and depth slightly smaller, 5.54Å and 3.03Å compared to 6.97Å and 4.85Å. In addition the vapor density of both DPCP and VX is approximately 9.2 (relative to air being 1). Both MIBK and DIPK mimic the size of GB very well with all having lengths of 6-7Å, widths of approximately 4 Å and depths of 3-5Å. While isopropanol does not mimic any of the CWAs it is found on the Occupational Safety and Heath Administration's (OSHA) list of toxic industrial chemicals (TICs), as well

as MIBK, which are defined as commonly produced chemicals that can be used as a weapon and pose a risk of severe adverse health effects.[93] Due to the new style of warfare faced in Afghanistan, Iraq and Iran, the presences of TICs have become of a greater concern to military personnel and therefore it is important to determine the protective capacity of the garment against such chemicals.[94] The test compound chosen for dynamic testing was diethyl ketone which also mimics the size of GB having lengths of approximately 7Å, widths of approximately 4 Å and depths of 3-4Å.

5.2.1 Method Development for Static Chemical Threat Testing

While various methods have been used to determine the maximum adsorption, the method developed for this research was similar to the method used by Rivin.[92] The test exposed samples to a saturated environment and measured the resulting mass increase over time using a recording micro-balance contained in a Dynamic Contact Angle Analyzer (DCA).

The chamber was sealed at each edge, both inside and out, and around the moving stage located inside the chamber using aluminum tape in order to prevent vapor from escaping the testing chamber. Initial runs were performed using the apparatus configuration observed in Figure 5.13 in which the test compound, isopropanol, was at room temperature.

108
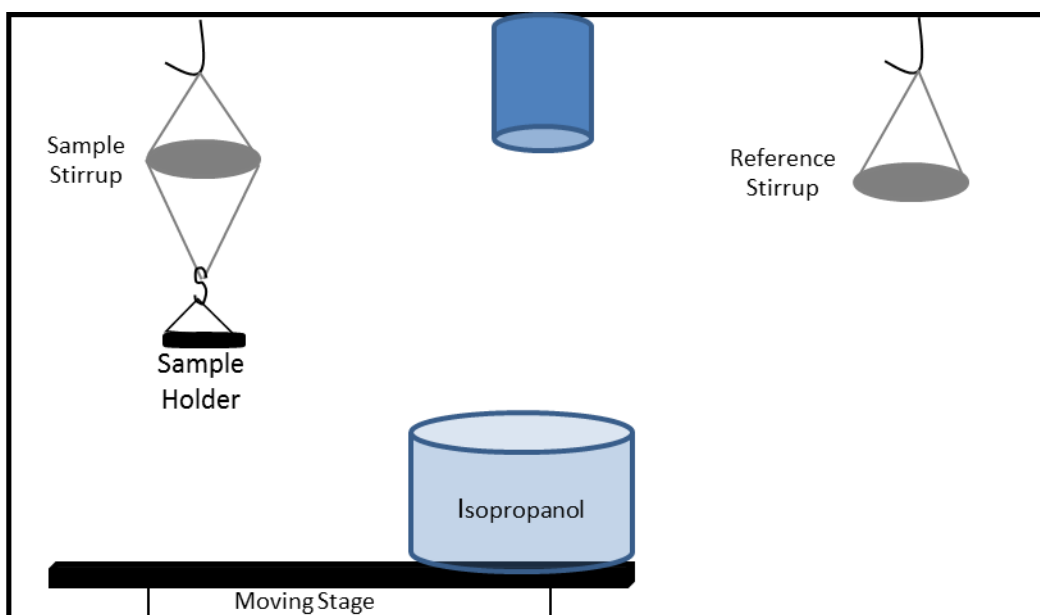
Figure 5.13. Preliminary set-up of the microbalance chamber

5.2.1.1 Preliminary Data

The initial goals of preliminary testing were to determine the time required for the sample to reach full saturation, to ensure that the chamber was completely sealed, and to confirm the sensitivity of the microbalance for this purpose. Three tests were run lasting for 1.5hrs, 4hrs, and 2 days. Zeolite particles from UOP LLC were used for this study as they were readily available, inexpensive and known to have a high surface area.[95]

The data was normalized using absorbance in mg of isopropanol per mg of sample in order to provide a direct correlation between samples. The mass of each sample and mass gain are presented in Table 5.2 in addition to the calculated theoretical maximum adsorption which was discussed in Section 3.4. These results are presented in Figure 5.14, confirmed that the microbalance was sensitive enough to measure the mass gain

www.manaraa.com

of isopropanol by the zeolite particles with mass gain occurring within the first 60 seconds of the test.

Run	Zeolite Sample Mass (mg)	Max Isopropanol Adsorbed (mg)	Theoretical Max Isopropanol Adsorbed (mg)
1	7.93	0.654	1.33
2	8.37	0.774	1.40
3	7.96	0.567	1.33

Table 5.2. Zeolite particle trial run 1-3 sample masses, measured maximum adsorption and calculated theoretical maximum adsorption
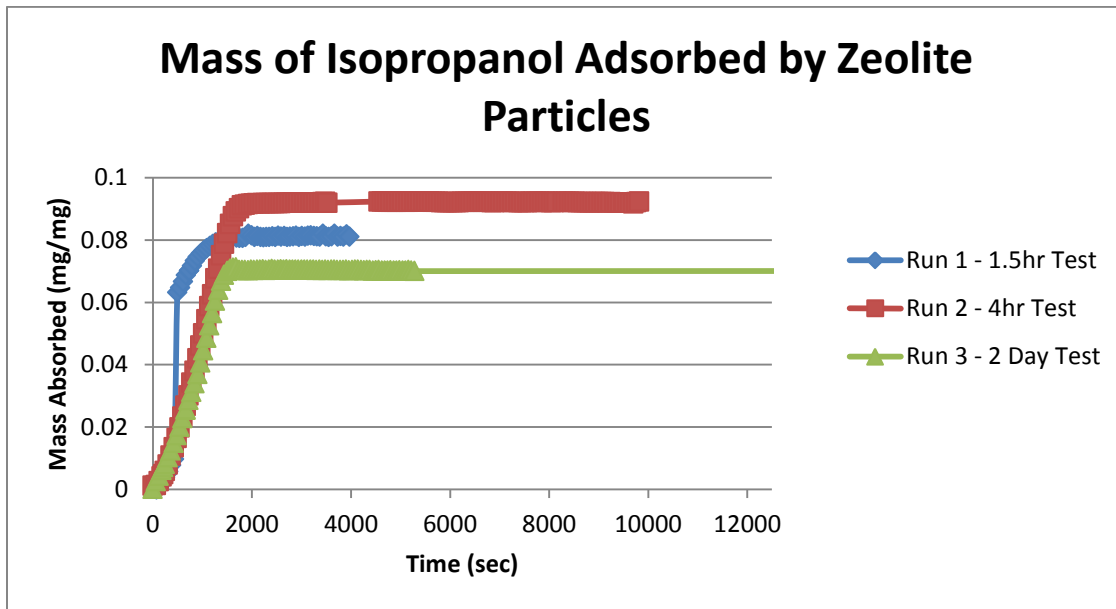
Figure 5.14. Mass (mg) of isopropanol adsorbed per mg of zeolite particles tested

During the first run no condensation was observed inside the chamber which indicated the chamber was not completely saturated, which was the goal. For the following run the door was sealed to prevent vapor from escaping the test chamber which resulted in an increase in adsorption, from 0.08mg/mg sample to 0.09mg/mg sample. However, it was still observed that there was a lack of condensation on the inside of the chamber. The samples were also only adsorbing approximately 50% of their calculated theoretical

110

maximum adsorption, for example Run 2 adsorbed 0.774mg but theoretically should

adsorb 1.40mg. It was thought that if the chamber was completely saturated the

sample would come closer to adsorbing its maximum capacity. This issue will be

addressed in Section 5.2.1.2.

The results also revealed that each sample reached a maximum adsorption, 0.654mg,

0.774mg and 0.567mg respectively for Runs 1-3, and remained at that level until the end

of the test. Even though each test length proved adequate for the sample to reach a

maximum adsorption the intermediate test length, 4 hrs, was chosen to ensure

equilibrium was reached for all samples.

5.2.1.2   *Optimizing Testing Conditions*

Once the feasibility of using the instrument in this manner was established a heat

source (150W high intensity, tungsten halogen light source) was placed inside the

chamber, as illustrated in Figure 5.15, to increase vaporization of the test compound

and ensure complete saturation of the test chamber. The temperature of both the test

compound and the chamber were monitored using Thermochron iButtons, one of which

was placed in a waterproof capsule before submerging in the test compound liquid. The

second sensor was placed in a sealed environment to protect it from any volatilized

chemicals present in the main body of the chamber.   Neat zeolite particles, i.e. without

the nonwoven substrate, were used for both Run 4 and 5 and the test length was 4

hours. Both runs used the heat source but for Run 5 the chamber had been pre-

saturated for two hours with the test compound to determine if the sample would then

be able to adsorb a greater amount of the test compound.
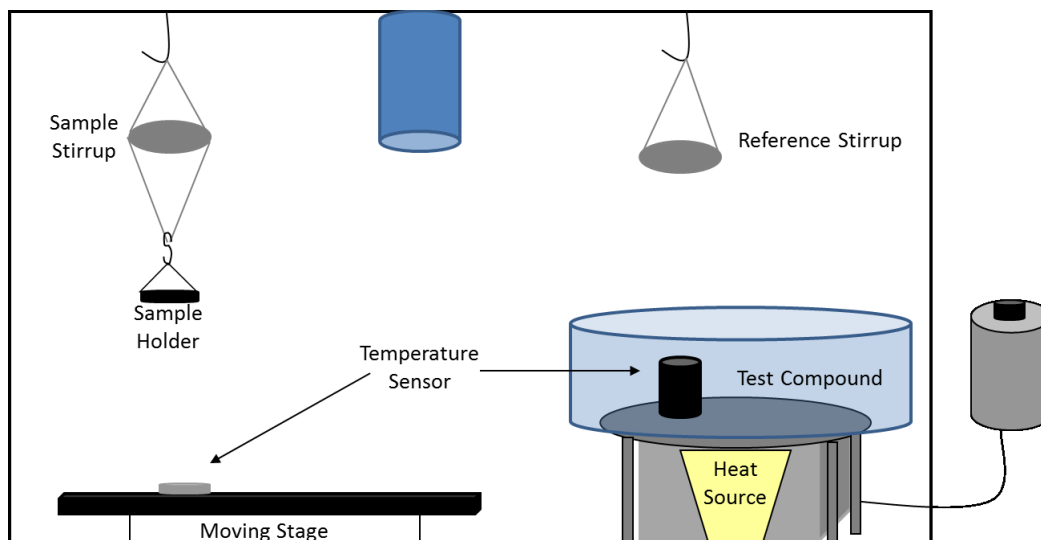
Figure 5.15. Set-up of the microbalance chamber with the addition of a heat source for the test compound

Again the data was normalized using absorbance in mg of isopropanol per mg of sample

in order to give a direct correlation between samples, Figure 5.16. The mass of each

sample, mass gain and calculated theoretical maximum adsorption for each sample is

presented in Table 5.3. For both Runs 4 and 5 the isopropanol was heated to 53°C and

resulted in the largest mass gain by the zeolite particles, ~0.11mg/mg sample as

compared to 0.09mg/mg sample for Run 2 (which had no heat source but was tested for

the same duration). In addition condensation of vapor was observed in the chamber

indicating a saturated environment, which was the goal of adding the heat source to the

chamber.

www.manaraa.com

Figure 5.16 shows that the mass gain for Run 5 occurred much faster than that of Run 4. The reason for the increased rate was due to the pre-saturated chamber; however the pre-saturation did not cause an increase in the overall mass gain, 0.109mg/mg sample for Run 4 compared to 0.107mg/mg sample for Run 5, and therefore pre-saturation was not be used for future testing.

Run	Zeolite Sample Mass (mg)	Max Isopropanol Adsorbed (mg)	Theoretical Max Isopropanol Adsorbed (mg)
4	8.14	0.884	1.36
5	6.83	0.728	1.14

Table 5.3. Zeolite particle trial run 4-5 sample masses, measured maximum adsorption and calculated theoretical maximum adsorption
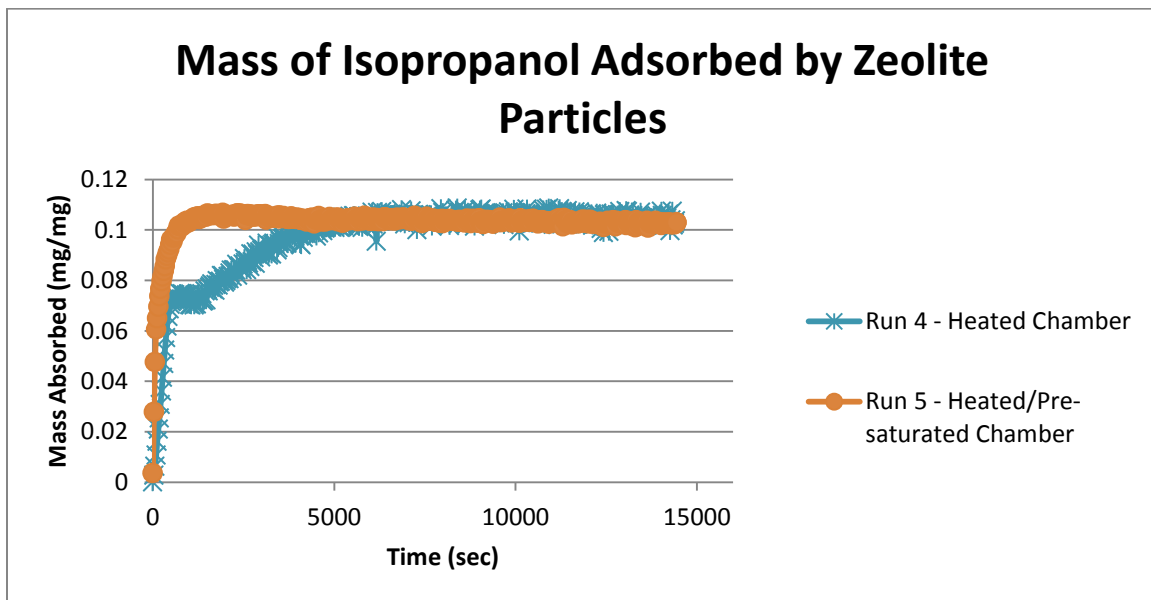
Figure 5.16. Mass of isopropanol adsorbed by zeolite particles normalized by mass of particles

5.2.1.3   Control Runs

While the addition of the heat source accomplished greater volatilization of the test compounds, resulting in observed condensation inside the chamber, there was also an

113

increase in point to point variations within the data set. While it was assumed that the heat source had caused the increased level of variation, it was unclear exactly how and was examined more closely during the control runs.

Control runs were performed to determine the degree of mass gain that could be attributed to vapors condensing on the sample stirrup while trying to reduce point to point variation. Control Run 1 was performed with the chamber set up as seen in Figure 5.15 (with the sample pan removed). In Control Run 2 the system was dampened from external vibrations using dampening blocks. In Control Run 3 a cap was placed over the reference stirrup, as depicted previously in Figure 2.6 of Section 2.9.2, to protect the reference stirrup from the volatilized test compounds.

All three control runs were performed with heated isopropanol and lasted for four hours. In order to directly compare the difference in point to point variation the last 4,000 seconds were plotted and normalized to run with the greatest variation (Control Run 2), as presented in Figure 5.17. Dampening the system did not appear to decrease the point to point variation and thus the dampening blocks were removed permanently. It was thought that the convection current from the vaporizing test compound was causing the reference stirrup (which is located directly above the test compound reservoir) to move and cause the variations from one data point to the next. The results for Control Run 3 show a significant reduction in the amount of noise.

114

Figure 5.17. Mass gain of isopropanol by the sample stirrup during Control Runs 1-3

115

5.2.2 Static Testing

From the trial runs on the zeolite particles and the control runs on the empty chamber it was determined that the microbalance could be used for static testing of the primary functional layer of the composite sample. A test protocol of 4 hrs at approximately 60°C was established. Placement of a cap over the reference stirrup reduced the high variability in the data obtained caused by the vaporization of the test compound below the reference stirrup.

5.2.2.1 Particle Free Nonwoven Samples

As would be expected the nonwoven samples without particles loaded onto the surface adsorbed minimal amounts (0.06 to 0.22 mg) of any of the test compounds especially as compared to a particle loaded sample, as presented in Figure 5.18. Any mass gained by these samples would be expected to be attributed to the test compound condensing within the channels of the CCP fibers.
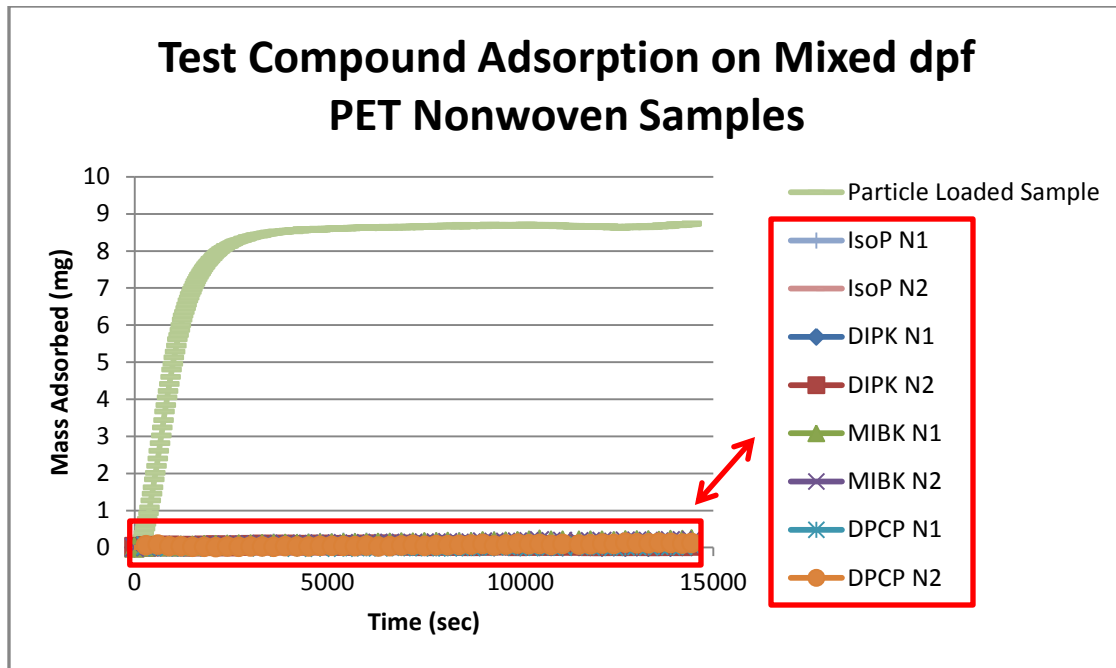
Figure 5.18. Results of test compound adsorption on mixed dpf PET nonwoven samples as compared to a particle loaded sample

The theoretical maximum adsorption of each test compound on each sample was then calculated as discussed in Section 3.4; the results are tabulated in Table 5.4. The measured maximum adsorption ranged from 0.06 mg to 0.22 mg whereas the calculated theoretical maximums ranged from 0.015 mg to 0.035 mg. As previously mentioned the mass gain observed for these samples would be expected to be due to condensation of the test compounds in the fiber channels and/or the effect of the reference stirrup being capped. C-CP^{TM} shaped fibers have been used previously for fluid adsorption and transport due to their increased surface area as compared to traditional round fibers and their inherent ability to wick fluids.[96] Therefore it is not surprising for mass gain to occur in a non-adsorbent nonwoven made of C-CP^{TM} fibers.

117

Sample ID	Nonwoven Mass (mg)	Max Test Compound Adsorption (mg)	Theoretical Max Test Compound Adsorption (mg)
DIPK_N1	92.10	0.09	0.018
DIPK_N2	77.20	0.08	0.015
MIBK_N1	102.90	0.22	0.020
MIBK_N2	99.70	0.19	0.019
DPCP_N1	95.40	0.06	0.035
DPCP_N2	96.4	0.13	0.035

Table 5.4. Nonwoven sample mass, maximum measured adsorption and theoretical calculated maximum adsorption for each test compound

5.2.2.2 Zeolite Loaded Nonwoven Samples

Samples, which consisted of zeolite loaded adsorptive functional layers, had a target

loading level of 4.3 g/ft^2 ± 10%. In order to directly compare experimental runs the data

was normalized by adsorbance in mg of test compound per mg of zeolite particle loaded

on the sample. These results are presented in Figure 5.19. The mass of the nonwoven

was not taken into account because the runs with the nonwoven showed minimal

amounts of mass gain (0.06 to 0.22mg). Sample mass, actual mass gain and the

calculated theoretical maximum adsorption are tabulated in Table 5.5.

Sample ID	Final Sample Mass (mg)	Zeolite Particle Mass (mg)	Max Test Compound Adsorption (mg)	Calculated Max Test Compound Adsorption (mg)
IsoP_Z1	145.9	59.80	7.83	9.45
IsoP_Z2	142.0	62.00	9.34	9.80
DIPK_Z1	170.8	60.00	5.50	11.94
DIPK_Z3	158.6	67.5	9.67	12.83
MIBK_Z1	165.8	65.60	8.51	11.40
MIBK_Z2	156.8	60.00	6.37	22.91
DPCP_Z1	147.7	63.1	8.73	22.29
DPCP_Z2	136.7	61.4	7.94	32.17

Table 5.5. Zeolite loaded nonwoven sample mass, particle mass, maximum measured adsorption and theoretical calculated maximum adsorption for all test compounds

118
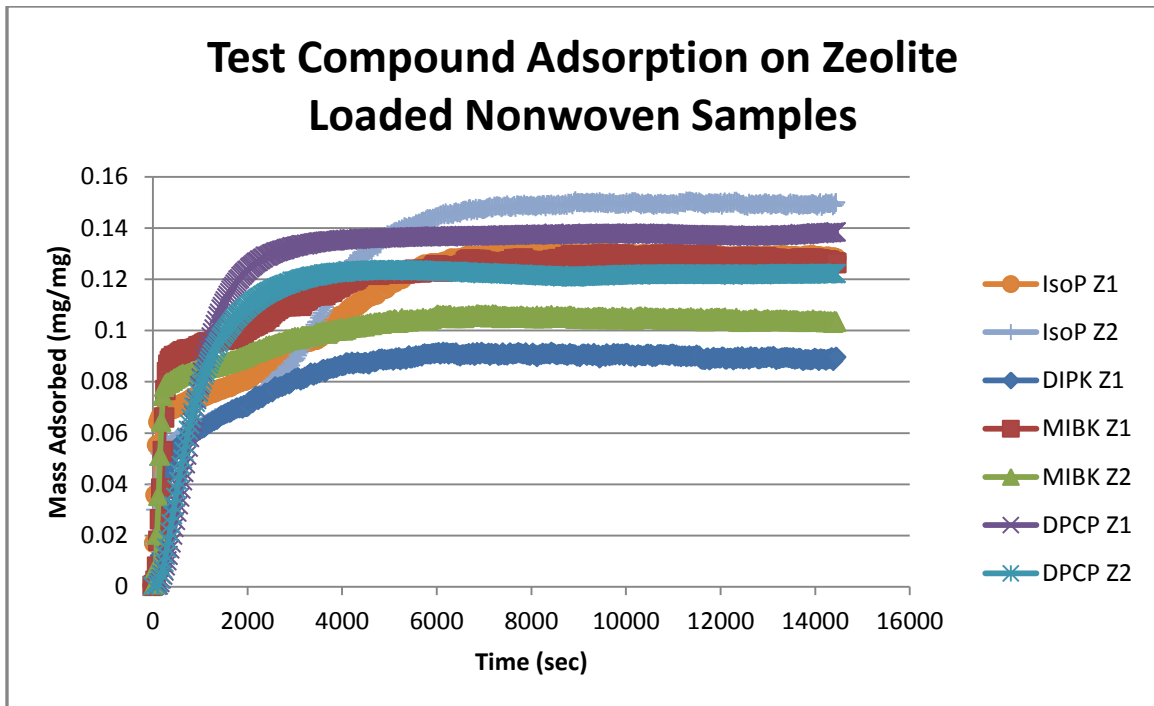
Figure 5.19. Results of test compound adsorption on zeolite loaded mixed dpf PET nonwoven samples

As would be expected, for a given pair of samples, those with a greater mass of particles

loaded onto the sample adsorbed higher amounts of the test compound. For example

MIBK Z1 had 65.6mg of zeolite particles loaded onto the sample and had a maximum

adsorption of 8.51mg of MIBK as compared to MIBK Z2 which had 60mg of particles and

adsorbed 6.37mg of MIBK. When examining the effect of test compound molecular size

on adsorption it was found that for samples with similar loading levels (IsoP Z1, MIBK Z2

and DIPK Z1 with 59.8, 60 and 60mg respectively) adsorption was greatest for the

smallest test compound molecule, in this case isopropanol.

All samples adsorbed less than the calculated theoretical maximums (Figure 5.20). It

was noted that as molecular size of the test compound increased, the measured

119

adsorption (as compared to the theoretical adsorption) decreased. For example, isopropanol (the smallest test compound) had an average adsorption of 0.14 mg/mg which was approximately 89% of the theoretical adsorption. DPCP (the largest test compound), however, had an average adsorption of 0.13 mg/mg which was approximately 37% of the theoretical adsorption. In addition to being the largest molecule, DPCP has a more rod-like shape as compared to the other test compounds.
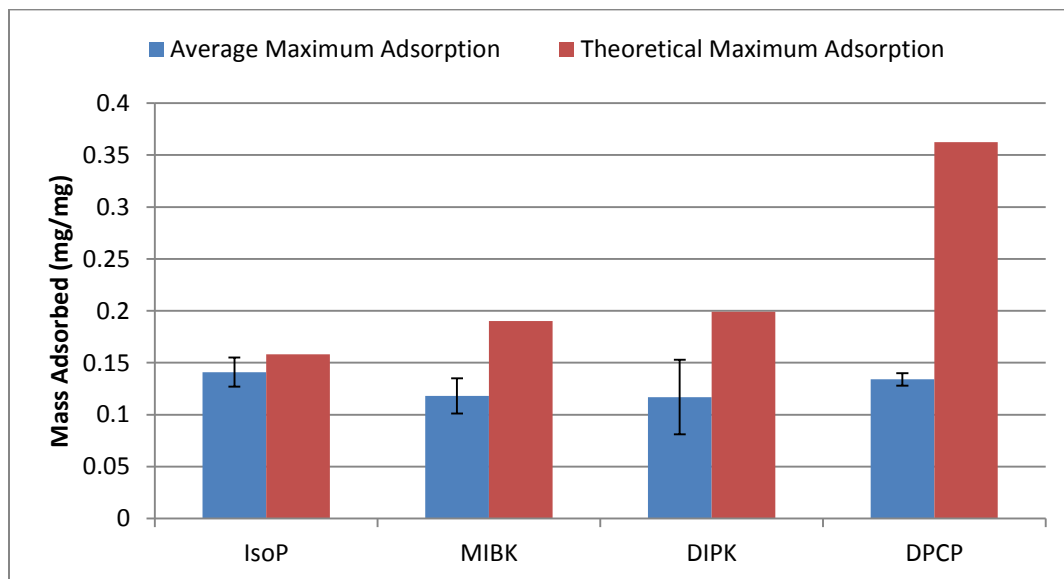
Figure 5.20. Comparison of average maximum adsorption and calculated theoretical maximum adsoption for zeolite loaded samples

In order to determine the protective capacity of the samples, the adsorption data was compared to the dermal LD50, which is the dose that would be lethal to 50% of the population, for CWAs of interest, VX and GB. The dermal LD50 for GB is 1.7g/70kg man and for VX it is 10mg/70kg man (Zajtchuk, Bellamy 1997). Wester *et al.* stated the total body surface area for a 70kg adult was 1.8m^2. Using this information the lethal dermal

exposure limit per area could be determined, Table 5.6, and compared to the adsorption data obtained for static testing, Table 5.7.

Chemical	LD50 (mg/kg)	Dermal Exposure Limit per 70kg man (mg/cm^2)
GB	24.29	9.44E-02
VX	0.14	5.44E-04

Table 5.6. Dermal LD50 and dermal exposure limit per area for GB, VX and isopropanol

Sample ID	Max Adsorption Mass (mg)	Max Adsorption per Area (mg/cm^2)
IsoP_Z1	7.83	0.54
IsoP_Z2	9.34	0.64
DIPK_Z1	5.50	0.38
MIBK_Z1	8.51	0.59
MIBK_Z2	6.37	0.44
DPCP_Z1	8.73	0.60
DPCP_Z2	7.94	0.55

Table 5.7. Max adsorption and max adsorption per area of zeolite loaded nonwovens

As stated previously DPCP was chosen to mimic VX based on molecular size. The results show that the average adsorption of DPCP on the zeolite loaded nonwoven samples was 0.58mg/cm^2 which is approximately three orders of magnitude greater than the lethal dermal limit shown in Table 5.6. Both MIBK and DIPK were chosen to mimic GB based on molecular size and the average adsorption of MIBK on the zeolite loaded samples was 0.52mg/cm^2 and the average adsorption of DIPK was 0.38mg/cm^2. These adsorptions are 7.7 and 5.6 times, for MIBK and DIPK respectively, greater than the lethal dermal limit show in Table 5.6.

5.2.2.3   mPS Loaded Nonwoven Samples

Samples loaded with mPS particles had the same loading level as the zeolite samples

(4.3 g/ft^2 ± 10%). The data was once again normalized by absorbance in mg of test

compound per mg of mPS particle loaded on the sample (Figure 5.21) and the mass of

the nonwoven was not taken into account. Sample mass, actual mass gain and the

calculated theoretical maximum adsorption are tabulated in Table 5.8.

Sample ID	Final Sample Mass (mg)	mPS Particle Mass (mg)	Max Test Compound Adsorption (mg)	Calculated Max Test Compound Adsorption (mg)
IsoP_P2	142.3	67.90	13.42	2.58
IsoP_P3	170.8	66.60	16.59	2.53
DIPK_P1	171.2	66.10	10.67	3.11
DIPK_P2	160.3	63.10	10.97	2.97
MIBK_P1	169.7	62.70	13.00	2.82
MIBK_P2	167.8	66.40	10.64	2.99
DPCP_P1	166.1	66.50	9.43	5.72
DPCP_P2	166.6	62.20	9.83	5.35

Table 5.8. Nonwoven sample mass, particle mass, maximum measured adsorption and theoretical calculated maximum adsorption for mPS loaded nonwoven samples

It would be expected to observe the same trend in adsorption as observed for the

zeolite loaded samples (samples with a greater mass of particles loaded adsorbed

greater amounts of the test compound). However, this trend was not observed for the

mPS loaded nonwoven samples (Table 5.8 and Figure 5.21). For example MIBK P1

adsorbed 13.0 mg of MIBK (62.7 mg of mPS particles loaded on to the sample) while

MIBK P2 adsorbed 10.6 mg of MIBK (66.4 mg of mPS particles loaded on to the sample).

This difference was less prominent in the two larger test compounds (less than 0.5 mg

difference for DIPK and DPCP samples). It is thought that this could be due to the mPS particles agglomerating. It was noted previously (Section 3.1, Figure 3.2) that the mPS agglomerate readily which reduces the number of particles that are accessible resulting in a lower adsorption. Comparing mPS loaded samples with similar loadings (MIBK P1, DIPK P2 and DPCP P2 with 62.7mg, 63.1mg, and 62.2mg respectively) sorption was greatest for the smallest test compound molecule (MIBK) and least for the largest test compound molecule (DPCP).
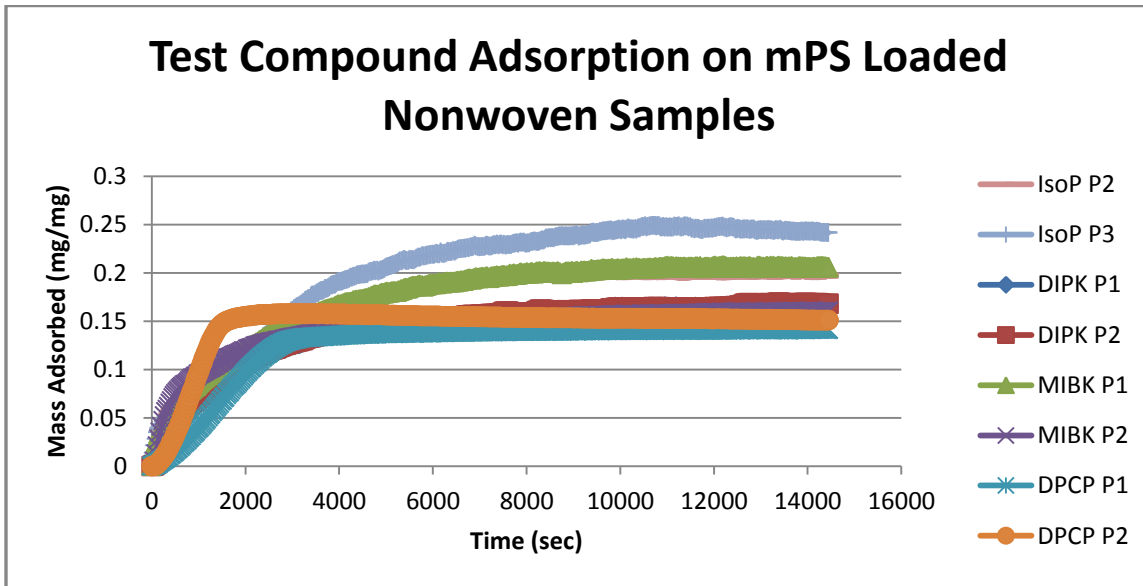
Figure 5.21. Results of test compound adsorption on mPS loaded mixed dpf PET nonwoven samples

All mPS loaded samples adsorbed significantly more of a given test compound than the calculated theoretical maximum, Figure 5.22. Again dependence was observed between amount adsorbed and molecular size. The mPS samples had an average adsorption of 0.22 mg isopropanol/mg sample (~590% greater than the theoretical adsorption) and

123

0.15 mg DPCP/mg sample (~173% greater than the theoretical adsorption). This data indicates that the assumption of pure physical adsorption was incorrect.

The mPS particles were amine modified, therefore it is likely that some of the adsorption occurring is due to chemisorption. The presence of chemisorption allows for the use of the Langmuir surface area which would account for some of the discrepancies observed (Figure 5.22). While isopropanol, MIBK and DIPK still adsorb more than the calculated theoretical maximum, DPCP does not. Chemisorption therefore properly models the adsorption process. It was likely that the remaining test compounds were not only adsorbing onto the mPS particles but also diffusing into the polymer matrix of the mPS particles via solution diffusion mechanism. This theory was then tested using PS free fall C-CP^{TM} fibers which will be discussed in Section 5.2.2.5.
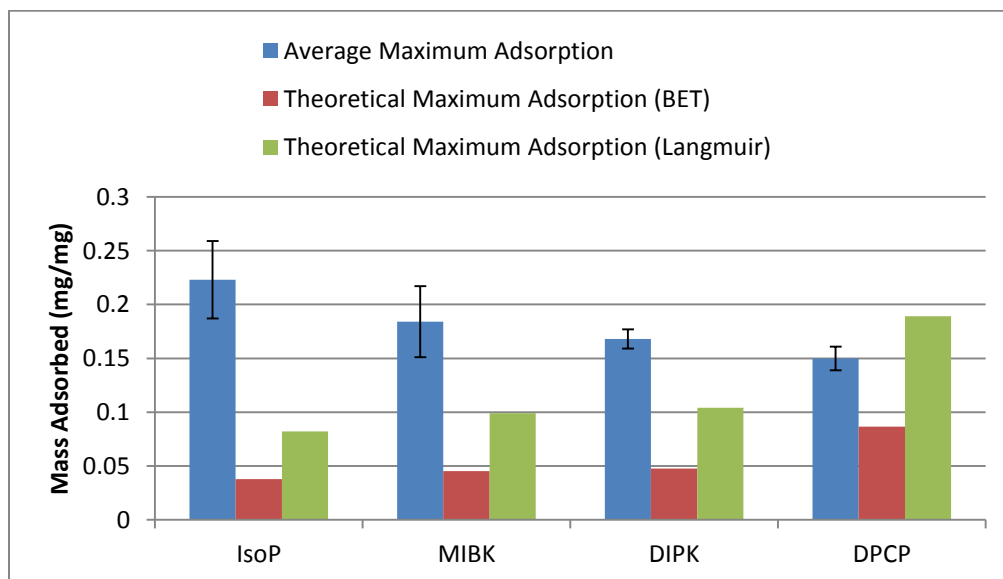
Figure 5.22. Comparison of average maximum adsorption and calculated theoretical maximum adsorption (using BET and Langmuir surface area) for mPS loaded samples

The protective capacity of each sample was determined by comparing the lethal dermal exposure limits (Table 5.6) to the calculated maximum adsorption of each test compound per area of sample (Table 5.9). The average adsorption of DPCP on the mPS loaded nonwoven samples was 0.67mg/cm^2 which was again more than three orders of magnitude greater than the lethal dermal exposure limit of VX. The average adsorption of DIPK by the mPS loaded samples was 0.75mg/cm^2 and average adsorption of MIBK was 0.82mg/cm^2 both of which are more than 10 times greater than the lethal dermal exposure limit for GB, indicating that all samples can sufficiently protect the wearer from a lethal dose of the simulated CWA's.

Sample ID	Max Adsorption Mass (mg)	Max Adsorption per Area (mg/cm^2)
IsoP_P2	13.42	0.93
IsoP_P3	16.59	1.14
DIPK_P1	10.67	0.74
DIPK_P2	10.97	0.76
MIBK_P1	13.00	0.90
MIBK_P2	10.64	0.73
DPCP_P1	9.43	0.65
DPCP_P2	9.83	0.68

Table 5.9. Max adsorption and max adsorption per area of mPS loaded nonwovens

5.2.2.4 50/50 Loaded Nonwoven Samples

The next set of samples contained equal masses of both zeolite and mPS particles. In order for the amount of each particle type present on the sample to be accurately known the particles were loaded onto the surface one at a time. For the initial set of 50/50 samples, the mPS particles were loaded first (target loading of 2.15 g/ft^2 ± 10%),

125

dried to a constant mass in a vacuum oven set at 60°C and weighed to obtain the mass of mPS particles loaded. The zeolite particles were then loaded on top of the mPS particles already present on the sample (target loading of 2.15 g/ft^2 ± 10%). A second set was made with the particles loaded in reverse order. Sample mass, actual mass gain and the calculated theoretical maximum adsorption for both sets of 50/50 samples are tabulated in Table 5.10 and Table 5.11, respectively. The theoretical maximum adsorption was calculated for the mass of each particle type present on the sample (as done previously, using the Langmuir surface area for the mPS particles) and then the sum of the two values was used for the final calculated theoretical maximum seen in Table 5.10 and Table 5.11.

Sample ID	Final Sample Mass (mg)	Zeolite Particle Mass (mg)	mPS Particle Mass (mg)	Max Test Compound Adsorption (mg)	Calculated Max Test Compound Adsorption (mg)
IsoP_ZP1	135.0	31.80	30.10	7.73	7.49
IsoP_ZP2	126.6	29.70	34.80	9.31	7.55
DIPK_ZP1	165.1	30.3	38.00	8.48	9.98
DIPK_ZP2	170.6	29.9	39.30	9.71	10.04
MIBK_ZP1	163.0	31.30	33.00	8.57	9.21
MIBK_ZP2	170.6	32.90	33.30	7.27	9.55
DPCP_ZP1	159.4	29.5	35.8	8.91	17.47
DPCP_ZP2	145	30.1	35.3	8.74	17.60

Table 5.10. Nonwoven sample mass, particle mass, maximum measured adsorption and theoretical calculated maximum adsorption for 50/50 mPS loaded first nonwoven samples

Sample ID	Final Sample Mass (mg)	Zeolite Particle Mass (mg)	mPS Particle Mass (mg)	Max Test Compound Adsorption (mg)	Calculated Max Test Compound Adsorption (mg)
IsoP PZ1	134.6	36.90	29.30	10.34	8.23
IsoP PZ2	140.5	33.70	30.10	9.75	7.79
DIPK PZ1	157.5	32.3	35.20	13.32	10.09
DIPK PZ2	160.9	36.7	36.60	13.41	11.11
MIBK PZ1	131.4	31.00	30.30	6.98	8.89
MIBK PZ2	130.2	31.00	33.10	14.98	9.17
DPCP PZ1	153.2	35.2	29.3	12.87	18.32
DPCP PZ2	155.6	33.6	33	9.29	18.43

Table 5.11. Nonwoven sample mass, particle mass, maximum measured adsorption and theoretical calculated maximum adsorption for 50/50 mPS loaded first nonwoven samples

The effect of the order in which the particles were loaded onto the nonwoven made a significant difference in the amount sorbed for both isopropanol and DIPK but not for MIBK and DPCP. Since the mPS loaded samples had sorbed more of the test compounds than the zeolite particles (9.43-16.59 mg as compared to 5.50-9.67 mg, respectively) it was expected that the second set of 50/50 samples would have greater sorption since the mPS particles were the last to be loaded.
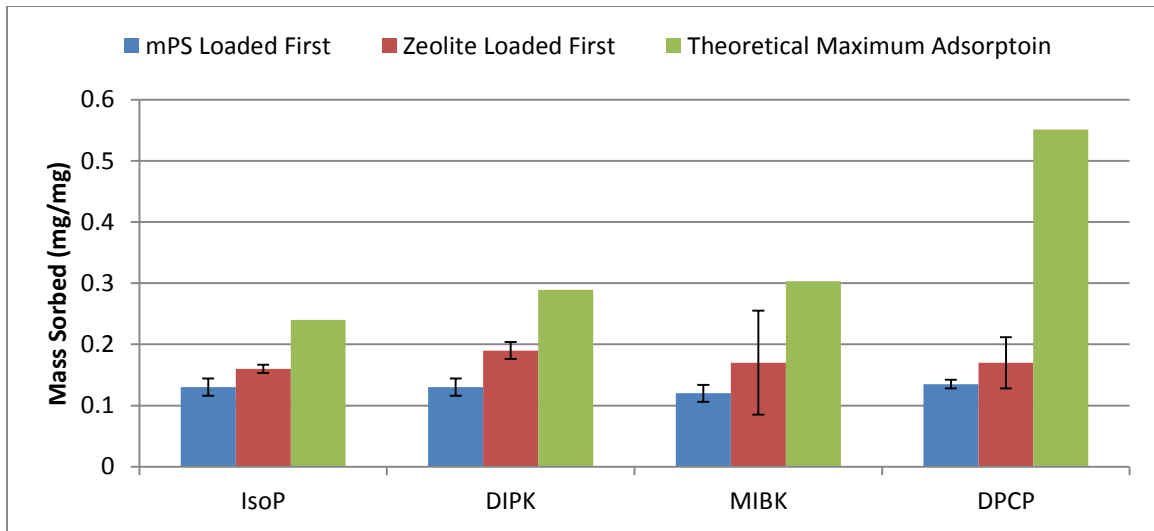
Figure 5.23. Comparison of average maximum adsorption and calculated theoretical maximum adsorption on 50/50 mPS loaded first mixed dpf PET nonwoven samples

The protective capacity of each sample was determined by comparing the lethal dermal

exposure limits (Table 5.6) to the calculated maximum adsorption of each test

compound per area of sample (Table 5.12). The 50/50 samples with the zeolite particles

loaded first had a greater average maximum adsorption per area. The average

adsorption of DPCP on both 50/50 loaded nonwoven samples was 0.61 and 0.76

mg/cm^2, respectively, which was more than four orders of magnitude greater than the

lethal dermal exposure limit of VX. The average adsorption of DIPK by the 50/50 mPS

loaded first samples was 0.55 mg/cm^2 and average adsorption of MIBK was 0.63

mg/cm^2, both of which are approximately 10 times greater than the lethal dermal

exposure limit for GB. The 50/50 zeolite loaded first sample had an average adsorption

of 0.76 mg/cm^2 for DIPK and of 0.92 mg/cm^2 for MIBK which was greater than 10 times

the lethal dermal exposure limit for GB, indicating that all samples can sufficiently

protect the wearer from a lethal dose of the simulated CWA's.

Sample/Test Compound		Average Max Adsorption Mass (mg)	AverageMax Adsorption per Area (mg/cm^2)
50/50 mPS Loaded First	IsoP	8.52 (1.1)	0.59 (0.08)
	MIBK	9.10 (0.87)	0.63 (0.06)
	DIPK	7.92 (0.92)	0.55 (0.06)
	DPCP	8.83 (0.12)	0.61 (0.01)
50/50 Zeolite Loaded First	IsoP	10.05 (0.42)	0.69 (0.03)
	MIBK	13.36 (0.06)	0.92 (0.004)
	DIPK	10.98 (5.7)	0.76 (0.39)
	DPCP	11.08 (2.5)	0.76 (0.17)

Table 5.12. Max adsorption and max adsorption per area of all 50/50 loaded nonwovens

By combining the both the mPS and zeolite particles adsorption capacities close to or equivalent to pure mPS loaded samples were obtained (Figure 5.24). Zeolite particles are relatively inexpensive adsorbents which are readily available and contain very high surface areas, hence their incorporation into this research. The mPS particles, however, are specially synthesized and therefore a more expensive product. Even though they have a decreased surface area they are able to sorb greater amounts of test compounds due to chemisorption. A combination of the two particles provides a cost efficient means to providing adequate protective capacity to the wearer from a lethal dose of the simulated chemical warfare agents.
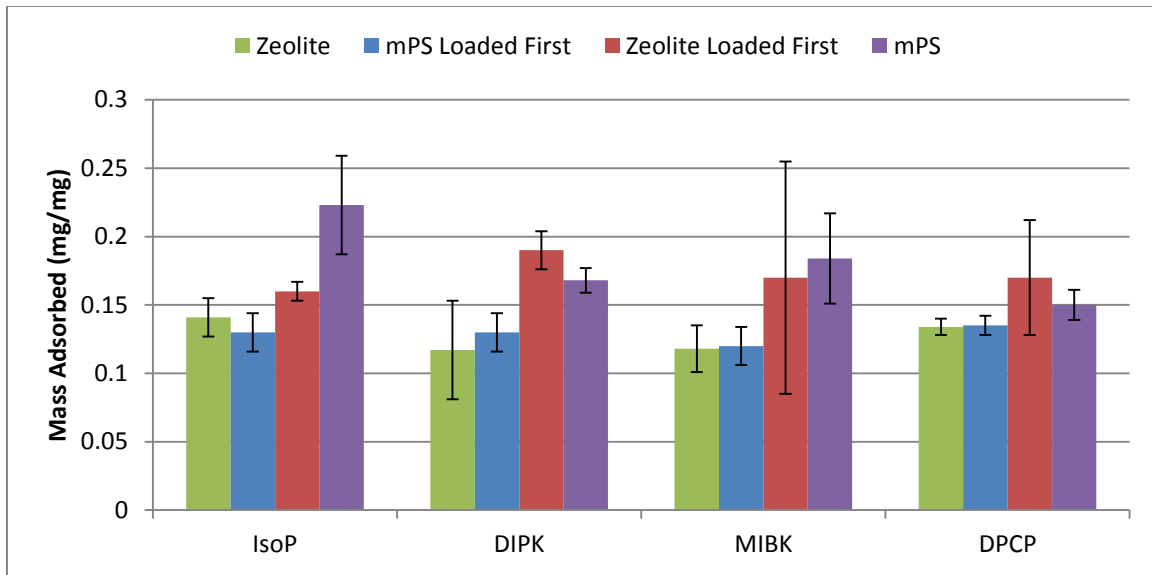
Figure 5.24. Comparison of average test compound sorption for zeolite loaded, mPS loaded first, zeolite loaded first and mPS loaded nonwoven samples

5.2.2.5 Melt Extruded PS Free Fall Samples

The results obtained for the mPS loaded nonwoven samples indicated that the test

compounds (IsoP, MIBK and DIPK in particular) were not adsorbing just on to the surface

of the particles but they were also absorbing into the polymer matrix. Therefore

samples of melt extruded PS C-CP[TM] free fall (polymer which is drawn due to the pull of

gravity and no other means) were run in the microbalance chamber with each test

compound. The absorption results, presented in Figure 5.25, confirmed the absorption

of both DIPK and MIBK into the PS free fall. The PS fiber samples absorbed

approximately a third of their mass in DIPK and MIBK test compounds while both

isopropanol and DPCP were barely absorbed.
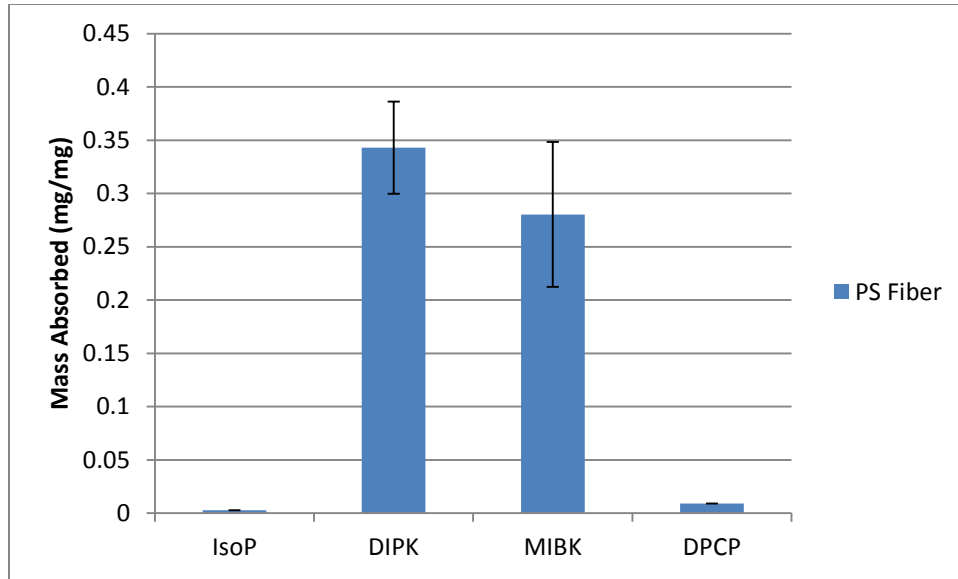
Figure 5.25. Average mass of test compound absorption per mass of PS free fall sample

Results obtained from static testing were confirmed via TGA (Figure 5.26). After the completion of the static test samples were immediately removed, weighed and a portion of the sample (~10 mg) was placed in the TGA which were run at 20°C/min to 600°C. The samples were not purged because total mass loss needed to be captured in the TGA themogram. A control run of an untested PS fiber sample was run first and, as shown in Figure 5.26, both the isopropanol and DPCP samples have identical thermograms indicating minimal absorption of either test compound. The samples that absorbed MIBK and DIPK lost approximately 26.5% of their mass before the onset of degradation of the polymer, which agrees with the static testing data.

131
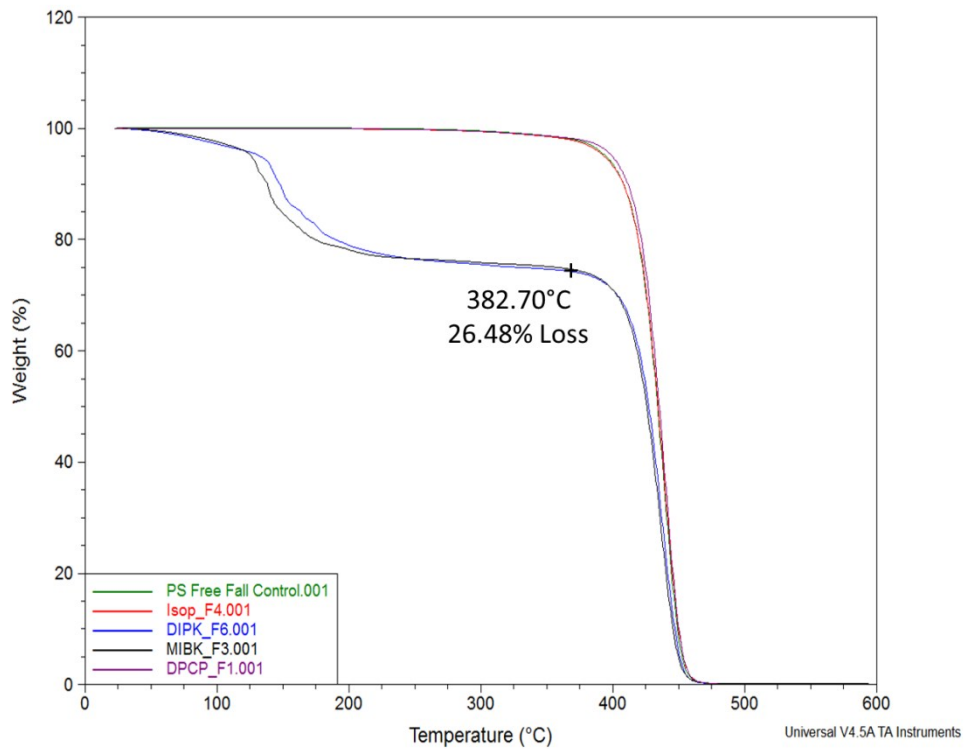
Figure 5.26. TGA thermogram of PS fiber samples, heated at a rate of 20°C/min to 600°C with no purge, immediately following static testing

These absorption results were also confirmed visually by examining the sample after testing was complete. During preparation of the sample for thermal analysis it was noted that the DIPK and MIBK samples were very pliable (due to plasticization) while the isopropanol and DPCP were still very rigid and brittle (Figure 5.27).
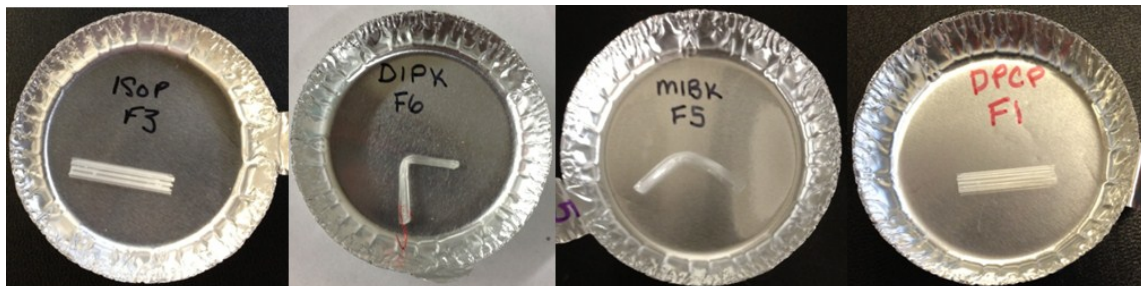
Figure 5.27. Photos of PS fiber samples after testing with each of the four test compounds

5.2.3 Dynamic Testing

After assessing the protective capacity of the composite in a static environment it was then subjected to dynamic testing to determine its ability to adsorb test compound vapors as they passed through the composite. The breakthrough time, which is the time required for the vapor to penetrate composite and reach the sensor, would be an indication of the ability of the composite to protect the wearer from a chemical threat. Typically analysis and detection of the breakthrough of chemical compounds was measured using a gas chromatograph coupled with a detector such as a flame ionization or mass spectrometer.[38, 97] However, a more economical means of detecting volatile organic compounds or chemical warfare agents is by the use of chemical sensors, which was employed for this research.[98, 99]

A schematic of the test set up used is shown in Figure 5.28 which incorporated a SC-210 Chemical Detection System (Seacoast Science, Inc.) to determine breakthrough of the test compound. The SC-210 is comprised of 8 chemicapacitive sensors. Each sensor has two conducting electrodes separated by a polymer which serves as the dielectric material for the capacitor. As the test compound passes through the sensor it interacts with the dielectric material causing physical changes to the polymer, such as swelling due to absorption. These changes affect the capacitance of the device, altering the electrical characteristics which are measured and recorded. The magnitude of the variation in capacitance can typically be used to determine the concentration of the test compound present in the sensor.[100]

Preliminary testing was performed to determine if the test set-up would work as shown, the type of data that would be obtained and what parameters would be important for future testing.   The test gas used was 86 parts per million (ppm) diethylketone (DIEK) in a balance of nitrogen (Airgas). This concentration was chosen based on the lower limit of detection of DIEK (1.5 ppm according to the manufacturer of the sensor) and because chemicapacitors are more likely to exhibit a linear response when measuring low concentrations.[98] The test compound was delivered to each sample at 2 mL/min (controlled by a flow meter) based on previous research.[97] Ideally the same test compounds used for static testing would be used again for dynamic testing, however, those compounds could not be obtained as a premixed vapor. Therefore, the closest analog that would still mimic a CWA based on molecular size was chosen (DIEK).   The data, temperature and humidity were collected and displayed in real time through the associated software on a computer.
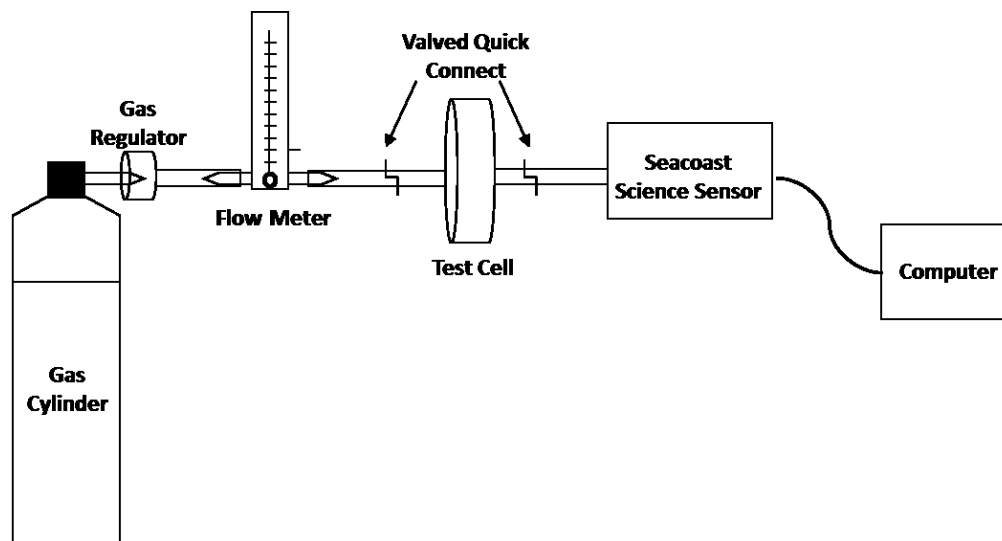
Figure 5.28. Schematic of dynamic flow testing set-up

134

5.2.3.1 Sensor Response

Testing began by determining the sensors response to both dry N_2 gas and the test compound, DIEK. Both gases were passed through the test setup (with no sample present) at 2 mL/min; the response of the sensor is presented in Figure 5.29. The results show an immediate response by the sensor to both gases. The nitrogen caused a decrease in the measured capacitance while the DIEK caused an initial increase in capacitance followed by a decrease. It should be noted that while four sensors had a response to N_2 and two responded to DIEK, the sensor with best response to DIEK (sensor 2) was chosen for all of the measurements.

According to Hierlemann *et al.* the output of a chemicapacitor reflects the permittivity of its dielectric material and the degree of change depends on four factors:[101]

1. Modifications to the chemical structure of the dielectric material due to reversible weak interactions, such as hydrogen bonding, dipole-dipole and van der Waals, with the test compound;

2. The amount of swelling of the dielectric material due to absorption of the test compound;

3. The permittivity of the test compound;

4. The amount of the test compound that is absorbed into the dielectric material.

It is thought that the response of the sensor to N_2 is not due to the interaction between the dielectric material and N_2, which is an inert gas, but instead due to the removal of

135

water from the sensor. This hypothesis is supported by the decrease in humidity (~6%) that was observed for each run. In addition, while the exact polymers used within the chemicapacitive microsensor were not reported, a paper published by the manufacturer has listed several polymers that have been used for targeted group of test compounds (nonpolar hydrocarbons, low polarity hydrocarbons, polar VOCs, etc.) as well as the dielectric constants for those polymers.[99] The polymers targeted to respond to low polarity hydrocarbons, such as DIEK, have a dielectric constant of ~4.[99, 102] Water on the other hand has a dielectric constant of 80; therefore the removal of water from the sensor would cause a decrease in the response due to decreasing the dielectric constant (or relative permittivity) which causes a decrease in the capacitance.[102] This run was repeated three times to determine how reproducible the measurements were and, as can be seen in Figure 5.29 A, the runs were very consistent.

The DIEK caused an initial rise in the capacitance until a maximum was reached and then the response decreased and leveled out. This response was due to absorption of DIEK (dielectric constant of 17.3) into the polymer (dielectric constant ~4) causing an increase in the relative permittivity and the measured capacitance.[102] However, the absorption of the test compound also caused the polymer to swell. Since the polymer is located within a fixed space in the microsensor, as it expands it can seep out of the capacitor gap causing a decrease in the response, according to Patel *et al.*[99] Swelling of the polymer reduces the density of polymer between the capacitor plates causing a decrease in the permittivity of the material as well. This occurs when the sensor is

136

exposed to a constant concentration of the test compound.[99] As can be seen for each of the DIEK runs (Figure 5.29 B), the sensor reaches a maximum and then almost immediately begins to decrease due to the constant concentration of test compound flowing through the sensor. The time required to reach this maximum for each of the three runs varied slightly (6, 4 and 9 seconds, respectively).
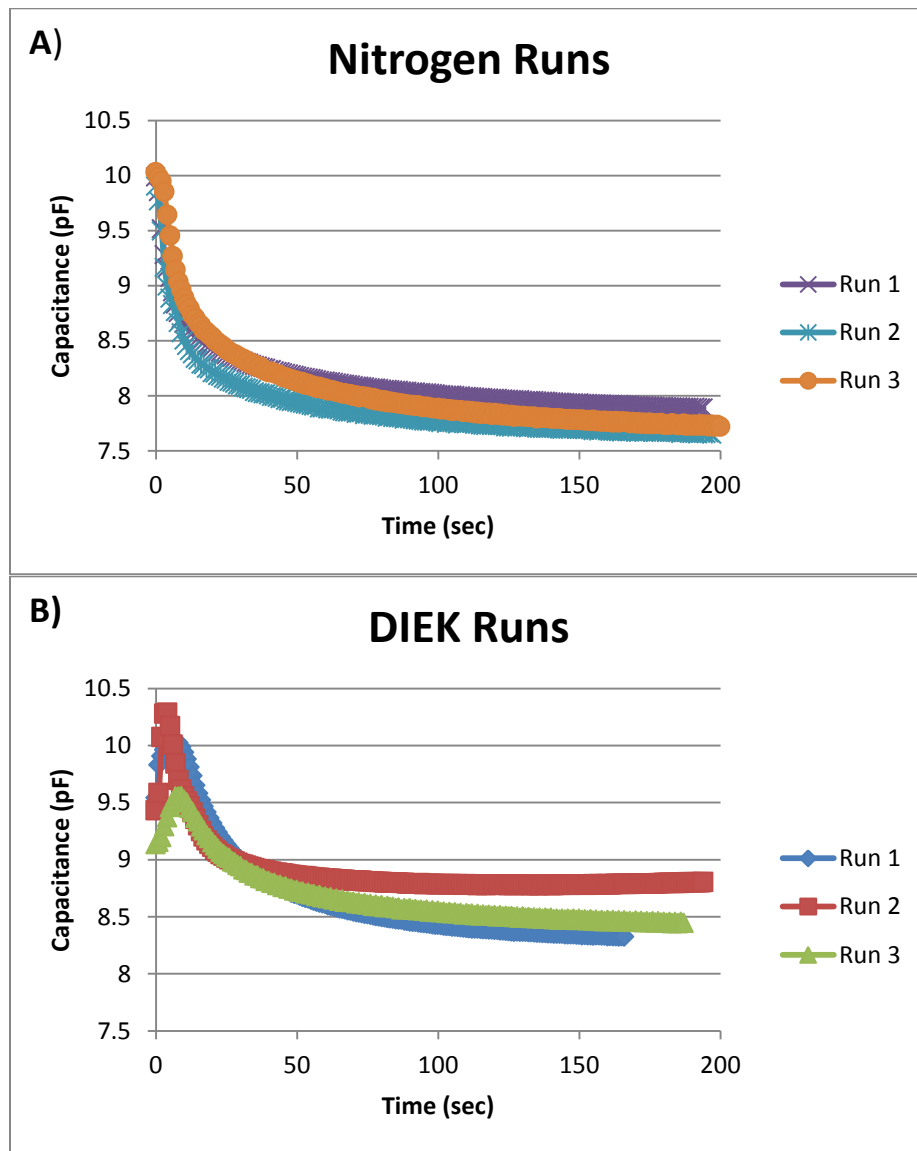
Figure 5.29. SC-210 Sensor response to A) dry N_2 gas and B) DIEK

137

5.2.3.2 Initial Testing

Several different samples were tested to determine how the response of the sensor changed in the presences of the following samples: those without adsorptive particles (C-CP™ nonwoven), with adsorptive particles (zeolite loaded sorptive functional layer) and in composite form (2nd generation, Figure 4.31). Prior to testing the samples were cut to have 48mm diameters and then dried at 60°C to a constant mass. Samples were placed in a desiccator to equilibrate to room before testing.
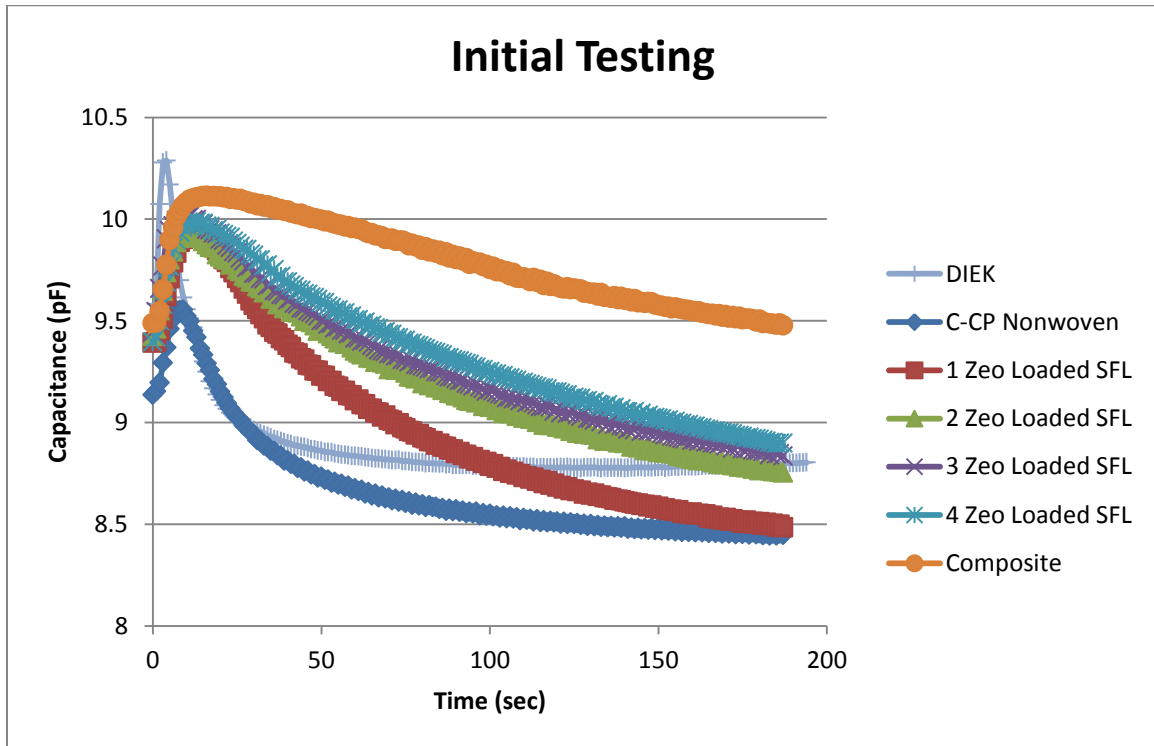
Figure 5.30. Sensor response to DIEK through a C-CP™ nonwoven, zeolite loaded sorptive functional layers (SFL) and the composite

As can be seen by the results (Figure 5.30), each sample type resulted in a different response from the sensor. The C-CP™ nonwoven, which did not have particles loaded on its surface, had a response very similar to DIEK runs with no sample present, as would be expected. A maximum capacitance was reached at approximately 9 seconds

138

which was the upper end of the range obtained in Section 5.2.3.1 for blank DIEK runs. The sorptive functional layers (see Section 4.2.4 for structure) loaded with zeolite particles (4.3 g/ft^2) reached a maximum capacitance between 10-13 seconds. As would be expected, the presence of the zeolite particles along with the structure of the sorptive functional layer caused an increase in time required to reach a maximum capacitance. In addition, the breadth of the peak had increased as compared to both DIEK and the C-CP^{TM} nonwoven, indicating it took longer for the sensor to detect a steady maximum concentration of the test compound. This was due to the adsorption of DIEK by the particles and the reduced flow rate due to the structure of the sample which caused a higher pressure drop across the sample and an increase in the tortuosity of the path the gas molecule had to travel. An increase in the number of layers of zeolite loaded sorptive functional layers tested also caused the breadth of the peak to expand. The most drastic change in the peak breadth was due to the composite sample which also had the longest time before the sensor reached its maximum capacitance (16 seconds). These results indicate that the composite structure does indeed provide more protection by adsorbing and reducing the breakthrough of the test compound.

5.2.3.3 Composite Testing

Both the 1st generation composite structure (Figure 4.1) loaded with zeolite particles (16 g/ft^2) and the 2nd generation composite structure (Figure 4.31) loaded with a 50/50 mixture of mPS and zeolite particles (4.3 g/ft^2) were examined as well as a control for

139

each which did not contain particles. The samples were prepared and tested as

described in Section 5.2.3.2. The sensor response is presented in

Figure 5.31.
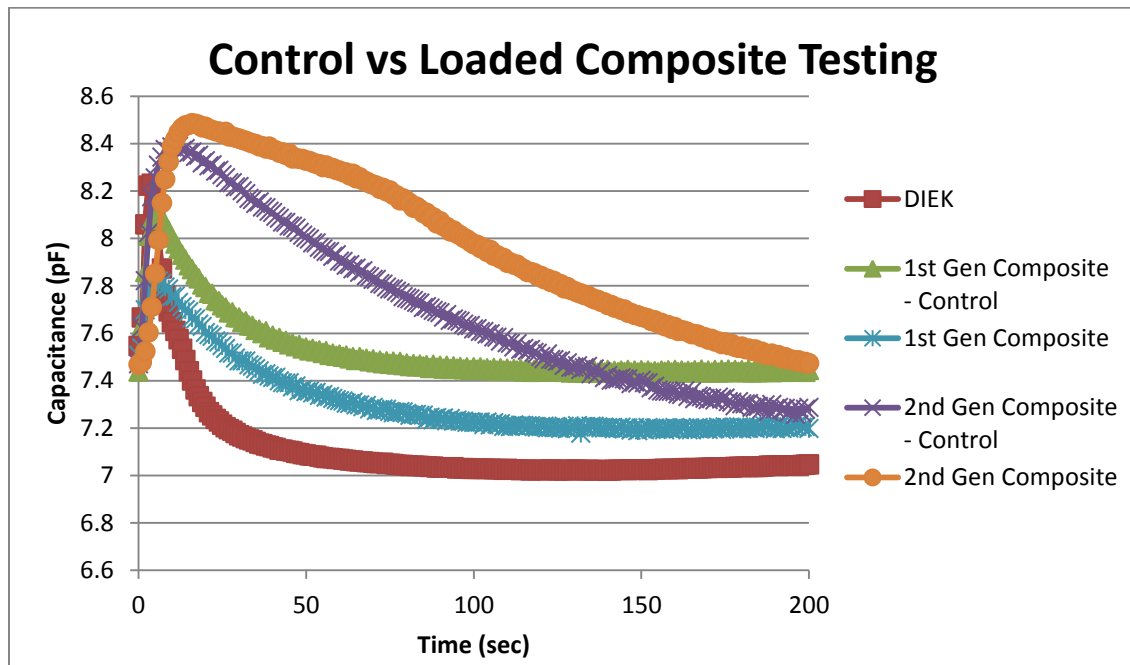
Figure 5.31. Sensor response to DIEK through 1st generation composites (control and zeolite loaded) and 2nd generation composites (control and 50/50 mPS/zeolite loaded)

There was a significant difference between the 1st and 2nd generation composites. The

sensor reached a maximum capacitance at 6 seconds for both 1st generation composite

samples where as it took 12 and 16 seconds to reach a maximum capacitance for the 2nd

generation composite control and 50/50 loaded samples, respectively. The time

required to reach a maximum capacitance for the 1st generation samples seemed

shorter than expected (based off of initial testing in Section 5.2.3.2). However, the 1st

generation composites with the original particle loading level (16 g/ft^3) had adhesion

140

problems due to significant amounts of dusting as discussed in Section 5.1.1. It is thought that the lack of proper adhesion throughout the sample contributed to the shorter time by providing the gas molecules a path with less resistance allowing them to breakthrough faster.

The breadths of the peaks for both 2nd generation composites were also substantially wider than either 1st generation peak. As would be expected, the addition of particles to either composite structure caused the breadth of the peak to increase due to adsorption of DIEK by the particles. In addition it can be seen that the 2nd generation composite structure itself caused a significant increase in the peak breadth. This is most likely due to the increased number of flow restrictive functional layers present in the composite as well as the added layers of binder present. The 1st generation composite had two flow restrictive functional layers (one located within the sorptive functional layer) while the 2nd generation composite had three (one also located within the sorptive functional layer).

These results indicate the 2nd generation composite structure loaded with 50/50 mixture of mPS and zeolite particles provides significantly more adsorption and protection as compared to both the control 2nd generation composite and the 1st generation composite (unloaded and loaded with particles). However, the results obtained are qualitative and have their limitations. In order to determine the actual level of protection, the concentration and permeation rate of the test compound

through the composite would need to be determined. This was not used with this test set-up because only a single concentration of the test compound was purchased and the equipment needed for accurate dilution of the test compound gas was not available. In addition, as the sensor was used more the results became less consistent. A common problem with this sensor is output drift due to chemical interactions of the polymer with the environment.[99] It was also noticed that the humidity affected the sensor results, which has been noted in other work, and though attempts were made to regulate the humidity, the sensor response remained inconsistent.[97, 99] While the sensor did not provide quantitative data for the research performed it was useful as a preliminary indication in the difference between samples and offered a cost effective means to test the samples in a dynamic environment.

6 Conclusions

This work investigated the production and characterization of a multi-functional fiber-based composite for use in protective clothing. The investigation of the fiber-based composite involved the characterization of two different sorptive particles, production of the sorptive functional layer and composite structure, analysis of the physical and mechanical properties of the composite, effective loading of the sorptive particles into the composite structure and determination of the protective capacity of the composite against simulated CWAs.

6.1   Particle Characterization

Both zeolite and mPS particles were investigated for use as adsorbents within the sorptive functional layer of the composite. The available surface area of each particle was measured in order to calculate the theoretical maximum adsorption of each test compound on each particle type. In all cases it was determined that the theoretical maximum adsorption was higher than the experimentally measured adsorption capacity for the zeolite particles due to residual bound and structural water within the pores of the particles which is not removed until temperatures above 300°C.

6.2   Development of the Composite Structure

The two functional components used within the composite were the sorptive layer and the flow restrictive layer. Use of C-CP^{TM} fibers to construct the sorptive functional layer allowed for greater retention of particles due to loading within the grooves which was

143

confirmed via SEM. The flow restrictive layer consisted of a meltblown PP nonwoven which had fiber diameters ranging from 0.05 μm to 5.7 μm (average diameter of 0.67 μm) and pore sizes ranging from 6.6 μm to 34 μm (average pore size 8.1 μm). These layers worked as a cohesive material due to the use of a binder which prevented delamination of the composite.

Upon designing the composite structure it was determined the composite must be strong enough to prevent rupture of the most delicate layer, the flow restrictive layer. Several approaches were taken in order to strengthen the composite including examining the use of a different binder, modification to the initial binder and the addition of a support layer. However it was determined the greatest adhesion was obtained by the Freudenberg which was also the lightest weight material. In addition, a layer of lightweight fiberglass fabric was incorporated to provide the required increase in strength in order to protect the flow restrictive layer.

The air permeability and pore size of several composite structures were examined. The results indicated that the limiting factor in the pore size was not the meltblown PP layer but the Freudenberg binder. Upon thermal bonding of the composite structure the binder became 'film' like and significantly reduced the pore sizes and resulting air permeability. Samples that did not contain the Freudenberg had both larger pore sizes (0.8-1.0 μm as compared to 0.35 μm, referencing smallest detected pore sizes) and higher air permeability (4.2-7.5 cfm/ft^2 as compared to 0.7-2.9 cfm/ft^2).

The individual component layers that made up the composite structure were also characterized to determine their pore sizes and air permeability. As was expected, the meltblown layer had the smallest detected pore size (6.58 ± 0.3 μm), however, it was determined that the 3 layer PET C-CP^{TM} carded nonwoven and the knitted outer layer (tested under minimal tension) had similar diameters for the smallest detected pore (6.86 ± 1.3 μm and 7.82 ± 0.25 μm respectively). The pore size distribution of the meltblown PP nonwoven, however, was significantly different than what was obtained for the carded nonwoven and knitted outer layer with the majority of its pores being 7-8 μm as compared to 30-80 μm and 60-100 μm for the carded nonwoven and knitted fabric, respectively. The measured pressure drop across the meltblown layer along with the air permeability confirmed its function as the flow restrictive layer.

The 2nd generation composite structure was developed which had the following attributes:

- Crimped C-CP^{TM} fibers provided a uniform sorptive functional layer;

- An increased number of meltblown layers a) reduced the number of particles lost during spraying and b) acted as a failsafe in case one layer ruptured;

- A support layer supplied the required strength to prevent rupture of the meltblown layer;

145

- The Fruedenberg binder provided consistent adhesion throughout the composite while also reducing the pore sizes causing an increase the residence time of the gas molecules (toxins) in contact with the adsorptive particles.

6.3 Composite Characterization and Testing

Uniform distribution of particles onto the surface of the sorptive functional layer was achieved through a spraying method and was confirmed via SEM. Upon fabrication it was determined that the initial loading level was too high due to an excessive mass of 'free particles' which were not physically retained by the grooves or by direct interaction with the fiber surface. These particles caused a significant amount of dusting and interfered with the adhesion of the sample. Incorporation of a layer of meltblown PP within the sorptive layer reduced the level of dusting and served a dual purpose by decreasing the amount of particles lost during spraying by providing another surface onto which the particles could load. A non-dusting loading level was also experimentally determined therefore alleviating this problem.

The maximum adsorption capacities of the samples were determined using an in-house developed static adsorption testing method in which a DCA was used as a recording micro balance and a heat source was used to vaporize test compounds. The test compounds were chosen to mimic chemical warfare agents based on molecular size due to the expected physical adsorption of the compounds. Samples loaded with only zeolite particles were able to adsorb $0.58 mg/cm^2$ of DPCP (used to simulate VX) which is

approximately three orders of magnitude greater than the lethal dermal limit of VX.

These samples were also able to adsorb 7.7 and 5.6 times more MIBK and DIPK (used to

simulate GB) than the dermal exposure limit of GB. Samples loaded with mPS particles

were able to sorb three orders of magnitude more than the lethal dermal limit of VX and

approximately 10 times more than the lethal dermal limit of GB. Static testing also

revealed that the mPS particles were not only physically adsorbing but also chemically

adsorbing the test compounds. When samples were loaded with equal amounts of mPS

and zeolite particles it was determined that the order of loading significantly affected

the adsorption capacity. Greater adsorption was obtained when the zeolite particles

were loaded first followed by the mPS particles. The combination of mPS and zeolite

particles resulted in adsorption capacities close to or equivalent to pure mPS loaded

samples. Therefore by combining the two particle types, a cost efficient, sorptive, fiber-

based composite can be produced which provides adequate protection to the wearer

from a lethal dose of chemical warfare agents based on the static adsorption testing

performed within this research.

Dynamic testing of composite samples was performed using a chemicapacitive sensor to

detect the breakthrough of a test compound and provide a comparative indication of

the protective capacity of tested samples. Samples containing adsorptive particles

clearly provided greater protection as compared to samples without adsorptive

particles. The most significant difference was obtained for composite structure due to

both adsorption of the test compound and reduction of flow rate. A reduction in flow

rate was due to the pressure drop across the sample and the tortuosity of path the test compound had to travel due to the structure of the composite. In addition, a comparison of the 2nd generation composite structure to the 1st generation resulted in the former providing greater protection. However, the results obtained were qualitative and have their limitations. In order to determine the actual level of protection, the concentration and permeation rate of the test compound through the composite would need to be determined.

7 Future Work

7.1 Composite Structure

During this research only a single meltblown structure was investigated for use as the flow restrictive layer. As discussed in Section 4.3 the meltblown layer had a very low extension before rupture and therefore a support layer had to be incorporated into the composite. Use of a meltblown or spunbond nonwoven that could withstand a greater extension before rupture could possibly prevent the need of a support layer which would reduce the number of layers required in the composite. In addition, other nanofiber webs production methods should be investigated such as ForceSpinning^{TM} (see Section 1.3.5). Since Forcespinning^{TM} can be used to spin both non-conductive and conductive solutions as well as solid materials that melt the polymer selection would be greatly increased.

In addition, integration of the sorptive and flow restrictive functional layers could significantly reduce the weight of the composite structure. At the time of this research the capability to produce C-CP^{TM} shaped fibers via a spunbond process was not available. The combination of fast production rates, a direct spun process and submicron shaped fibers could offer substantial benefits as compared to the C-CP^{TM} shaped carded nonwoven web and meltblown nonwoven that were used for this research. The direct production of a shaped fiber web would also remove the need for round binder fibers which were used within the carded nonwoven in this research.   The

149

removal of round binder fibers would increase the amount of shaped fiber content present and decrease the amount of binder within the composite structure. Other fiber shapes such as 'H' and 'Y' could also be investigated to determine if they provide greater loading capacities for the adsorptive particles.[96]
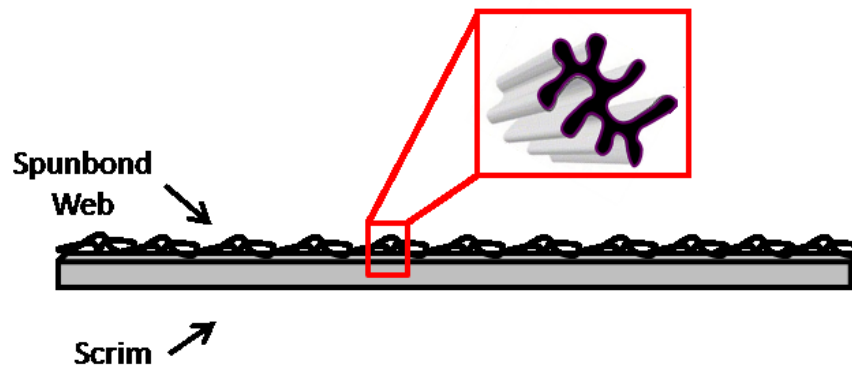
Figure 7.1. Schematic of spunbond nonwoven with C-CP[TM] fibers

7.2   Composite Testing

In order to more fully characterize the protective capacity of the fiber based composite that was developed during this research further dynamic testing should be performed, such as chemical permeation. As mentioned in Section 5.2.3 breakthrough detection and the permeation rate of chemicals through CPC is commonly measured using a gas chromatograph coupled with a detector such as a flame ionization or mass spectrometer due to the sensitivity of these analytical instruments.[38, 97] Testing according to ASTM F739, the Standard Test Method for Permeation of Liquids and Gases through Protective Clothing Materials under Conditions of Continuous Contact, should

150

be performed in order to provide a better comparison of the performance of the fiber based composites to materials that are currently being used as CPC.

Additional testing should be performed on the composite structure to further validate the performance and comfort of the composite. In order to determine the thermal comfort of the composite, testing such as moisture vapor permeability and water vapor flux should be conducted following ASTM E96, the Standard Test Method for Water Vapor Transmission of Materials, and ASTM F2298, the Standard Test Method for Water Vapor Diffusion Resistance and Air Flow Resistance of Clothing Materials Using the Dynamic Moisture Permeation Cell, respectively. Integrity of the composite structure should be examined using Federal Test Method Standard (FTMS) 191A Test Methods (TM) 5512 for bonding strength and TM2724 for delamination. Other physical properties of the composite should be examined such as torsional flexibility (FTMS101A TM2017), stiffness (FTMS191A TM5202) and abrasion resistance (FTMS191A TM5034).

References

(1) Lacombe, P.; Boutell, C. *Arms and Armour in Antiquity and the Middle Ages : Also a Descriptive Notice of Modern Weapons ; Translated from the French of M.P. Lacombe, and With a Preface, Notes, and One Additional Chapter on Arms and Armour in England;* Combined Books: 1996; pp 328p.

(2) Wilusz, E., Ed.; In *Military Textiles;* Woodhead Publishing Limited: Cambridge, England, 2008; pp 362.

(3) Scott, R. A., Ed.; In *Textiles for Protection;* Woodhead Publishing Limited: Cambridge England, 2005; pp 734.

(4) Romano, J. J. A.; Lukey, B. J.; Salem, H., Eds.; In *Chemical Warfare Agents: Chemistry, pharmacology, toxicology, and therapeutics;* CRC Press Taylor & Francis Group: Boca Raton, FL, 2008; pp 723.

(5) United Nations Office for Disarmament Affairs 1925 Geneva Protocol. *http://www.un.org/disarmament/WMD/Bio/1925GenevaProtocol.shtml* (accessed 10/13, 2012).

(6) Meselson, M.; Robinson, J. P. Chemical Warfare and Chemical Disarmament. *Scientific American* **1980**, *242*, 38-47.

(7) Sidell, F. R.; Takafugi, E. T.; Franz, D. R. *Textbook of Military Medicine: Medical Aspects of Chemical and Biological Warfare;* Office of The Surgeon General, Department of the Army: Washington, DC, 1997.

(8) U.S. Department of Health & Human Services Chemical Warfare: Classes of Chemical Agents. *http://sis.nlm.nih.gov/enviro/chemicalwarfare.html#a1* (accessed 2/1, 2013).

(9) AnonymousToxic Industrial Chemicals. *Journal of the Royal Medical Corps* **2002**, *148*, 371-381.

(10) Hincal, F.; Erkekoglu, P. Toxic Industrial Chemicals (TICs) - Chemical Warfare withouth Chemical Weapons. *FABAD Journal of Pharaceutical Sciences* **2006**, *31*, 220-229.

(11) Gilden, R. C.; Huffling, K.; Sattler, B. Pesticides and Health Risks. *Journal of Obstetric, Gynecologic, & Neonatal Nursing* **2010**, *39*, 103-110.

152

(12) Lejeune, K. E.; Dravis, B. C.; Yang, F. X.; Hetro, A. D.; Doctor, B. P.; Russell, A. J. Fighting nerve agent chemical weapons with enzyme technology. *Ann. NY Acad. Sci.* **1998**, *864*, 153-170.

(13) Bassil, K. L.; Vakil, C.; Sanborn, M.; Cole, D. C.; Kaur, J. S.; Kerr, K. J. Cancer health effects of pesticides. *Canadian Family Physician* **2007**, *53*, 1704-1711.

(14) Sanborn, M.; Kerr, K. J.; Sanin, L. H.; Cole, D. C.; Bassil, K. L.; Vakil, C. Non-cancer health effects of pesticides. *Canadian Family Physician* **2007**, *53*, 1712-1720.

(15) Wolfe, H. R.; Durham, W. F.; Armstrong, J. F. Exposure of Workers to Pesticides. *Archives of Environmental Contamination and Toxicology* **1967**, *14*, 622-633.

(16) Bureau of Labor Statistics Injuries, Illnesses, and Fatalities: Nonfatal occupational illness incidence rates by industry and category of illness, 2001. *http://www.bls.gov/iif/oshwc/osh/os/ostb1124.pdf* (accessed 10/13, 2012).

(17) Lee, S.; Obendorf, S. K. A statistical model to predict pesticide penetration through nonwoven chemical protective fabrics. *Text. Res. J.* **2001**, *71*, 1000-1009.

(18) Lee, S.; Obendorf, S. K. Barrier effectiveness and thermal comfort of protective clothing materials. *J. Text. Inst.* **2007**, *98*, 87-97.

(19) Hoechst Celanese *Dictionary of Fiber & Textile Technology;* Hoechst Celanese Corporation: Charlotte, NC, 1990; pp 218.

(20) Hutten, I. M. *Handbook of Nonwoven Filter Media;* Elsevier Ltd.: Oxford, UK, 2007; pp 473.

(21) Albrecht, W.; Fuchs, H.; Kittelmann, W., Eds.; In *Nonwoven Fabrics;* WILEY-VCH Verlag GmbH & Co. KGaA: Weinheim, 2003; Vol. 1, pp 748.

(22) Lim, H. A Review of Spun Bond Process. *Journal of Textile and Apparel, Technology and Management* **2010**, *6*, 1-13.

(23) Malkan, S. R. An overivew of spunbonding and meltblowing technologies. *Tappi Journal* **1995**, *78*, 185-190.

(24) Fedorova, N.; Pourdeyhimi, B. High strength nylon micro- and nanofiber based nonwovens via spunbonding. *Journal of Applied Polymer Science* **2007**, *104*, 3434-3442.

(25) Nonwovens Industry Reicofil Highlights Spunbond and Melt Blowing Lines. *http://www.nonwovens-industry.com/contents/view_breaking-news/2012-11-15/reicofil-highlights-spunbond-and-melt-blowing-lines/* (accessed 2/3, 2013).

(26) Kimberly Clark Wear it for Protection. Want it for Comfort. Kleengaurd Brand Saftey Product Catalog. **2008***, Winter*, 23-39.

(27) Dever, M.; Davis, W. T.; Hood, C. C. Development of an activated carbon loaded melt blown-spunbond laminate. *Tappi Journal* **1994***, 77*, 207-214.

(28) Brown, P. J.; Stevens, K., Eds.; In *Nanofibers and nanotechnology in textiles;* CRC Press LLC: Boca Raton, FL, 2007; pp 528.

(29) Lee, S.; Obendorf, S. K. Use of electrospun nanofiber web for protective textile materials as barriers to liquid penetration. *Text. Res. J.* **2007***, 77*, 696-702.

(30) Schreuder-Gibson, H.; Gibson, P.; Senecal, K.; Sennett, M.; Walker, J.; Yeomans, W.; Ziegler, D.; Tsai, P. Protective Textile Materials Based on Electrospun Nanofibers. *Journal of Advanced Materials* **2002***, 34*, 44-55.

(31) Reneker, D. H.; Fong, H., Eds.; In *Polymeric Nanofibers;* ACS Symposium Series 918; American Chemical Society: Washington, D.C., 2006; pp 430.

(32) Sarkar, K.; Gomez, C.; Zambrano, S.; Ramirez, M.; de Hoyos, E.; Vasquez, H.; Lozano, K. Electrospinning to Forcespinning^{TM}. *Materials Today* **2010***, 13*, 12-14.

(33) Shanmuganathan, K.; Fang, Y.; Chou, D. Y.; Sparks, S.; Hibbert, J.; Ellison, C. J. Solventless High Throughput Manufacturing of Poly(butylene terephthalate) Nanofibers. *Acs Macro Letters* **2012***, 1*, 960-964.

(34) Padron, S.; Patlan, R.; Gutierrez, J.; Santos, N.; Eubanks, T.; Lozano, K. Production and characterization of hybrid BEH-PPV/PEO conjugated polymer nanofibers by forcespinning (TM). *J Appl Polym Sci* **2012***, 125*, 3610-3616.

(35) Leonas, K. K. The Mechanism of Pesticide Transmission through Apparel Fabrics - a Comparison of Drop and Spray Exposure Methodologies. *Arch. Environ. Contam. Toxicol.* **1991***, 20*, 427-431.

(36) Csiszar, E.; Borsa, J.; Racz, I.; Obendorf, S. K. Reduction in Human Exposure to Pesticide Using Traditional Work Clothing Fabrics with Chemical Finishing: Carboxymethylation and Starch. *Archives of Environmental Contamination and Toxicology* **1998***, 35*, 129-134.

(37) Raheel, M.; Gitz, E. C. Effect of Fabric Geometry on Resistance to Pesticide Penetration and Degradation. *Archives of Environmental Contamination and Toxicology* **1985***, 14*, 273-279.

(38) Lee, S.; Obendorf, S. K. Statistical model of pesticide penetration through woven work clothing fabrics. *Arch. Environ. Contam. Toxicol.* **2005***, 49*, 266-273.

(39) Jain, R.; Raheel, M. Barrier Efficacy of Woven and Nonwoven Fabrics Used for Protective Clothing: Predictive Models. *Bulletin of Environmental Contamination and Toxicology* **2003***, 71*, 437-446.

(40) Zhang, X.; Raheel, M. Statistical Model for Predicting Pesticide Penetration in Woven Fabrics Used for Chemical Protective Clothing. *Bulletin of Environmental Contamination and Toxicology* **2003***, 70*, 652-659.

(41) DuPont DuPont Personal Protection Product Catalog. **2012**.

(42) Branson, D. H.; Ayers, G. S.; Henry, M. S. In *In Effectiveness of Selected Work Fabrics as Barriers to Pesticide Penetration;* Performance of protective clothing, ASTM STP 900; American Society for Testing and Materials: Philadelphia, PA, 1986; pp 114-120.

(43) Leonas, K. K.; Easter, E. P.; DeJonge, J. O. Effect of Fabric Characteristics on Pesticide Penetration through Selected Apparel Fabrics. *Bulletin of Environmental Contamination and Toxicology* **1989***, 43*, 231-238.

(44) Evans, K. M.; Hardy, J. K. Predicting solubility and permeation properties of organic solvents in viton glove material using Hansen's solubility parameters. *J Appl Polym Sci* **2004***, 93*, 2688-2698.

(45) Zellers, E. T. Three-Dimensional Solubility Parameters and Chemical Protective Clothing Permeation. 1. Modeling the Solubility of Organic sovents in Viton Gloves. *Journal of Applied Polymer Science* **1993***, 50*, 513-530.

(46) Zellers, E. T.; Zhang, G. Z. 3-Dimensional Solubility Parameters and Chemical Protective Clothing Permeation .2. Modeling Diffusion-Coefficients, Breakthrough Times, and Steady-State Permeation Rates of Organic-Solvents in Viton(r) Gloves. *J Appl Polym Sci* **1993***, 50*, 531-540.

(47) Pal, T.; Griffin, G. D.; Miller, G. H.; Watson, A. P.; Daugherty, M. L.; Vodinh, T. Permeation Measurements of Chemical-Agent Simulants through Protective Clothing Materials. *J. Hazard. Mater.* **1993***, 33*, 123-141.

(48) Schreuder-Gibson, H. L.; Truong, Q.; Walker, J. E.; Owens, J. R.; Wander, J. D.; Jones, W. E. Chemical and biological protection and detection in fabrics for protective clothing. *MRS Bull* **2003**, *28*, 574-578.

(49) U.S. Department of Health & Human Services Personal Protective Equipment (PPE) Classification Systems. *http://www.remm.nlm.gov/ppe_classification.htm* (accessed 11/18, 2012).

(50) U.S. Department of Health & Human Services PPE Classification System from OSHA and EPA. *http://www.remm.nlm.gov/osha_epa_ppe.htm* (accessed 11/18, 2012).

(51) U.S. Department of Health & Human Services Mission Oriented Protective Posture (MOPP) Gear: Military PPE. *http://www.remm.nlm.gov/MOPP.htm* (accessed 11/18, 2012).

(52) DOD 4120.24.M DSP Policies & Procedures. *Office of the Undersecretary of Defense (Acquisition, Technology and Logistics)* **2000**, *March*.

(53) Raushel, F. M. Bacterial detoxification of organophosphate nerve agents. *Curr. Opin. Microbiol.* **2002**, *5*, 288-295.

(54) Dyguda-Kazimierowicz, E.; Sokalski, W. A.; Leszczynski, J. Gas-phase mechanisms of degradation of hazardous organophosphorus compounds: Do they follow a common pattern of alkaline hydrolysis reaction as in phosphotriesterase. *J Phys Chem B* **2008**, *112*, 9982-9991.

(55) Richins, R. D.; Kaneva, I.; Mulchandani, A.; Chen, W. Biodegradation of organophosphorus pesticides by surface-expressed organophosphorus hydrolase. *Nat. Biotechnol.* **1997**, *15*, 984-987.

(56) Singh, A.; Lee, Y.; Dressick, W. ?. Self-Cleaning Fabrics for Decontamination of Organophosphorous Pesticides and Related Chemical Agents. *Adv Mater* **2004**, *16*, 2112-2115.

(57) Xiong, Y.; Zhan, C. G. Reaction pathways and free energy barriers for alkaline hydrolysis of insecticide 2-trimethylammonioethyl methylphosphonofluoridate and related organophosphorus compounds: Electrostatic and steric effects. *J. Org. Chem.* **2004**, *69*, 8451-8458.

156

(58) Zheng, F.; Zhan, C. G.; Ornstein, R. L. Theoretical studies of reaction pathways and energy barriers for alkaline hydrolysis of phosphotriesterase substrates paraoxon and related toxic phosphofluoridate nerve agents. *J. Chem. Soc. -Perkin Trans. 2* **2001**, 2355-2363.

(59) Chen, L.; Bromberg, L.; Schreuder-Gibson, H.; Walker, J.; Hatton, T. A.; Rutledge, G. C. Chemical protection fabrics via surface oximation of electrospun polyacrylonitrile fiber mats. *J. Mater. Chem.* **2009**, *19*, 2432-2438.

(60) Salter, B.; Owens, J.; Hayn, R.; McDonald, R.; Shannon, E. N-chloramide modified Nomex(A (R)) as a regenerable self-decontaminating material for protection against chemical warfare agents. *J. Mater. Sci.* **2009**, *44*, 2069-2078.

(61) Grandcolas, M.; Sinault, L.; Mosset, F.; Louvet, A.; Keller, N.; Keller, V. Self-decontaminating layer-by-layer functionalized textiles based on WO3-modified titanate nanotubes. Application to the solar photocatalytic removal of chemical warfare agents. *Appl. Catal. A-Gen.* **2011**, *391*, 455-467.

(62) Prasad, G. K.; Singh, B.; Vijayaraghavan, R. Respiratory protection against chemical and biological warfare agents. *Def. Sci. J.* **2008**, *58*, 686-697.

(63) Srivastava, A. K.; Shah, D.; Saxena, A.; Mahato, T. H.; Singh, B.; Verma, A. K.; Shrivastava, S.; Roy, A.; Shrivastava, A. R.; Gutch, P. K. Vapour breakthrough behaviour of carbon tetrachloride - a simulant for chemical warfare agent on ASZMT carbon. *J. Sci. Ind. Res.* **2012**, *71*, 748-756.

(64) LI, Y.; KOPER, O.; ATTEYA, M.; KLABUNDE, K. Adsorption and Decomposition of Organophosphorus Compounds on Nanoscale Metal-Oxide Particles - Insitu Gc-Ms Studies of Pulsed Microreactions Over Magnesium-Oxide. *Chem. Mat.* **1992**, *4*, 323-330.

(65) Sundarrajan, S.; Chandrasekaran, A. R.; Ramakrishna, S. An Update on Nanomaterials-Based Textiles for Protection and Decontamination. *J Am Ceram Soc* **2010**, *93*, 3955-3975.

(66) Grancaric, A. M.; Tarbuk, A.; Kovacek, I. Nanoparticles of Activated Natural Zeolite on Textiles for Protection and Therapy. *Chemical Industry & Chemical Engineering Quarterly* **2009**, *15*, 203-210.

(67) Breck, D. *Zeolite Molecular Sieves: Structure, Chemistry and Use;* John Wiley & Sons, Inc.: New York, NY, 1974; pp 771.

157

(68) Hudiono, Y. C.; Miller,A.Lee,,II; Gibson, P. W.; LaFrate, A. L.; Noble, R. D.; Gin, D. L. A Highly Breathable Organic/Inorganic Barrier Material that Blocks the Passage of Mustard Agent Simulants. *Ind Eng Chem Res* **2012**, *51*, 7453-7456.

(69) Satya, A. R.; Subramanian, S.; Seeram, R. Functionalized Cellulose: PET Polymer Fibers with Zeolites for Detoxification Against Nerve Agents. *J. Inorg. Mater.* **2012**, *27*, 332-336.

(70) Sing, K. S. W.; et al. Reporting Physisorption Data for Gas/Solid Systems with Special Reference to the Determination of Surface Area and Porosity (Recommedations 1984). *Pure & Applied Chemistry* **1985**, *57*, 603-619.

(71) Gregg, S. J.; Sing, K. S. W. *Adsorption, Surface Area and Porosity;* Academic Press Inc.: New York, New York, 1967; pp 371.

(72) Webb, P. A.; Orr, C. In *Surface Area and Pore Structure by Gas Adsorption;* Analytical Methods in Fine Particle Technology; Micromeritics Instrument Corp.: Norcross, GA, 1997; pp 53-153.

(73) Brunauer, S.; Deming, L. S.; Deming, W. E.; Teller, E. On a Theory of the van der Waals Adsorption of Gases. *Journal of the American Chemical Society* **1940**, *62*, 1723-1732.

(74) Cejka, J.; et al., Eds.; In *Introduction to Zeolite Science and Practice;* Elsevier B.V.: Amsterdam, The Netherlands, 2007; pp 1058.

(75) Do, D. D. *Adsorption Analysis: Equilibria and Kinetics;* Series on Chemical Engineering; Imperial College Press: London, England, 1998; Vol. 2, pp 892.

(76) Langmuir, I. The adsorption of gases on plane surfaces of glass, mica and platinum. *Journal of the American Chemical Society* **1918**, *40*, 1361-1403.

(77) Yang, R. T. In *Adsorbents and Adsorption Isotherms;* Gas Separation by Adsorption Processes; Butterworth Publishers: Stoneham, MA, 1987; pp 9-39.

(78) Fowler, R. H. A Statistical Derivation of Langmuir's Adsorption Isotherm. *Mathematical Proceedings of the Cambridge Philosophical Society* **1935**, *31*, 260-264.

(79) Miyamoto, S. On the theory of adsorption. *Colloid & Polymer Science* **1935**, *70*, 275-277.

(80) DeBoer, J. H.; Zwicker, C. The polarization due to adsorption isotherms. *Z. Phys. Chem* **1929**, *3*, 407-418.

(81) Bradley, R. S. Polymoleular adsorped films. Part I. The adsorption of argon on salt crystals at low temperatures, and the determination of surface fields. *Journal of the Chemical Society* **1936**, 1467-1474.

(82) Balci, S. Effect of heating and acid pre-treatment on pore size distribution of sepiolite. *Clay Minerals* **1999**, *34*, 647-655.

(83) Korotchenko, V. N.; Gagne´, M. R. Fluorophobic enhanced decontamination of a mustard simulant by porous monolithic flow-through columns. *Reactive & Functional Polymers* **2007**, *67*, 422-431.

(84) Brandrup, J.; Immergut, E. H.; Grulke, E. A., Eds.; In *Polymer Handbook, 4th Edition;* Wiley-Interscience: 1999; pp 3336.

(85) Moellmer, J.; et.al. Insights on Adsorption Characterization of Metal-Organic Frameworks: A benchmark Study on the Novel soc-MOF. *Microporous and Mesoporous Materials* **2009**, *129*, 345-353.

(86) Bae, Y.; Yazaydin, O.; Snurr, R. Evaluation of the BET Method for Determining Surface Areas of MOFs and Zeolites that Contain Ultra-Micropores. *Langmuir* **2010**, *26*, 5475-5483.

(87) Sing, K. The use of nitrogen adsorption for the characterisation of porous materials. *Colloids and Surfaces A-Physicochemical and Engineering Aspects* **2001**, *187-188*, 3-9.

(88) Rouquerol, J.; Llewwellyn, P.; Rouquerol, F. Is the BET equation applicable to microporous adsorbents? *Studies in Surface Science and Catalysis* **2007**, *160*, 49-56.

(89) Vaughn, E.; Ramachandran, G. Fiberglass vs. synthetic air filtration media. *INJ* **2002**, *Fall*, 41-53.

(90) Kisilak D. A New Method of Evaluating Spherical Fabric Deformations. *Text. Res. J.* **1999**, *69*, 908-913.

(91) Wester, R. M.; Tanojo, H.; Maibach, H. I.; Wester, R. C. Predicted chemical warfare agent VX toxicity to uniformed soldier using parathion in vitro human skin exposure and absorption. *Toxicol. Appl. Pharmacol.* **2000**, *168*, 149-152.

(92) Rivin, D.; Kendrick, C. E. Adsorption Properties of Vapor-Protective Fabrics Conating Activated Carbon. *Carbon* **1997**, *35*, 1295.

(93) OSHA Toxic and Hazardous Substances: Limits for Air Contaminants. *1910.1000*.

(94) Force Health Protection & Readiness Toxic Industrial Chemicals/Toxic Industrial Materials (TICS/TIMs) – Awareness and Preventive Measures. *http://deploymenthealthlibrary.fhp.osd.mil/Product/RetrieveFile?prodId=301* (accessed 5/18, 2012).

(95) Roostaei, N.; Tezel, F. Removal of phenol from aqueous solutions by adsorption. *J. Environ. Manage.* **2004**, *70*, 157-164.

(96) Fuller, L. Production and Characterization of Novel Shaped Fibers for Fluid Adsorption and Transport, Dissertation, Clemson University, Clemson, SC, 2009.

(97) Muse, W. T.; Thomson, S.; Crouse, C.; Matson, K. Generation, sampling, and analysis for low-level GB (sarin) and GF (cyclosarin) vapor for inhalation toxicology studies. *Inhal. Toxicol.* **2006**, *18*, 1101-1108.

(98) Mlsna, T.; Cemalovic, S.; Warburton, M.; Hobson, S.; Mlsna, D.; Patel, S. Chemicapacitive microsensors for chemical warfare agent and toxic industrial chemical detection. *Sensors and Actuators B-Chemical* **2006**, *116*, 192-201.

(99) Patel, S.; Mlsna, T.; Fruhberger, B.; Klaassen, E.; Cemalovic, S.; Baselt, D. Chemicapacitive microsensors for volatile organic compound detection. *Sensors and Actuators B-Chemical* **2003**, *96*, 541-553.

(100) Plum, T. J. Design and Fabrication of a MEMS Chemicapacitive Sensor for the Detection of Volatile Organic Compounds, Boise State University, Boise, Idaho, 2006.

(101) Hierlemann, A.; Lange, D.; Hagleitner, C.; Kerness, N.; Koll, A.; Brand, O.; Baltes, H. Application-specific sensor systems based on CMOS chemical microsensors. *Sensors and Actuators B-Chemical* **2000**, *70*, 2-11.

(102) RaFoG Space Energy Development Corporation Dielectric Constants of Common Materials. *http://www.rafoeg.de/20,Dokumentenarchiv/20,Daten/dielectric_chart.pdf* (accessed 1/26, 2013).